ADAPTIVE CONTROL OF COMBUSTION INSTABILITIES USING REAL-TIME MODES OBSERVATION

A Thesis

Presented to

The Academic Faculty

by

Clifford Edgar Johnson

In Partial Fulfillment

Of the Requirements for the Degree

Doctor of Philosophy in Mechanical Engineering

Georgia Institute of Technology

May, 2006

ADAPTIVE CONTROL OF COMBUSTION INSTABILITIES USING REAL-TIME MODES OBSERVATION

Approved by:

Dr. Ben T. Zinn, Advisor
School of Mechanical Engineering
Georgia Institute of Technology

Dr. Yedidia Neumeier
School of Aerospace Engineering
Georgia Institute of Technology

Dr. Ari Glezer
School of Mechanical Engineering
Georgia Institute of Technology

Dr. Tim Lieuwen
School of Aerospace Engineering
Georgia Institute of Technology

Dr. Samuel Shelton
School of Mechanical Engineering
Georgia Institute of Technology

Date Approved: February 13, 2006

To my Lord and Savior, Jesus Christ, my wife Laura, and my family, thank you for your sustaining love and support.

ACKNOWLEDGEMENTS

I would like to acknowledge several people who have supported and encouraged me in completing this thesis.

First, I would like to thank my thesis advisor, Dr. Ben T. Zinn, for his encouragement, guidance and support throughout my research, and for providing numerous opportunities to research interesting subjects.

I would like to thank Dr. Yedidia Neumeier for serving on my committee, for the countless hours of research mentorship, and for continually challenging me to think "outside the box."

I would like to thank Dr. Tim Lieuwen for serving on my committee, for his contributions to my research and his friendship.

I would also like to thank Dr. Ari Glezer and Dr. Samuel Shelton for serving on my committee.

I would like to thank Dr. Jerry Seitzmann and Dr. Jechiel Jagoda for their help and advice in the Georgia Tech Combustion Lab.

I would like to give a special thanks to thank all of the graduate students, post-docs and research engineers of the Georgia Tech Combustion Laboratory for their collaboration and friendship, especially: Dr. Larry Matta, Bob Daniels, Dr. Eugene Lubarsky, Dr. Maël Disseau, David Scarborough, Jason Faulkner, Jacob Cohen, and Jae-Yeon Lee.

Finally, I would like to acknowledge the financial support of the National Science Foundation, the United States Department of Energy through the Advanced Gas Turbines Systems Research, and Siemens Power Generation.

TABLE OF CONTENTS

LIST OF TABLES

LIST OF FIGURES

NOMENCLATURE

A	pressure amplitude
f	frequency in Hz
G(x)	Rayleigh integral
K_c	control gain
K_{ident}	online identification amplitude
L_i	energy loss process
L_x,L_y,L_z	length in the x,y,z directions, respectively
n_x,n_y,n_z	acoustic mode number in x,y,z directions, respectively
P	acoustic pressure
P_0	limit cycle pressure amplitude
Q	total heat release rate
q	local heat release rate
r	Pearson's product moment coefficient
R	mean square correlation coefficient
t	time
T	oscillation period
T_{ident}	duration of the online identification sweep
U	control signal
V	volume
x	spatial location
x_j	cosine of identification control phase
y_j	amplitude of pressure oscillations

Greek symbols

χ	cosine correlation function for online identification
$\Delta\phi_{max}$	maximum adaptation step size
ε	van der Pol oscillator damping
Φ	equivalence ratio
ϕ	phase
$\phi_{rel,mean}$	relative mean phase: difference between control phase and optimum control phase
η	filter constant
κ	transfer function
θ	amplitude of control phase modulation
$\Theta_{p/q}$	phase difference between acoustic pressure and heat release for siren driving
$\Theta_{q/p}$	phase difference between acoustic pressure and heat release for flame driving
σ	sine correlation function for online identification
τ	Characteristic time delay
ω	angular frequency, $2\pi f$

SUMMARY

This thesis describes an investigation into the prediction and control of combustion instabilities. The main contribution of this research is to enable the development of a "bolt-on" active control system that can be used on a variety of combustors without *a priori* knowledge of the instability characteristics of the combustor. An industrial version of such an active control system would reduce the amount of time required to field test a new combustor design by providing protection against damaging combustion instabilities. In addition to the active controller development and characterization, this thesis discusses a novel experimental method for determining combustor stability margin and limitations of controllability of unstable combustors due to system noise and time delays.

The first part of the thesis describes an experimental method for predicting the stability margin of a combustion system. This method measures the transfer functions that describe 1) the influence of the combustor pressure oscillations on the heat release and 2) the influence of the fluctuating heat release on the combustor dynamic pressure oscillations. Using these two transfer functions, the overall system gain and phase are determined, which provides an estimate of the tendency of the combustor to exhibit combustion instability.

The second part of the thesis describes the development of an adaptive controller for damping combustion instabilities. Two methods are presented: 1) an online identification method that provides a rapid, semi-automatic calculation of the optimum control phase, and 2) an adaptive method that continually adjusts the control system to

operate at the optimum control phase to provide maximum damping. The adaptive controller performance is characterized and its limitations are discussed.

The last part of the thesis describes an investigation into the factors that limit the ability of an active control system to damp combustion instability, i.e., its controllability. In particular, the effects of system noise and time delays are examined through experiments and a linear model.

Finally, several ideas are presented for further research and development in each of the areas described above.

CHAPTER 1

INTRODUCTION AND LITERATURE REVIEW

This thesis describes an investigation of active control of combustion instabilities in Dry Low NO_x (DLN) Gas Turbine combustors. This work primarily consists of two tasks: 1) developing an experimental method for evaluating the stability of a combustor, and 2) developing and testing an adaptive active control system for actively controlling the combustion process heat release and pressure oscillations in an unstable gas turbine combustor. The results of this investigation provide new methods for predicting and controlling detrimental combustion instabilities, which can shorten combustor lifetime, cause catastrophic failure of a gas turbine engine, and prevent operating combustors at their optimum design point.

1.1 Background

Interest in gas turbines for power generation has increased significantly in recent years due to their advantages over traditional methods of power generation. For example, gas turbines cost less to install and maintain than other methods of power generation (e.g., coal-fired boilers, nuclear reactors)[1]. Gas turbines also provide a reliable, efficient method of power generation and are well suited for increasing the peak capacity of existing powerplants [2]. One of the most significant benefit of gas turbines is their lower pollutant emissions, especially oxides of nitrogen (NO_x)[3].

Dry Low NO_x (DLN) engines achieve very low NO_x emissions levels by burning premixed fuel and air at a low equivalence ratio. Lean premixed flames burn at much lower temperatures than diffusion flames, which traditionally have been used in other combustion-based power generation systems. NO_x production is strongly dependent on

flame temperature, and lowering the flame temperature significantly reduces NO_x emissions. The lean premixed mode of combustion is illustrated in the schematic of a generic DLN combustor in Fig. 1.1 [4]. Compressed air enters through an inlet section at the left of the figure. Fuel is injected into the air stream, where it begins to mix with the inlet air. As the fuel and air pass through the mixing section, they are further mixed by the swirl vanes before entering the combustion zone. The flame is typically anchored by a bluff body, by a stabilizing pilot flame, or by a turbulent recirculation region caused by a rapid expansion of gases at the "dump plane" as shown in Fig. 1.1. The hot exhaust products exit downstream to the turbine section, where they drive the turbine blades to convert the combustion process heat release to mechanical power.

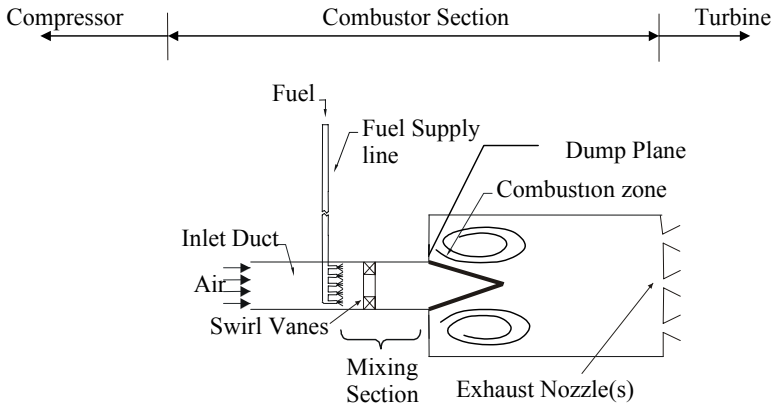

Figure 1.1: Generic schematic of an DLN combustor, see [4]

1.2 Combustion Instabilities

The development of DLN combustors has been hindered by their susceptibility to combustion instabilities that can cause degraded performance and premature wear of system components, and in some cases catastrophic failure of the system. Additionally, combustion instabilities can change the fuel-air mixing, which may result in higher NOx emissions. Combustion instability is a generic term that describes coherent, large-

amplitude pressure and heat release oscillations that are associated with the excitation of one or more natural acoustic modes of the combustor. Combustion instabilities have been observed in many types of combustors, including rocket motors, ramjets, and DLN [5,6,7]. The increased interest in the application of lean premixed technology in DLN combustors has increased the importance of understanding and controlling their instabilities, which is the subject matter of this research.

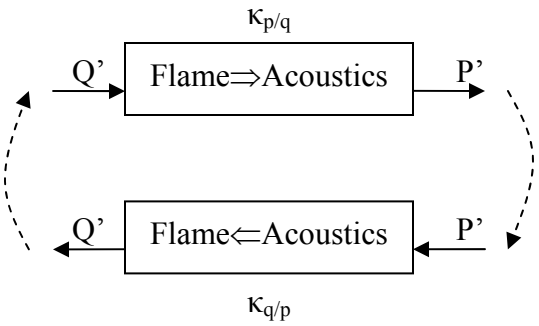

Figure 1.2: Feedback loop that drives combustion instabilities

Combustion instabilities are caused by complex interactions between pressure and heat release oscillations in a combustor. These interactions comprise a feedback loop, which consists of two branches as illustrated in Fig. 1.2. In the forward branch (top), heat release oscillations (denoted by Q') excite acoustic velocity and pressure oscillations P' in the combustor, which, in turn, excite heat release oscillations Q' in the combustor via the backward (bottom) branch of the feedback loop. Under appropriate conditions, this feedback process results in a rapid growth in the amplitudes of the combustor pressure and heat release oscillations. At some point, nonlinear processes saturate the growth of the oscillation amplitude, resulting in limit cycle oscillations in the combustor. Figure 1.3 illustrates this transition from stable combustion to unstable limit cycle pressure oscillations in a DLN combustor. In this example "stable" combustion occurs until t = 1.8 seconds, and is characterized by low-level turbulent fluctuations in the acoustic

pressure. At this time, the instability is triggered by a change in operating conditions and the oscillation amplitude grows exponentially until the amplitude saturates when t = 3.7 seconds. The limit cycle oscillations tend to persist either until the operating conditions are changed or active control is applied (see Section 1.4). As mentioned previously, these large amplitude limit cycle oscillations are undesirable since they can significantly shorten the life of the combustor or other system components and lead to catastrophic failure of the system (gas turbine, rocket motor, etc.).

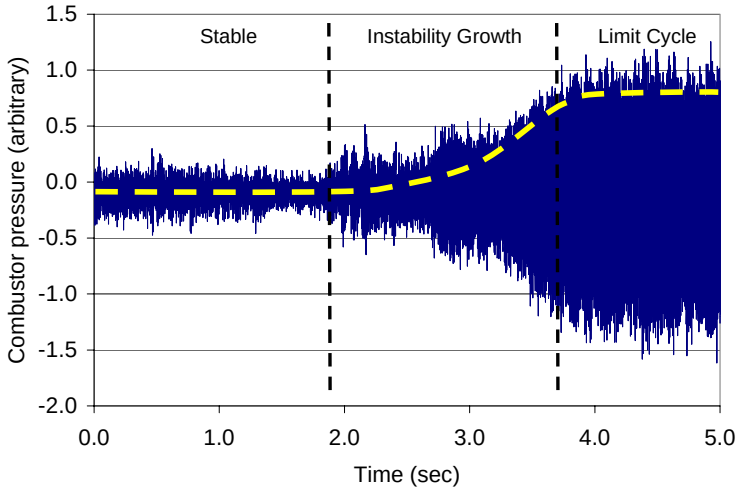

Figure 1.3: Transition from stable combustion to unstable limit cycle oscillations.

Combustion instabilities are generally encountered only for certain operating conditions. There are a number of factors, such as combustor geometry, fuel and air flow rates, and combustor pressure and temperature that determine whether the combustor is susceptible to instability for a given operating condition. This is due to the specific requirements that must be met in order to generate coherent heat release and pressure oscillations that excite and maintain the combustion instability feedback loop. Lord Rayleigh first described these requirements in his *Theory of Sound* [8]. Rayleigh's criterion states that if the local pressure and heat release oscillations are in phase, there is a net local addition of energy to the acoustic field. Conversely, if the pressure and heat

release are out of phase, there is a net local removal of energy from the acoustic field. The "Rayleigh index," G(x), can be used to quantify the spatial variation of this coupling between the heat release and pressure oscillations [9]:

$$G(x) = \frac{1}{T}\int q'(x,t)p'(x,t)dt \tag{1.1}$$

where T is the period of an oscillation and q' and p' represent the fluctuating parts of the heat release and pressure, respectively. Local acoustic driving occurs where the Rayleigh index is positive at a location (x), i.e., G(x) > 0. For harmonic oscillations, this condition is met when the magnitude of the phase ϕ between the heat release and pressure is less than 90 degrees; i.e., $-\pi/2 < \phi < \pi/2$. On the other hand, if the phase between the heat release and the pressure oscillations is larger than 90 degrees, the Rayleigh index at location (x) is negative and the heat release oscillations damp the acoustic field at that location. By integrating the Rayleigh index over the entire flame, the net acoustic energy addition can be calculated. A combustor is unstable when the total rate of acoustic energy addition to the combustor is greater than the rate of acoustic energy losses through other processes (e.g., convection, viscous dissipation, heat transfer, acoustic radiation through nozzles); i.e., [4,10]

$$\int_V \int_T p'(x,t)q'(x,t)dtdV \geq \int_V \int_T \sum_i L_i(x,t)dtdV \tag{1.2}$$

where L_i represents the various energy loss processes in the combustor. During the transition to limit cycle, the term on the left is greater than the term on the right. Once the limit cycle amplitude has been reached, the two terms are equal at a higher amplitude than the previous "stable" state.

Rayleigh's criterion shows that combustion instability occurs when the heat release and pressure are in phase. To predict analytically or numerically the conditions for instability, it is necessary to understand the physical mechanisms that contribute to the

driving and damping of the pressure and heat release oscillations. Lieuwen, *et al*., have described a mechanism in lean premixed DLN combustors in which the feedback cycle for combustion instabilities is driven by oscillations in the combustion equivalence ratio [4,12]. The phase relationship between pressure and heat release can also be controlled by the distortion or displacement of the flame due to acoustic interactions. There are many factors that control the phase between the pressure and heat release oscillations, including combustor geometry, flame dynamics, convection of the reactants and products of combustion. Other factors, such as vortex shedding and turbulence noise also influence the dynamics and may enhance or inhibit the feedback mechanism. In summary, instability can be excited by a complex interaction of several of these factors.

Because of the importance of understanding the roles of various mechanisms that can drive combustion instabilities, considerable effort has been invested in understanding and characterizing these mechanisms [4,11,12,13,14,15,16,17,18,19,20] in different types of combustors. The main goal of these studies was to provide engineers with the knowledge needed to design stable combustors. Unfortunately, current understanding of the phenomena that are responsible for driving these instabilities in different combustors has not reached the level required to design stable combustors. Therefore, it is nearly impossible to predict (through analysis or numerical simulation) whether, and under what operating conditions, combustion instabilities will occur. Consequently, efforts to control combustion instabilities usually begin when they are first encountered during testing. However, at this stage major design changes become more costly and generally cause production delays. A compromise that is sometimes employed is to avoid certain operating conditions under which the combustor becomes unstable. However, this compromise may be costly in terms of preventing engine operation at peak efficiency or peak power [21] or preventing ultra-clean (low emissions) operation near the lean blowout limit [19].

To maximize the potential of lean-premixed combustor technology, it is necessary to develop and implement technologies that prevent or limit the amplitude of combustion instabilities. The primary goal is to develop tools that allow engineers to design stable combustors. However, these tools require sophisticated models that are not available at present. Since we cannot analytically or numerically predict the conditions for instability, it would be very useful to explore methods for quickly determining how likely a combustor is to become unstable. Once an instability has been identified, control measures are required that can quickly and effectively damp these instabilities.

1.3 Combustor Stability Prediction

As mentioned above, it would be very useful to have tools that can predict the occurrence of combustion instabilities by accounting for flow and combustion dynamics, chemical kinetics, and combustor geometry. Unfortunately, such commercial tools do not exist for predicting combustion instabilities in gas turbine combustors, due mostly to the complexity of the interactions and the range of timescales that contribute to the problem. Reliable tools may someday be available to model these processes and utilize them to aid in designing combustors. In the meantime, it would be useful to develop technologies that allow engineers to determine experimentally how likely a combustor is to become unstable under certain operating conditions.

Traditionally, combustor stability characteristics have been determined by operating the combustor at a number of different operating points. If the combustor pressure oscillations are deemed acceptable, then the combustor can be deployed for field testing. If the pressure oscillations are unacceptable, then the combustor may have to be redesigned, or control measures may have to be implemented (see next section). The problem with this method of testing is that it does not provide any indication of how design changes or slight changes in operating conditions will affect a marginally stable combustor. This method only indicates whether a combustor is stable or unstable for a

given set of operating conditions that are encountered during testing. What is needed is a systematic method for determining whether a combustor is marginally stable, and if so, what changes would be likely to increase or decrease the stability margin of the combustor. Once the stability characteristics of a combustor have been determined, proper control measures can be developed to minimize pressure oscillations in the combustor. Chapter 3 presents a new method that was developed for experimentally determining the stability of a combustor.

1.4 Combustion Instability Control

After it has been determined that control measures are required, a number of options are available to reduce the amplitude of combustion dynamics. However, there are several challenges associated with the control of combustion instabilities. As mentioned above, the mechanisms that drive combustion instabilities are not completely understood. Also, many combustors have several natural modes that can be excited under various operating conditions, and in some cases, two or more modes are simultaneously excited [22,23,24,25]. Harmonics of the fundamental mode are often damped when the fundamental mode is controlled. However, in some cases distinct, independent modes can be present simultaneously. This multiple mode behavior complicates the control problem and renders some control approaches ineffective [26]. Suppression of one mode can lead to the destabilization of another mode in the combustor, and thus several iterations of control parameters may be required to eliminate the instability. Another complication is the cycle-to-cycle variation of the oscillating pressure's phase and amplitude in an unstable combustor [27,28,29]. Lastly, the stability characteristics of different combustors vary widely; in some combustors the oscillations can be easily prevented or damped, whereas in other combustors the persistent nature of the oscillations makes control very difficult. The persistence of combustor pressure

oscillations depends upon the damping of the combustion system and the driving mechanism; a noise-driven oscillator has different stability characteristics than a pure feedback instability.

Traditionally, efforts to prevent combustion instabilities have utilized passive approaches to accomplish one or more of the following: 1) increase the damping of the unstable modes by, e.g., nozzle modifications, Helmholtz resonators, or acoustic liners, 2) modify the combustion process to decrease the driving of the unstable modes, or 3) change the natural frequencies of the acoustic modes of the combustor [7,30]. These passive solutions are generally very costly, are combustor specific, are only effective over a limited range of operating conditions, and significantly increase the cost and development time of the system.

As an alternative to passive control systems, active control systems (ACS) have received significant attention in recent years. Active control of combustion instability involves adding energy to the system in a periodic manner so that the pressure oscillations are damped. This can be accomplished by forcing the system in such a manner that the feedback cycle is altered or by adding energy out of phase with respect to the pressure oscillations in the combustor. Though early work on active control systems was published in the 1950s [31,32], recent advances in computing performance and the development of new actuators have made active control of combustion instability in DLN combustors more practical. A properly designed ACS can be effective over a wide range of operating conditions and can be applied to a variety of combustors with little or no modification to the combustor, thus providing cost savings over traditional passive control approaches. An ACS can also be employed as a temporary measure to allow engine operation until design changes or passive control measures can be implemented.

There are two general classes of active controllers for combustion instabilities: open-loop and closed-loop. The characteristics of each type of controller are summarized in the following subsections.

1.4.1 Open-Loop Control

Open-loop control systems use actuators (types of actuators are discussed in the next subsection) to disrupt the feedback mechanism that creates an unstable system. The controller does not require any feedback (e.g., pressure or heat release measurement) to generate the control signal, and is thus relatively simple to implement. A schematic of an open-loop controller is shown in Fig 1.4 .

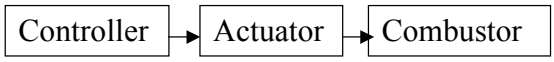

Figure 1.4: Typical open-loop controller block diagram

An open-loop ACS can be used to decouple the feedback mechanism that drives combustion instability by, e.g., periodic forcing of the shear layer [33,34]. McManus *et al*. showed that shear layer excitation modifies the normal formation of coherent vortical structures and found that by setting the control parameters properly, this method can lead to improved mixing and heat release while lowering the RMS amplitude of pressure oscillations. Richards *et al*. obtained similar results with open loop forcing by pulsed fuel injection [35]. The open loop control parameters are generally independent of the combustion instability characteristics. For example, Richards, *et al*. used 50Hz modulation of the fuel injection with varying duty cycle to control a 300Hz combustor pressure oscillation. A trial and error approach was used to experimentally determine the optimum open loop control parameters for maximum damping.

1.4.2 Closed-Loop Control

In contrast, closed-loop controllers attempt to damp combustor pressure oscillations by adding energy out of phase with the naturally occurring combustor

pressure oscillations, in accordance with Rayleigh's criterion [8]. Figure 1.5 shows a simple closed-loop ACS block diagram.

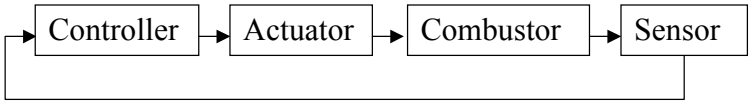

Figure 1.5: Typical closed-loop control block diagram

A closed loop ACS generally consists of one or more sensors that measure the combustor pressure and/or heat release oscillations, a controller that analyzes the measured pressure/heat release data to generate a control signal, and an actuator that generates secondary heat release or pressure oscillations in the combustor that damp the natural instability. Examples of sensors include transducers [36] that measure oscillating pressure, diode-laser arrays [37] that measure fluctuating local temperature or mole fraction of combustion reactants/products, and photomultipliers [22] that measure local or global chemiluminescence oscillations due to the formation and destruction of radicals in the course of an oscillating reaction process. Examples of actuators include loudspeakers that drive pressure oscillations in the combustor [23,38], piezoelectric airfoils that perturb the shear layer near the flame [34,39], and high-frequency fuel valves/injectors (e.g., solenoid injectors, piezoelectric stack injectors, magnetostrictive actuator injectors) that modulate the fuel flow rate to generate secondary heat release oscillations in the combustor[21,35,40].

The mechanism for controlling the combustion instability depends upon the choice of actuator. Laboratory experiments sometimes employ loudspeakers to drive pressure oscillations in the combustor that are out of phase with the limit cycle oscillations of the combustion instability. In contrast, a fast-response fuel valve provides heat release oscillations that are out of phase with the limit cycle pressure oscillations. Though laboratory experiments have demonstrated effective use of loudspeakers for

active control, a fast-response valve for fuel flow modulation is generally a more practical solution for the harsh operating environment of full-scale DLN combustors. In addition, a fast-response valve can introduce large energy reaction rate oscillations that to damp the combustion instability by modulating a relatively small fraction of the total fuel flow rate rather than attempting to modulate the pressure directly.

The heart of an ACS is its controller, which is typically implemented through analog circuitry or a computer. Several controllers have been employed with varying success in the active control of combustion instabilities. A common practice is to filter and phase shift the oscillating pressure/heat release signal to generate the actuator command signal [40,41,42]. This method can work in simple combustors that have a single, dominant unstable mode. However, as mentioned previously, many combustors have multiple modes that must be controlled, and these simple controllers can destabilize other modes in the combustor [22,23]. This method also requires knowledge of the exact frequencies of the unstable modes for all operating conditions in order to set the filter cutoff frequencies. Another approach to active control is to use model-based algorithms that attempt to account for combustor geometry, time delays, actuator dynamics and flame dynamics in order to predict combustor behavior under different operating conditions. The model provides a transfer function that is used to generate the actuator control signal from a measured pressure signal. Model-based algorithms have been demonstrated in the laboratory where the combustor geometry and dynamics are reasonably well known [38]. However, current modeling techniques are generally not capable of providing a transfer function for the complex dynamics of full-scale practical combustors [43].

In order to bypass the two main problems associated with the above control methods, a fast multiple-mode observer was developed at Georgia Tech [24]. This observer does not require a model of the combustion system, and by isolating multiple modes it is able to control one mode without destabilizing another. Appendix A provides

a description of the observer algorithm. This observer transforms the pressure signal from the time domain to the frequency domain, thus calculating the frequencies, phases and amplitudes of the dominant mode(s) in the combustor. Because the observer only calculates parameters that are relevant to the dominant mode(s), it is more efficient numerically (i.e., faster) than an FFT, which calculates the entire pressure signal frequency spectrum (see [25]). The controller uses the information from the observer to calculate a command signal that can control multiple modes simultaneously by setting the control gain and phase independently for each mode. These control parameters are generally determined in offline testing by manually adjusting the control phase and gain until the maximum damping is achieved [44]. When the controller is activated, it can damp the dominant mode(s) without destabilizing other modes in the combustor.

All three of the above control concepts (i.e., filter/phase shifter, model-based, and observer-based) require extensive offline testing to determine the control parameters properly. The offline testing results are used to determine the frequency response of the combustor to excitation by the ACS actuator, and the data from these tests are then used to determine the control phase and gain for damping different modes in the combustor. As operating conditions change, the control parameters must be adjusted. If operating conditions in the field vary from those in the test facility, the offline testing may not provide sufficient information needed to determine the proper control parameters. If design changes are made, the offline testing may need to be repeated in order to determine whether any changes in the control parameters are necessary. The necessity for offline testing is a significant obstacle to designing industry-ready control systems for active control of combustion instabilities.

1.5 Overview of Present Work

This thesis describes the development of an adaptive control system that automatically identifies the optimum control parameters for minimizing the amplitude of

the pressure oscillations in an unstable combustor without *a priori* knowledge of the combustor stability characteristics. Thus, the adaptive controller eliminates all or part of the offline testing that is presently required to implement active control. The results of this research are directly applicable to industrial DLN combustors, thus increasing the likelihood that a "bolt-on" ACS can be developed and applied to various combustors. The developed ACS does not require additional modeling or testing of combustor characteristics; thus, it can be easily configured for use on different combustors with slight modifications to the control hardware (actuator, piping, etc.).

Other "adaptive" algorithms have been developed for active control of combustion instability. However, these algorithms have typically been based upon some kind of model that will be substantially dependent of the type of combustor that is to be controlled. For example, Annaswamy, *et al.* developed a self-tuning scheme that is based upon a model of combustor dynamics [45]. As conditions change, the model parameters are adjusted in order to optimize the controller effectiveness. Koshigoe, *et al*. used a similar model-based approach, in which an online identification scheme is used to determine the correct model parameters that correctly describe the dynamics of the investigated system [46]. Bowman, *et al.* used a filtered-X LMS algorithm for parameter optimization [47]. The limitation of all of these approaches is that the control parameters require some model of the combustion system and control hardware, and must account for a number of time delays, including convection, valve actuation, combustion process heat release, and acoustic response. While it is theoretically possible to model all of the components that contribute to combustion instability, the time and effort required to model these process increases rapidly as the combustor complexity grows. Also, these models must account for a variety of operating conditions that depend upon, e.g., ambient temperature and fuel flow distribution in the combustor as a function of engine load. The above-mentioned adaptive schemes are designed to compensate for these uncertainties, but they require that the model parameters can be properly adjusted in order to adapt to

these changing conditions. In addition, it is likely that a given model will not apply to a wide variety of combustor designs, which thus limits the "bolt-on" capability of these systems. This thesis describes the development of an adaptive algorithm that eliminates the need for such models.

To present the results of this study, Chapter 2 first describes the various experimental setups that were used in this research. Next, Chapter 3 presents a method that was developed to experimentally determine the stability of a combustor. Subsequently, Chapters 4 and 5 describe the developed adaptive controller. These chapters include the algorithm development, implementation, and experimental investigation of the algorithm performance. Chapter 6 then presents an investigation of the limitations of the control authority imposed by the unstable system. This thesis closes with Chapter 7, which presents the conclusions of this research and recommendations for future work. Appendices are provided that describe the observer algorithm, background on computer programming for real-time control, and the algorithm used for controlling the mean fuel flow rate through the actuator.

CHAPTER 2

EXPERIMENTAL AND COMPUTING FACILITIES

This chapter describes the experimental and computing facilities that were used in the course of this research. Sections 2.1-2.3 discuss the experimental setups that were used for conducting active control tests and for characterizing the stability of a DLN combustor simulator. These experimental setups are described in detail in this chapter for reference in subsequent chapters. Section 2.4 describes the computing facilities that were used for active control and data acquisition.

The three experimental setups used were:

- An acoustic feedback setup was used to test the performance of the developed controller without the complexities of operating a combustion test facility. This setup also allowed more accurate measurements of controller performance and the effects of parameter variation.
- A high pressure Dry Low NOx (DLN) Gas Turbine simulator was developed to study a various problems encountered in gas-fired DLN combustors, including active control. This simulator was designed to exhibit instabilities at multiple frequencies, and provide a realistic simulation of a DLN combustor, which experiences combustion instabilities at low equivalence ratios.
- An atmospheric liquid-fueled ramjet simulator was developed for testing active control techniques in a liquid-fuel combustor. This facility provided the added complexity of droplet evaporation to the active control loop. In contrast to the DLN simulator, this test rig was most susceptible to high

amplitude combustion instability as the equivalence ratio approaches 1.0 (stoichiometric condition).

2.1 Acoustic Feedback Setup

The acoustic feedback setup is a resonant box in which the unstable combustion dynamics have been simulated by an acoustic feedback circuit. The system is much like a public address system in which the microphone senses the amplified output from the speaker. The acoustic system was used to test the various stages of development of the active control software and algorithms without the expense of operating an actual combustor. A schematic of the developed acoustic feedback setup is shown in Fig. 2.1. It consisted of a rectangular box 27.5 in long, 8.0 in wide, and 5.0 in high. The bottom of the box was constructed from ¾" plywood and the sides and top from ¾" Lexan. Three fast-response Kistler pressure transducers (i.e., T_A, T_B, T_C) were installed at various locations on the sides of the box. Transducer A was part of a feedback loop used to drive a positive feedback instability with an acoustic driver. The signal from this transducer was routed through a low-pass analog filter (Krohn-Hite Model 3343), an analog phase shifter, and an audio amplifier (Radio Shack MPA-101) before it was supplied to one of the acoustic drivers (Whelen SA-340-TSA 100 watt sirens). When the gain on the amplifier was increased from zero, a limit cycle instability was excited by the feedback loop. The analog filter and phase shifter combination allowed selection of the unstable mode, see Table 2.1, to be analyzed and controlled. The signal from transducer B could be used in similar fashion to set up a second feedback loop that generated an instability of a different frequency. Alternatively, the second amplifier and loudspeaker could be used to drive oscillations in the acoustic box from a noise source or a function generator by switching the input to the amplifier, as shown in Fig. 2.1.

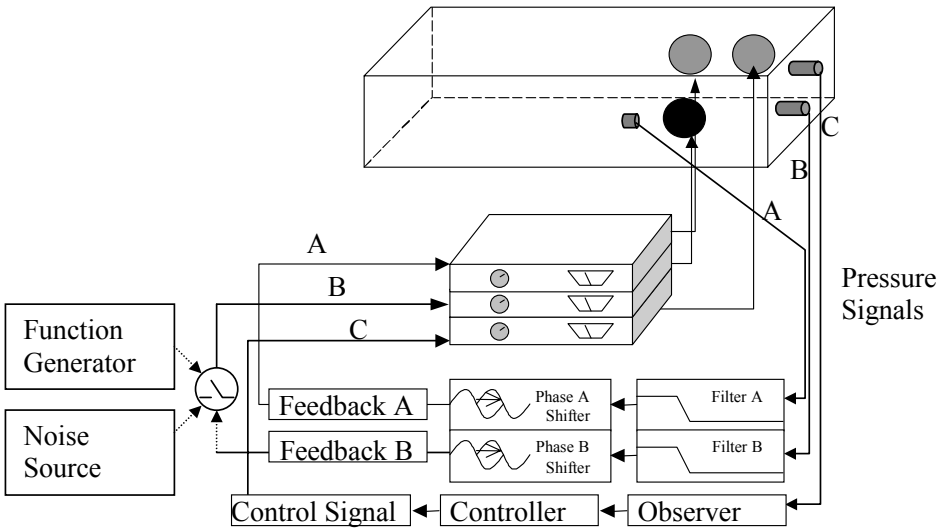

Figure 2.1: A schematic of the developed acoustic feedback setup

The signal from the third pressure transducer, T_c, was conditioned through a low-pass filter before being sent to the control computer, described in Section 2.5, which runs the observer and controller algorithms. The observer, as described in [25], determined the frequencies, phases and amplitudes of the unstable modes in the acoustic box. The controller utilized these data to generate a control signal, which was amplified and delivered to the control actuator, i.e., another speaker.

This acoustic feedback setup offered a number of advantages for development and testing of the control algorithms that will be discussed in later chapters. It was much less expensive to operate this experiment than any of the combustion experiments that are described later in this chapter. More importantly, it was much easier to control the characteristics of the oscillations in the acoustic feedback setup than in any of the combustors. For example, the amplitude of the feedback signal representing the combustion feedback could be adjusted by simply changing the gain on the amplifier or changing the phase shift. In a combustor, the feedback gain and phase are functions of the physical characteristics of the combustor and the operating conditions, such as the air and fuel flow rates. While the combustor operating conditions can be controlled to some

degree, some factors that influence the combustor stability, e.g., flame location, cannot be easily controlled. However, in the acoustic feedback setup, feedback oscillations could always be driven with deterministic feedback gain if the pressure sensor and speaker were properly located.

The lowest natural acoustic mode frequencies of this box were calculated for room temperature using the equation for determining the eigenfrequencies of the solution for the wave equation in a closed box with rigid walls, i.e., [48]

$$f_n = \frac{c}{2}\sqrt{\left(\frac{n_x}{L_x}\right)^2 + \left(\frac{n_y}{L_y}\right)^2 + \left(\frac{n_z}{L_z}\right)^2} \tag{2.1}$$

where c is the speed of sound (345 m/s at room temperature), and n_x, n_y, n_z represent the n^{th} modes in the x, y, and z directions, respectively. L_x, L_y, L_z represent the dimensions of the rectangular box. The first several natural modes of the acoustic feedback system were calculated using Eq. (2.1), and are shown in Table 2.1. The experiments on this setup were typically run using the lowest frequency natural acoustic mode (247Hz).

Table 2.1: Natural modes of the acoustic feedback system

n_x	n_y	n_z	f_{nat} (Hz)
1	0	0	247
2	0	0	494
3	0	0	740
0	1	0	850
0	2	0	1700
0	0	1	1358
1	1	0	885
2	1	0	983
3	1	0	1127
4	1	0	1302
1	0	1	1381

2.2 DLN Combustor Simulator

The second experimental setup, used for experiments in both active control of combustion instabilities and in the experimental determination of combustor stability margin, was a small-scale lean-premixed DLN combustor simulator with variable geometry. A schematic of this facility is shown in Fig. 2.2. Both the length of the air inlet and the location of the fuel injector could be varied to change the stability characteristics of the combustor (the double-ended arrows in Fig. 2.2 indicate the movable sections.) The configurable geometry allowed the primary longitudinal acoustic resonance and the fuel mixing length to be changed, thus giving additional ways to configure the combustor so that oscillations were excited.

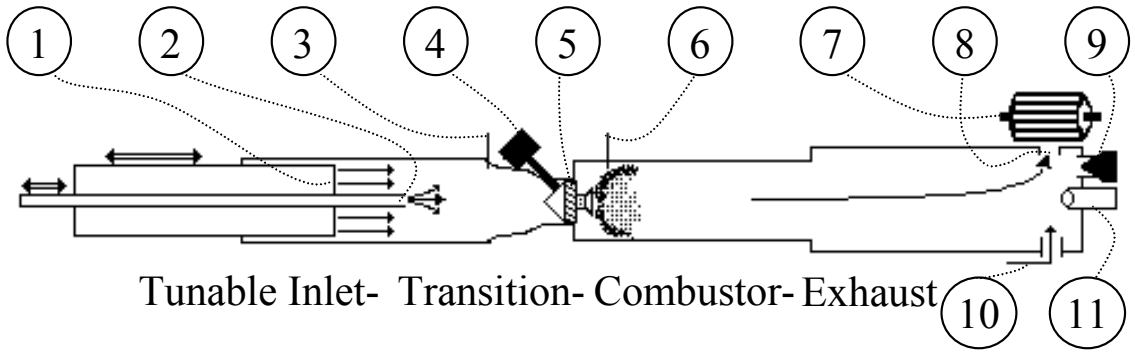

Figure 2.2: Laboratory scale DLN combustor: (1) choked air inlet (moveable), (2) primary fuel injector (moveable), (3) upstream pressure transducer, (4) fuel injector actuator, (5) swirler/flameholder assembly, (6) combustor pressure transducer, (7) siren, (8) siren nozzle, (9) bypass valve, (10) combustor cooling air, (11) photomultiplier assembly.

During a test, air entered the circular 1.87in diameter inlet section through a porous plate (1) made of sintered granular steel, which produced a rigid acoustic interface at its upstream end. The air inlet pipe could be moved axially with a ball screw driven by a stepper motor, thus changing the length of the inlet section between 41.0 in and 64.5 in. Primary fuel (industrial grade methane) was supplied through a choked fuel injection tube

(2) that protruded into the inlet section through the center of the air injector and could be moved axially to vary the fuel injection location between 40.2 in and 63.7 in upstream of the flame holder. The maximum travel of the fuel injector location was limited by the position of the tunable air inlet. For example, if the air inlet was moved as far back as possible, the fuel inlet could travel its maximum range of approximately 24in. However, if the air inlet was moved as far forward as possible, the range of fuel injection locations was very limited, to approximately 0.8in. The primary fuel and air mixed in the inlet section and then passed through a swirler (5) for further mixing prior to entering the combustor. A secondary fuel stream could be supplied through the fuel injector actuator (4), which was integrated with the swirler and flame holder. The second fuel stream was supplied through a choked orifice and subsequently injected radially into the air stream just upstream of the flame holder, where it was partially premixed with the incoming fuel/air mixture before reaching the flame zone. Combustion occurred in the 2x2x20in square combustor downstream of the conical flame holder. The combustion products then flowed through a circular 3in diameter, 77in long exhaust section before leaving the system. A separate high-pressure air stream cooled the combustor walls and was injected through a tube (10) into the exhaust section where it mixed with the combustion products. The "combined" flow exited the setup through an exhaust nozzle (8), whose area could be modulated by the siren (7), and an adjustable bypass valve (9). It should be noted that by increasing the flow rate of the cooling air it was possible to significantly increase the combustor pressure without altering the flow rates of the reactants. The siren (7), driven by a variable speed DC motor, provided capability for changing the frequency of the exhaust modulation between approximately 20Hz and 1000Hz. With the bypass valve (9) closed, the siren modulated the mean exhaust area by +/-30 percent. Opening the bypass valve dramatically reduced the percentage of the exhaust area modulations. The combustor could also be operated without the siren active.

Combustion process heat release and pressure oscillations could be measured simultaneously. Kistler pressure transducers (3) and (6), see Fig. 2.2, were mounted 13in upstream and 2.0in downstream of the flame holder, respectively. The relative magnitude of the combustion heat release oscillations was obtained by measuring the global CH* chemiluminescence with a photomultiplier (PMT) (11) fitted with a 10 nm bandwidth filter centered at 430 nm. The PMT was installed downstream of a quartz window at the rear end of the setup in a manner that permitted it to "view" the chemiluminescence from the entire combustion zone, see Fig. 2.2. The combustion process could also be viewed from the side, as a pair of windows was installed on each side of the combustor, with a flow of high pressure, cold air flowing through the gap between the windows. This design was used to minimize the stress on the windows. The inner quartz window was exposed to the high pressure, high temperature combustion process on one side, and high pressure, low temperature cooling air on the other side in order to minimize the pressure gradient across this window. The outer Pyrex window was exposed to high pressure, low temperature cooling air on one side, and low temperature, low-pressure ambient air on the other side in order to minimize the temperature gradient across the outer window.

The fuel injector actuator assembly was a critical component of the experimental setup. In order to generate controlled heat release oscillations in the combustor, high-pressure methane (400 psi supply pressure) was connected to the upstream end of the reed valve assembly that controlled the "secondary" fuel flow rate through the actuator assembly. A schematic of the reed valve assembly (not to scale) connected to the flameholder assembly is shown in Fig. 2.3. The reed valve position was controlled by a Terfenol D magnetostrictive actuator manufactured by Etrema Corp. (model # AA140J025-ES1). When supplied with a positive current, the actuator expanded, thus closing the reed valve; when a negative current was applied, the actuator contracted, thus opening the reed valve and allowing more fuel to flow through the actuator. Current to the actuator was provided by an Advanced Motion Controls model 30A20ACT pulse-

width modulated servo amplifier. With this configuration, it was possible to provide fuel flow modulations from DC to 1500Hz. Details of actuator characteristics and performance are given in Appendix A.

As mentioned above, the fuel flow modulations provided by this novel valve design were used to generate controlled heat release oscillations in the combustor. In this setup, the valve injected the "secondary" fuel flow into the flame zone via six 1.0mm holes that were drilled into the conical flameholder assembly, see Fig. 2.3. By injecting very close to the flame, the fuel flow oscillations were closely coupled to the heat release oscillations at the flame front. In contrast, if the fuel were modulated further upstream, in the premixing section, the coherence of the fuel pulses would be reduced by the "smearing" of the fuel flow oscillations due to diffusion of the fuel pockets as they were convected towards the flame. The fuel injector actuator assembly was used in "closed-loop" to control pressure oscillations in the combustor, and in "open-loop" to drive heat release oscillations at specific frequencies.

The DLN combustor simulator exhibited longitudinal mode instabilities under certain operating conditions. These oscillations typically occurred when the velocity of the reacting flow was slowed by restricting the exit area of the combustor exhaust, see [4]. Due to the geometry of the combustor and the temperature of the combustion products, the fundamental longitudinal mode was observed at approximately 100Hz, with an amplitude of approximately 1.0psi. Strong longitudinal oscillations were also observed at 180-200Hz, again depending upon operating conditions.

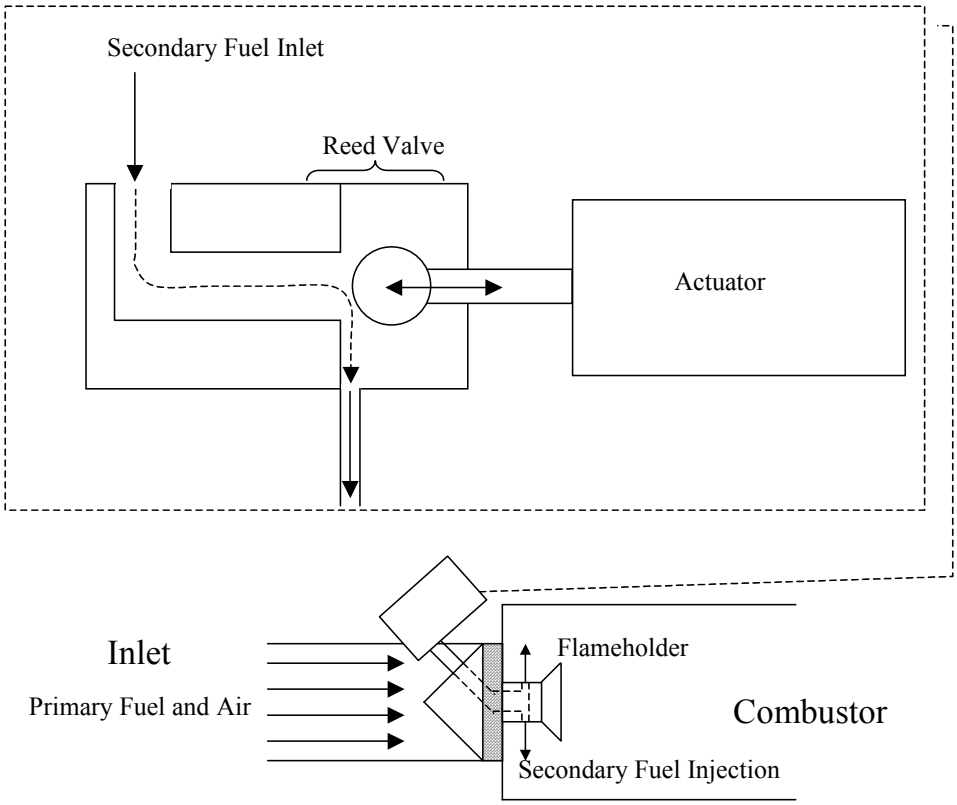

Figure 2.3: Schematic of the Fuel Injector Actuator with connection to swirler/flameholder assembly (not to scale)

2.3 Liquid Fuel Ramjet Combustor Simulator

Another experimental setup used in the study of active control of combustion instabilities was a liquid fuel ramjet combustor simulator, consisting of air and fuel supply systems, a fuel injector actuator (FIA) with flame holder, and a quartz combustor. The FIA consisted of an Etrema Terfenol D magnetostrictive actuator connected to a pintle-type injector, see Fig. 2.4. The actuator was driven by an Advanced Motion Controls model 30A20ACT pulse-width modulated servo amplifier. The time dependence of the liquid flow rate through the FIA was controlled by sending control current through the actuator, which changed the length of the magnetostrictive rod (1), as described in Section 2.2. As the actuator's length changed, it pushed the pintle (2) against a pressure force exerted by the liquid fuel supplied into the volume (3) between the

pintle's conical termination and the FIA's casing. The resulting force imbalance set the pintle in motion. As the pintle moved backward, the annular clearance (4) between the two cones expanded and allowed liquid fuel to flow through the plenum (5) into the nozzle (6). The pressure difference across the nozzle (6) changed as the width of the cross sectional area of the annular clearance (4) was changed. This pressure difference forced the liquid to move through the nozzle and produce a spray in the combustor.

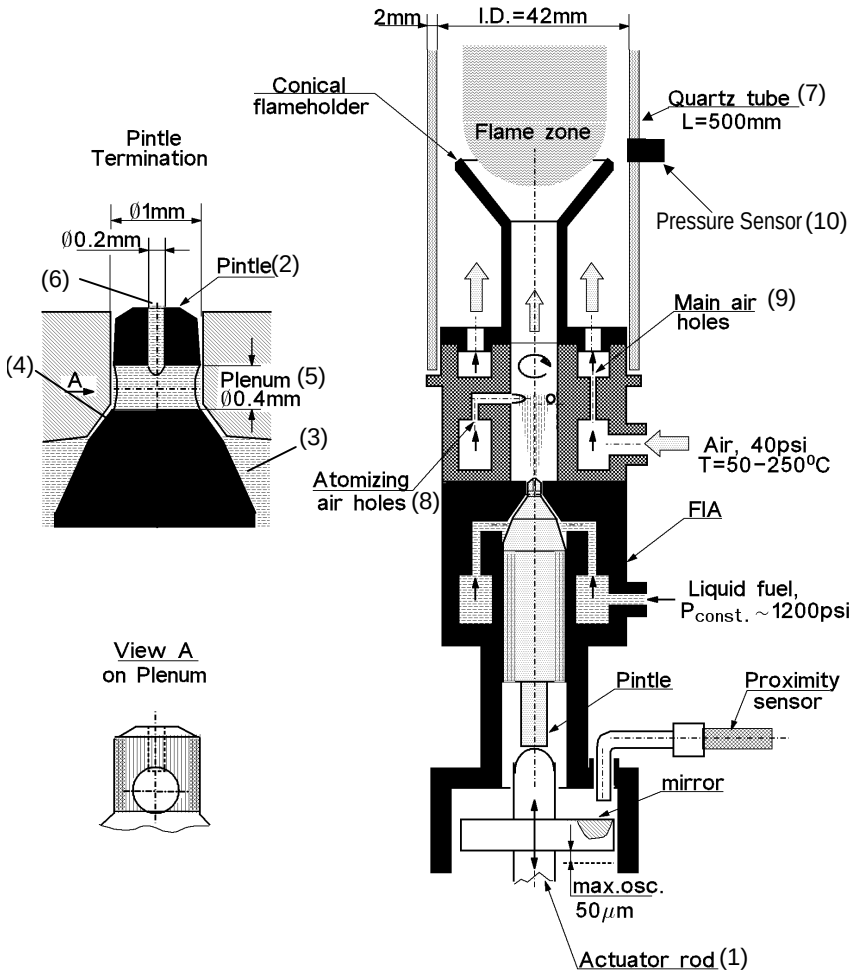

Figure 2.4: A schematic of the liquid fuel ramjet combustor setup, consisting of the following components: (1) magnetic rod, (2) pintle, (3) fuel supply, (4) annular clearance, (5) fuel plenum, (6) fuel nozzle, (7) quartz combustor, (8) air swirl holes, (9) annular air holes, and (10) pressure sensor.

The investigated combustor consisted of the air supply system, which was integrated with the FIA, a conical flame holder, and a 500mm long quartz pipe section (7) open at its downstream end. Thirty three percent of the air flow rate was directly injected with swirl into the liquid spray through a set of tangentially oriented orifices (8) and the remaining air (9) was supplied into the flame region in an annular stream that moved around the periphery of the conical flame holder. The maximum air supply was 15g/sec, and the maximum inlet air temperature was 200°C. The fuel in all experiments was n-heptane (C_7H_{16}) and the maximum investigated fuel flow rate was 1g/sec. The velocity of the combustion products was measured with a high speed Kodak EktaPro camera to be approximately 80m/s by tracking droplets as they moved through the combustor before evaporating. Pressure oscillations in the combustor were measured with an air-cooled piezoelectric pressure sensor (10).

This combustor exhibited instabilities at equivalence ratios of $0.6 < \Phi < 1.0$. As the fuel flow into the combustor, and thus the equivalence ratio, was increased, the amplitude of the instability grew stronger, reaching a maximum amplitude of approximately 1.0 psi, or approximately 7 percent of the mean pressure under atmospheric operating conditions. During limit-cycle oscillations, the combustor exhibited quarter-wave longitudinal mode instabilities of 400-440Hz, depending upon the temperature of the combustion products.

2.4 Computing and Data Acquisition Facilities

This section describes the computers that were used for active control and for data acquisition.

2.4.3 Active Control

The active control system was programmed in the "C" programming language on a PC running the QNX 4.0 real-time operating system. Analog Devices RTI-800 and

RTI-802 boards were used for real-time input and output, respectively, each with a total sampling rate of 40kS/s. These boards provide non-buffered real-time input and output from the control computer at the sampling rate.

2.4.4 Data Acquisition

Data acquisition was performed with a PC that used a National Instruments AT-MIO-16X input board with a sampling rate of 100kS/s divided over 2,4,8 or16 input channels. Labview software was used to collect voltage data from pressure transducers, photomultipliers, flowmeters and the control computer. The resolution of the National Instruments board was 12 bits over a range of +/-10V, thus giving a resolution of 4.8mV.

Two Labview programs were used for data acquisition. The first program measured time varying signals for up to 16 channels and recorded the raw data to a file. Typically, the sampling rate was set to 5kHz, which was at least ten times the natural (unstable) frequency of the oscillations for all of the experimental setups. This "time-trace" data was post-processed and analyzed using Matlab or Excel. A modified version of the Labview Dynamic Signal Analyzer program was used to calculate the Fourier transform (FFT) of two signals simultaneously. This program allowed rapid determination of the phase and gain between two signals. Chapter 3 described how this capability was used for determining the stability characteristics of a combustor.

CHAPTER 3

EXPERIMENTAL DETERMINATION OF COMBUSTOR STABILITY

It is important to assess whether combustion pressure oscillations are likely to be excited under normal or off-design operating conditions. Such knowledge allows engineers to determine whether design changes are required to limit the amplitude of combustion instabilities. This chapter describes a method that was developed to characterize the stability of a gas turbine combustor by independently examining the transfer functions that describe: 1) the effect of oscillating heat release on the pressure in the combustor, and 2) the effect of oscillating pressure on the heat release in the combustor. In what follows, Section 3.1 introduces the concept of combustor stability and the governing transfer functions, Section 3.2 presents the experimental procedure that was used to determine these transfer functions, and Section 3.3 provides a summary of the experimental results from the DLN combustor simulator.

3.1 Background

One of the significant needs of combustion engineers is the ability to predict whether and under what operating conditions a combustor is likely to become unstable during operation. Computer models that allow engineers to determine whether specific design changes will alter the stability characteristics of a combustor may someday be available. However, existing models do not adequately capture all of the complex interactions that drive combustion instabilities in order to allow reliable predictions of the stability of a particular design. Present computer models are generally only capable of giving qualitative information about the trends that can be expected from particular design changes, and experimental validation is generally required to verify the results.

There exists a need for dependable approaches that could predict the stability margin of combustors. Such an approach would enable combustion engineers to determine whether a specific combustor is marginally stable and, thus, likely to become unstable in the field, due to slight changes in operating conditions. Such *a priori* determination of a combustor's stability would greatly reduce unexpected incidence of combustion instabilities in the field, thus preventing costly system malfunctions and delays in the introduction of new propulsion systems and gas turbines. This predictive capability would be especially useful for determining whether active or passive control measures are necessary in order to bring an engine into production.

Determining the stability characteristics of a combustor involves characterization of the flame response to the acoustic field and the acoustic response of the combustor to flame fluctuations. While flame-acoustic wave interactions have been investigated theoretically, [49,50,51,52], current modeling capabilities are too immature to describe these phenomena in realistic combustion systems. The flame response to acoustic oscillations has also been studied experimentally. Zinn et al. [53] used the impedance tube technique and Matsui [54] used microphones upstream and downstream of the flame to measure the flame response. Also, Poinsot et al. [55] describe a method for measuring the reflection coefficient of a premixed flame in a duct. Additional descriptions of the efforts by Panchenko in this area are described in Ref. [56]. A passive method for determining combustor stability limits has been recently published by Lieuwen [57].

This chapter presents a new approach for determining combustor stability margin that takes advantage of the magnetostrictive fuel injector actuator for active control of combustion instabilities that is described in Sec. 2.2. While the technique presented herein was developed as part of an investigation of combustion instabilities in lean premixed gas turbine combustors, it can also be applied to determine the stability margin of other combustion systems.

As discussed in Chapter 1, combustion instabilities are driven by a feedback mechanism involving interactions between flow and combustion process oscillations. We can assign each branch of the feedback loop a complex transfer function that relates the magnitudes and phases of the input and output of the branch. We describe the transfer functions of the upper and lower branches of the feedback loop in Fig. 3.1 by $\kappa_{p/q}(\omega, |P'|)$, and $\kappa_{q/p}(\omega, |P'|)$ respectively, indicating their possible dependence upon frequency and magnitude of the pressure oscillations. Note that system losses (e.g., heat transfer to walls, acoustic damping) play an important role in this feedback cycle. These losses are not explicitly described in the illustration, but are incorporated into the transfer functions. For example, acoustic damping is considered in the transfer function $\kappa_{q/p}$ – the effect of the pressure fluctuations on the flame is reduced by acoustic damping in the system. Alternatively, this acoustic damping could be described by another transfer function on the right side of the diagram; however, we cannot measure this loss (or other system losses) directly. Therefore, all such losses are incorporated into the two transfer functions already described.

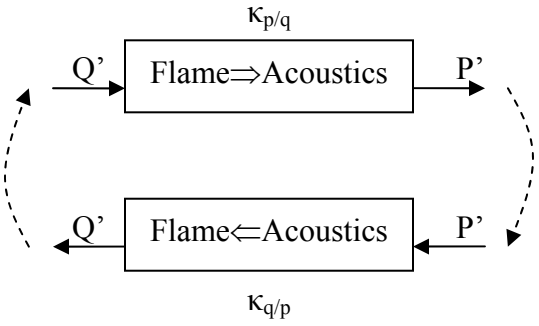

Figure 3.1: Transfer functions $\kappa_{p/q}$ and $\kappa_{q/p}$ describe the interactions between heat release and acoustics in a combustor

While both of the transfer functions $\kappa_{p/q}$ and $\kappa_{q/p}$ relate important information about the relative contribution of different processes to the feedback loop, the product of these transfer functions, i.e., $\kappa_{p/q}\kappa_{q/p}$ gives an indication of the overall stability of the

system. If the magnitude of this product is less than unity, i.e., $|\kappa_{p/q}\kappa_{q/p}| < 1$, the combustor is stable, and a feedback loop between the heat release and acoustics cannot be sustained. However, if the magnitude of this product is greater than unity, i.e., $|\kappa_{p/q}\kappa_{q/p}| > 1$, an instability is triggered, and the magnitude of the pressure and heat release oscillations are increasing for some period of time until reaching the limit cycle condition described below, see Fig. 1.3. Note that triggering the instability requires overcoming the system losses as described above. Referring to Fig. 3.1, this feedback cycle can be understood as follows. If the product of the transfer functions is less than 1.0, the amplitude of the pressure (and heat release) fluctuations diminishes from one cycle to the next. If the product is greater than 1.0, the amplitude increases from one cycle to the next. Finally, when nonlinear processes saturate the growth of the instability, the oscillations will tend to maintain a constant *limit cycle* amplitude, which signifies that the product of the transfer functions is equal to unity, i.e., $\kappa_{q/p}\kappa_{p/q}=1.0$. To satisfy this condition, the product of the magnitudes of $\kappa_{q/p}$ and $\kappa_{p/q}$ must equal one and the sum of the phases of $\kappa_{q/p}$ and $\kappa_{p/q}$ must be zero, i.e., $\Theta_{q/p} + \Theta_{p/q} = 0$. If $\kappa_{q/p}\kappa_{p/q}<1$ for all frequencies and pressure amplitudes, the combustor is "globally" stable.

The above discussion indicates that a combustor's stability over a range of frequencies could be determined if the frequency dependence of the magnitudes and phases of the transfer functions $\kappa_{q/p}$ and $\kappa_{p/q}$ could be determined. An experimental approach was developed for determining the frequency dependence of these transfer functions, and applying the measured transfer functions in determining the stability of a combustor. In this study, both transfer functions were determined from acoustic pressure and heat release oscillations measured simultaneously by the pressure transducer in the combustor (6) and the PMT (11), respectively, see Fig. 2.2. The transfer functions are dimensionless, as the magnitude of the oscillating heat release and pressure were normalized with respect to the mean heat release and mean combustor pressure, respectively. The transfer function $\kappa_{q/p}$ was determined from the ratio Q'/P' measured in

open loop tests in which the siren drove acoustic oscillations in the setup at specific frequencies. Similarly, the transfer function $\kappa_{p/q}$ was determined from the ratio P'/Q' measured in open loop tests in which the fuel injector actuator (4) periodically modulated the fuel injection rate into the combustor, thus generating heat release oscillations Q' in the setup. These tests are described schematically in Fig. 3.2. An examination of Fig. 3.2-a reveals that when the setup is driven by the siren, the effect of siren driving on heat release oscillations ($\kappa_{q/p}$) can be measured. All of the heat release oscillations in the combustor result from the pressure fluctuations when the combustor pressure is driven by the siren at a *stable* operating point. However, the "contribution" of the heat release oscillations to the pressure oscillations ($\kappa_{p/q}$) cannot be determined because it cannot be isolated from the contribution of the siren to the pressure oscillations. Similarly, for tests in which the fuel injector actuator drives combustion process heat release oscillations in the setup, Fig. 3.2-b shows that only $\kappa_{p/q}$ can be determined. Finally, Fig. 3.2-c shows that when the combustor is self-excited, both transfer functions can be determined, though only at the unstable frequency. Note that the tests must be conducted at stable operating conditions, at a stable combustor operating point, for these tests to be accurate. Self-excited oscillations may add an unwanted source term (in addition to the siren driving or fuel modulation), thus distorting the transfer function measurements, especially if the self-excited oscillations occur near the frequency of the external driving.

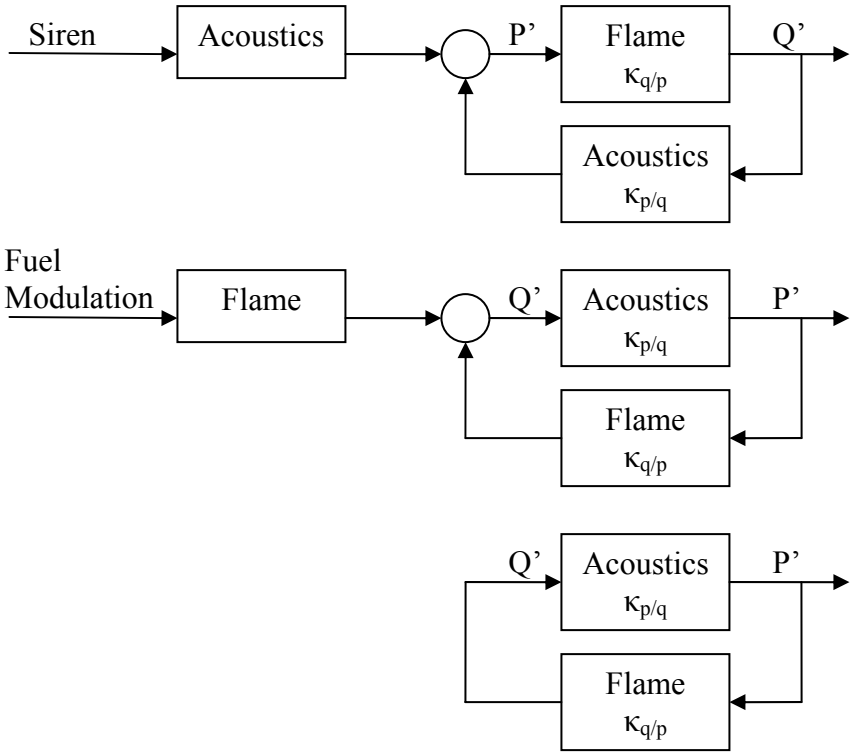

Figure 3.2 - Schematics of the feedback loops when the experiment is (a) siren driven, (b) driven by fuel injection rate modulation, (c) self-excited

The experimental setup that was developed to perform such driving experiments and measuring the corresponding transfer functions is described in Section 2.2. The experimental procedure is described in the next section.

3.2 Experimental Procedure

The DLN combustor simulator described in Section 2.2 has two important components that were essential for this study. The first component is the exhaust siren that allowed modulation of the combustor exhaust area, thus exciting pressure oscillations in the combustion chamber and exhaust pipe sections. The frequency of the pressure oscillations in the combustion chamber was varied between approximately 10Hz and 350Hz in order to determine the frequency response of the pressure and heat release to the siren (the natural combustor modes are 100HZ and 200Hz). The second component

required for this setup was a fuel injector actuator that was capable of modulating up to 50 percent of the fuel flow rate into the combustor. The frequency of these oscillations could be varied between zero and 1500Hz, and the amplitude could be adjusted from zero to the maximum amplitude that corresponded with 50 percent of the fuel flow rate into the combustor. Although both the siren and fuel actuator had sufficient bandwidth to drive high frequency oscillations of the pressure and heat release, respectively, the range of frequencies investigated in these experiments was 50-350Hz. Limitations imposed by the siren motor made it difficult to get repeatable results below 50 Hz. Above 350Hz, the coherence between the pressure and the heat release oscillations diminished rapidly, thus making it difficult to determine the gain and phase between the two signals.

In the first set of experiments, the response of the combustor pressure oscillations to fuel flow modulation was measured by injecting the fuel through the fuel injector actuator. The siren was locked into a fixed position to keep the exit area of the combustor constant and the mean static pressure in the combustor (with combustion) at 105 psia. The fuel injector actuator was used to modulate the fuel injection rate into the combustor at chosen, discrete frequencies. The pressure transducer in the combustor was used to measure the acoustic pressure oscillations in the combustion chamber and the photomultiplier was used to measure the time dependence of the global heat release in the combustion zone. The Labview Dynamic Signal Analyzer was used to measure the amplitude and phase of both signals in real time, thus enabling the calculation of the transfer function $\kappa_{p/q}$ at discrete frequencies between 50 and 350Hz. The magnitude of $\kappa_{p/q}$ was obtained from:

$$\left|\kappa_{p/q}\right| = \frac{\left|P'\right|/\left|\overline{P}\right|}{\left|Q'\right|/\left|\overline{Q}\right|}$$

where P' and Q' are the measured amplitudes of the pressure and heat release oscillations as measured by the dynamic pressure transducer and the PMT, respectively, and $\overline{P}$ and

$\overline{Q}$ are the mean pressure and heat release, as measured by the static combustor pressure gauge (corrected to absolute pressure) and the PMT, respectively. The amplitudes of the pressure and heat release were measured only at the frequency of the driven oscillations, which was the frequency of the input command to the actuator. The phase $\Theta_{p/q}$ was calculated by subtracting the phase of the acoustic pressure from the phase of the oscillating heat release at the driven frequency. At each test point, the frequency of the combustion process driving was held constant, and tests were conducted at different frequencies between 50 and 350Hz.

In the second set of experiments, the open loop response of the combustion process heat release to acoustic pressure was studied by forcing the combustor with the exhaust siren. Fuel and air were mixed in the inlet section, and the mixture was burned in the combustor. As in the first set of experiments, the acoustic pressure in the combustor was measured with the combustor pressure transducer and the global heat release rate oscillations were measured with the photomultiplier mounted in the exhaust section. The magnitude of $\kappa_{q/p}$ was determined in a similar manner as in the second set of experiments, from the expression,

$$\left|\kappa_{q/p}\right| = \frac{\left|Q'\right|/\left|\overline{Q}\right|}{\left|P'\right|/\left|\overline{P}\right|}$$

The phase calculation for the second set of experiments was identical to that for the first set of experiments, i.e., the phase of the transfer function was calculated by subtracting the phase of the pressure signal from that of the PMT signal at the driven frequency, using the modified Labview Dynamic Signal Analyzer (FFT). The phase and magnitude data for $\kappa_{q/p}$ were measured at discrete data points between 50 and 350Hz. Some limitations of the siren controller prevented obtaining data at the exact frequencies used in the second set of experiments; therefore interpolation was used to calculate the overall transfer function described in section 3.4.

In the final set of experiments, naturally driven feedback instabilities were investigated at operating conditions near those used for the other two sets of tests. In this case, the natural instability frequency was 180Hz.

3.3 Results

Figures 3.3 and 3.4 show the acoustic pressure and normalized heat release measured in all three experiments. Figure 3.3 shows that the siren driving produced very large amplitude pressure oscillations at the natural acoustic mode frequencies. At the fundamental acoustic mode frequency of 180Hz the siren drove oscillations whose amplitude was more than five times larger than the limit cycle amplitude of the natural instability. The flame driving experiments exhibited a similar behavior, but with much lower amplitudes. In these cases, the acoustic pressure amplitude was approximately equal to what was measured in experiments in which the combustor was unstable. While the acoustic pressure amplitude was highest at similar frequencies for both flame driving and siren driving, Fig. 3.4 shows that the normalized heat release response differed depending upon the driving mechanism. In particular, when flame driving was used, the normalized heat release was low at frequencies where the siren driving produced a high amplitude response in the flame (e.g., 100Hz). This difference in heat release response to acoustic perturbations versus fuel flow rate modulations highlights the complicated nature of the flame response to different inputs and why it is difficult to model this flame response. The flame responds to external forcing from the siren in a predictable manner, i.e., large amplitude pressure oscillations drive large amplitude flame response, especially when the phase is aligned in accordance with Rayleigh's criterion. However, modulating the fuel flow rate causes two forces to act upon the flame: 1) direct "internal" forcing of heat release oscillations by the fuel flow modulations, and 2) indirect "external" forcing of heat release fluctuations by the induced pressure oscillations in the combustor. If the phase between the two forces are aligned properly, they will act together to drive larger

heat release oscillations; however, if these two forces are acting against each other, the heat release oscillations may be partially damped. At certain frequencies, the pressure oscillations and fuel flow rate modulations work together to drive the heat release oscillations, and at other frequencies these forces work against each other. This relationship is dependent upon several factors including flame shape, actuator location, nozzle design, flameholding mechanism, and so on.

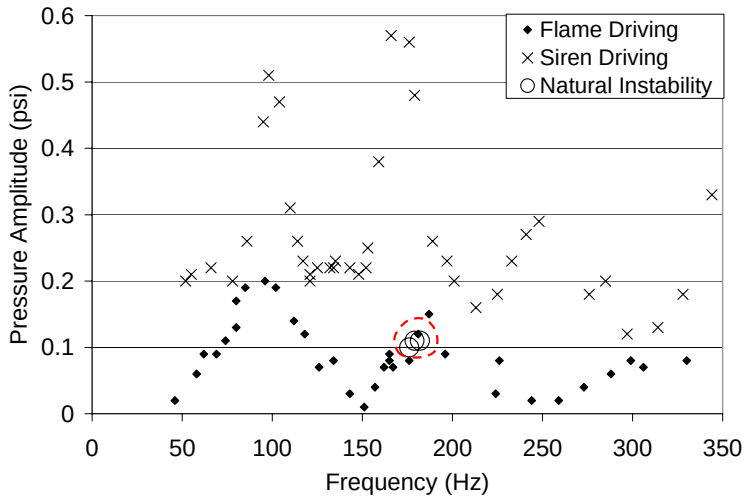

Figure 3.3 - The frequency dependence of the measured acoustic pressure for (a) siren driving, (b) flame driving (fuel modulation), and (c) natural instability

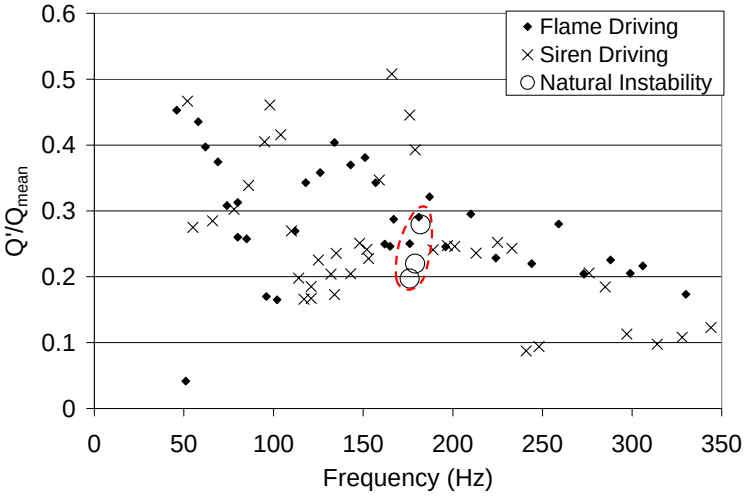

Figure 3.4 - The frequency dependence of the measured heat release fluctuations for (a) siren driving, (b) flame driving (fuel modulation), and (c) natural instability

Figures 3.5-a,b describe the frequency dependence of the magnitude and phase of $\kappa_{p/q}$ measured in experiments in which all of the fuel was supplied by the fuel injector actuator and a fraction of the fuel flow rate was periodically modulated to produce heat release oscillations Q'. It is important to note that the magnitudes and phases of $\kappa_{p/q}$ measured in driven experiments and the "naturally" unstable experiments are in good agreement. This figure indicates that the acoustic response of the combustor to heat release oscillations, $\kappa_{p/q}$ is the same regardless of whether the heat release oscillations are driven by the closed loop feedback cycle of the natural instability or by open loop modulation of the fuel flow rate. This result is very important, as it shows that the pressure response to the flame driving did not "saturate" due to overdriving of the fuel actuator, i.e., the pressure response to flame driving was linear, up to the limit cycle pressure amplitude. By contrast, it will be shown later that it was possible to drive the pressure amplitude high enough to saturate the flame response, i.e., the heat release oscillations increase with dynamic pressure oscillations driven by the siren up to the "saturation point." Once this level is exceeded, the flame response drops off rapidly, ,no longer providing an increase in heat release oscillations for an increase in the driven pressure oscillations.

Note that the phase between the heat release and the pressure is designated $\Theta_{p/q}$ to indicate that it represents the phase during experiments in which fuel injection rate modulation was used to drive the flame. Phase data from tests with siren driving are designated $\Theta_{q/p}$. However, in both test configurations, the phase difference between the photomultiplier and the pressure transducer measurements was always determined in the same manner, i.e., $\Theta_{p/q} \sim \Theta_{q/p} \sim < \Theta_{\text{photomultiplier}} - \Theta_{\text{pressure transducer}}$.

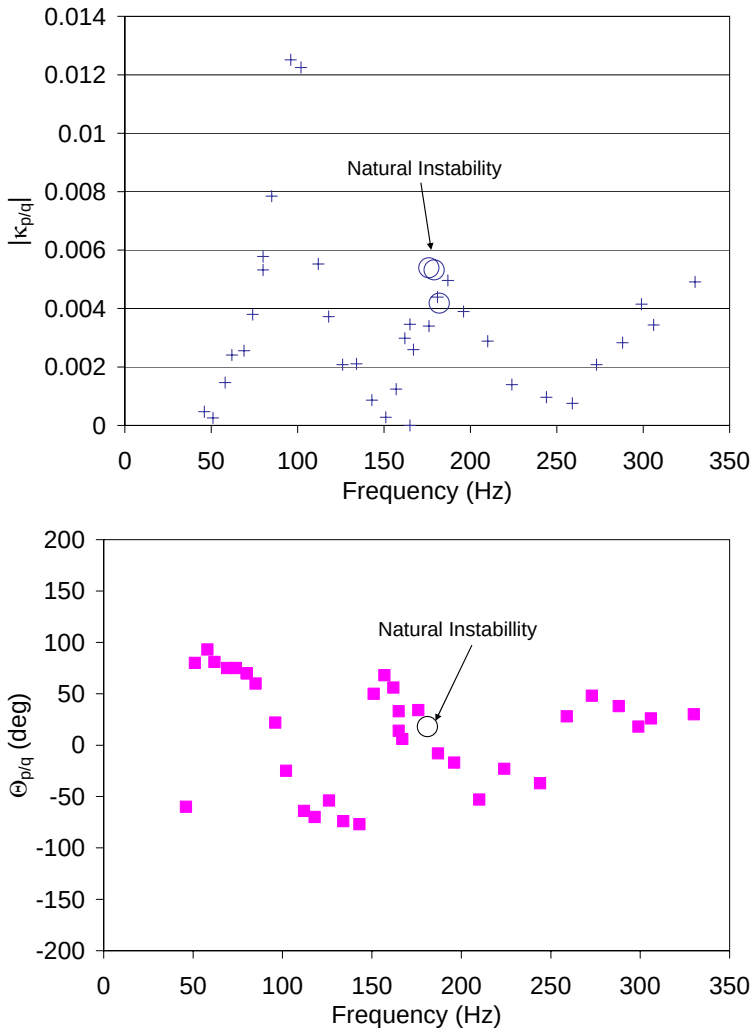

Figure 3.5 - The frequency dependence of measured (a) magnitude and (b) phase of the transfer function $\kappa_{p/q}$.

Figures 3.6-a,b describe the frequency dependence of the magnitude and phase of the transfer function $\kappa_{q/p}$ measured in experiments with siren driving and in experiments with natural instability (i.e., without any external driving). Figure 3.6-a shows that the magnitude of the transfer function $\kappa_{q/p}$ measured when the combustor was driven by the siren at 180Hz is nearly half that measured in the combustor when it is "inherently" unstable at this frequency. Figure 3.6-b shows that the phase of $\kappa_{q/p}$ monotonically increases with frequency and that the phases measured at the unstable frequency in the

driven and "inherently" unstable combustor are practically the same. In comparing the data from the driven experiments and data from the unstable combustor (both at 180 Hz) it should be noted that the amplitude of the pressure oscillations in the former and latter were 0.5 and 1.0 psi, respectively. The data in Figs. 3.6-a,b, thus, suggests that the magnitude of $\kappa_{q/p}$ is a function of the pressure amplitude and the phase is not. For limit cycle oscillations to develop, the magnitude and/or phase of the product of the transfer functions $\kappa_{q/p}\kappa_{p/q}$ must be a function of the pressure amplitude. Since the magnitude of $\kappa_{q/p}$ is the only pressure dependent parameter, it should control the amplitude of limit cycle oscillations for this combustor. Moreover, for a stable limit cycle, the magnitude of $\kappa_{q/p}$ (i.e., Q'/P') must be a decreasing function of the pressure amplitude, a trend that is exhibited in the data shown in Fig. 3.6-a. It should be noted that while the frequency dependence of the magnitude and phase of $\kappa_{p/q}$ likely could be predicted with a relatively simple linear model, no capabilities for modeling the amplitude and phase dependence of the flame response, $\kappa_{q/p}$, to acoustic perturbations for realistic turbulent flames are currently available.

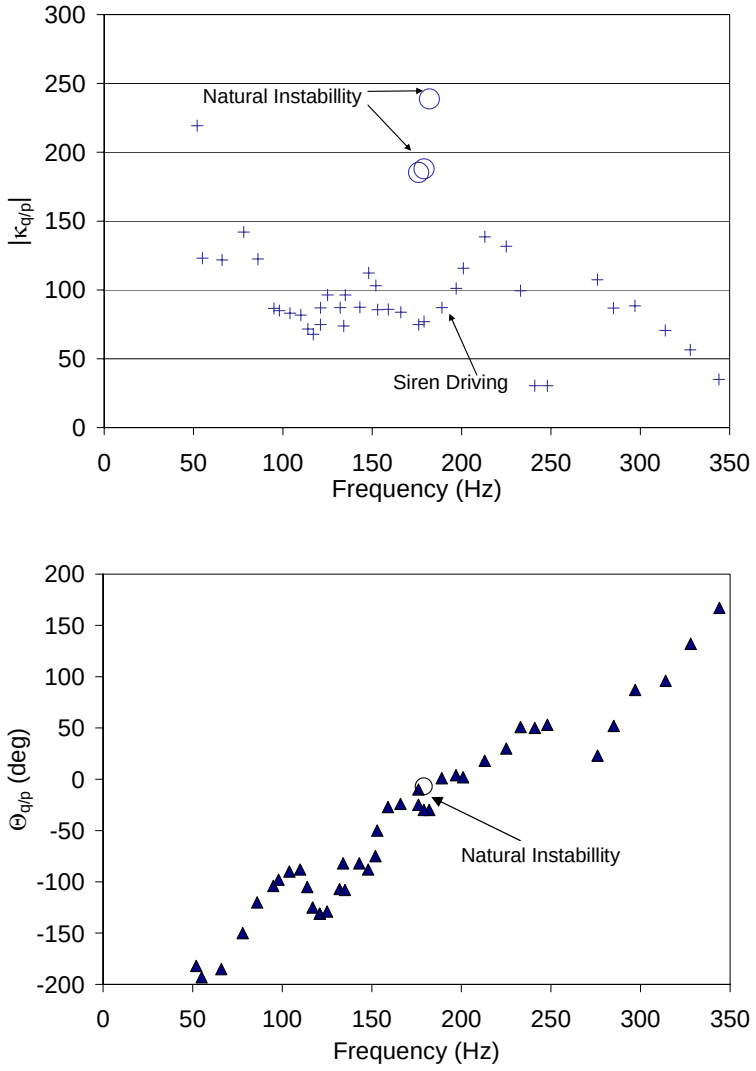

Figure 3.6 - The frequency dependence of measured (a) magnitude and (b) phase of the transfer function $\kappa_{q/p}$.

Next, we examine the frequency dependence of the product of the measured transfer functions $\kappa_{p/q}$ and $\kappa_{q/p}$, see Eq. (1). Figures 3.7-a,b show the product and sum of the transfer function magnitude and phase, respectively. In accordance with the discussion in the Section 3.1, a limit cycle occurs when the product of the magnitudes of $\kappa_{p/q}$ and $\kappa_{q/p}$ equals unity and the sum of their phases equals zero. Since the phases of both transfer functions were plotted as positive quantities in Fig. 3.7-b, their sum equals zero

where the plots of the two phases "intersect" in the figure. Accordingly, Fig. 3.7-b indicates that instabilities could occur around 140 and 180 Hz where these phases are equal. On the other hand, Fig. 3.7-a indicates that the product of the magnitudes of these transfer functions exceeds unity near 100 Hz, suggesting that instability could occur at this frequency. However, the phase difference at 100Hz is approximately 135 degrees., see Fig. 3.7-b. Therefore, the combustor should be stable at this frequency, in agreement with observations during this set of tests. This discussion and measured transfer functions indicate, however, that while the combustor did not become unstable at 100 Hz, it may become unstable with relatively modest changes in operating conditions at this frequency due to its narrow phase margin. In fact, other tests in this combustor at slightly different operating conditions have demonstrated self-excited oscillations at 100Hz, see [4].

We now examine the magnitude and phase of the product of the transfer functions at 180 Hz, the frequency at which the combustor is unstable. Figure 3.7-a shows that the product $\left|\kappa_{p/q}\right\|\kappa_{q/p}\right|$ measured during unstable operation is indeed close to unity (i.e., the circles in Fig. 3.7-a vary between 0.8 and 1.0) and Fig. 3.7-b shows that the phases of the two transfer functions measured during unstable operation equal one another at this frequency. Figure 3.7-a also shows, however, that the product $\left|\kappa_{p/q}\right\|\kappa_{q/p}\right|$ determined from measurements of $\kappa_{p/q}$ and $\kappa_{q/p}$ in the two (different) driven experiments at the 180Hz is only around 0.4. It is important to note, however, that the amplitudes of the pressure oscillations in the inherently unstable combustor and siren driven experiment were 0.1 and 0.5 psi (compared to a mean pressure of 105psi), respectively, when both operated at 180Hz, indicating that the amplitude of the oscillations in the driven experiment was five times larger than that in the unstable combustor. Consequently, the observation that the driven experiments provide $\left|\kappa_{p/q}\right\|\kappa_{q/p}\right|$=0.4, see Fig. 3.7-a, indicates that the combustor cannot sustain limit cycle oscillations at this amplitude (i.e., 0.5 psi) for the operating condition of the tests. In other words, the saturation mechanism that controls the limit

cycle amplitude (i.e., the flame response to dynamic pressure) does not permit limit cycle amplitudes to reach the amplitudes that were driven with the siren…the limit cycle amplitude is much lower than these values. Furthermore, in accordance with theory, the above results show that the product $\left|\kappa_{p/q}\right|\left|\kappa_{q/p}\right|$ indeed decreases as the pressure amplitude increases.

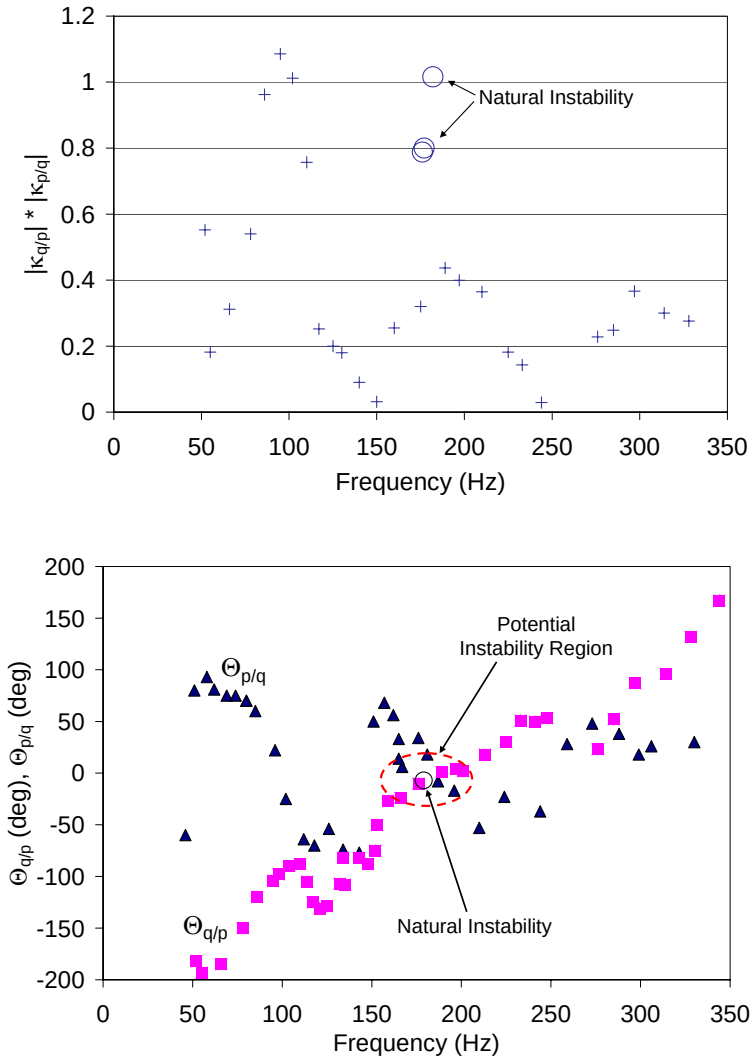

Figure 3.7 - Frequency dependence of (a) the product of the magnitudes of $\kappa_{q/p}$ and $\kappa_{p/q}$ and (b) the phases of $\kappa_{q/p}$ and $\kappa_{p/q}$.

The observations that $\left|\kappa_{p/q}\right|\left|\kappa_{q/p}\right| \approx 1$ and that the phases of these transfer functions are nearly equal at 100 Hz, see Figs. 3.7-a,b, also suggest that the combustor is nearly unstable at or near 100 Hz. A slight change in operating conditions that causes the phases to align would allow the combustor to become unstable, in which limit cycle oscillations could be expected at amplitudes of approximately 0.5psi, the pressure amplitude at which the overall system gain was measured at 1.0.

3.4 Summary

An experimental method was developed to determine the amplitude and frequency of naturally occurring combustion instabilities. The predicted amplitude and frequency of the combustion instability was compared with those occurring when the combustor was naturally unstable.

There are two conditions that must be met for instability to occur:

1) The phase plots relating heat release and pressure oscillations must be equal. By plotting the phase relation of the heat release to acoustic pressure for both the siren driving and flame driving experiments, it is possible to see which frequencies are most likely to become unstable (in this case, 180Hz). It is also possible to see other frequencies where the phase plots nearly intersect, indicating a potential instability at these frequencies if the gain condition is met.
2) The gain of the system must be greater than 1.0 at these frequencies to sustain an instability.

The only frequency where both conditions was met was 180Hz. At 100Hz, thee system gain is very high, but the phases do not align properly. However, a slight change in operating conditions may cause this mode to be unstable.

Finally, this study was somewhat limited by the inability to control the amplitude of the siren driving. For future experiments, it is recommended that an actuator capable of controlling both the frequency and amplitude of the driven pressure oscillations be used.

CHAPTER 4

ONLINE IDENTIFICATION OF OPTIMUM CONTROL PHASE

As a first step toward development of an adaptive control algorithm, an online identification algorithm was developed for determining the optimum control phase to be used for damping pressure oscillations in an unstable combustor. This chapter provides the background for this development and describes theoretical and experimental studies of the developed online identification procedure. The performance of this algorithm is investigated theoretically using a model of a van der Pol oscillator and experimentally in the positive feedback acoustic setup and the unstable DLN combustor simulator described in Chapter 2. Predicted and measured results demonstrate that the developed algorithm effectively and rapidly identifies the optimum control phase, which is applied to control the instability immediately after completion of the identification procedure.

4.1 Background

As discussed in Chapter 1, active control systems (ACS) would benefit from a method that eliminates some or all of the offline testing that is required prior to their use. This offline testing is typically used to determine control parameters, such as gain and phase, which are then employed in an ACS in order to damp the instabilities that may arise during normal operation. There are two problems with this procedure. First, offline testing designed to "map" the regions of operation where active control is necessary can be time consuming and expensive. Second, "unmapped" operating conditions may be encountered with different instability characteristics, in which case it would be helpful to have a flexible ACS that can quickly determine the optimum control parameters in order to regain control of the unstable combustor.

The online identification algorithm described in this chapter was developed to address these problems by rapidly determining the optimum control phase for an observer-based ACS that was previously developed at Georgia Tech.

Before discussing the online identification algorithm, a brief description of the observer-based active controller is given below. For more information on the observer-based controller, see Appendix A or [25].

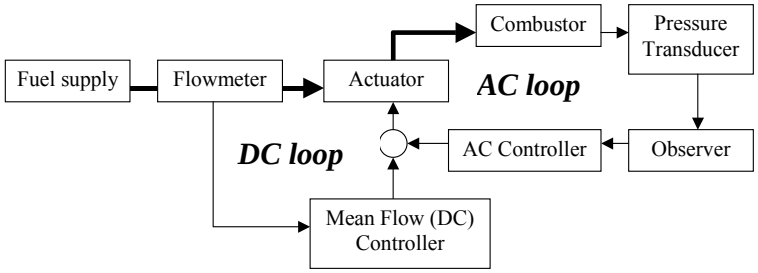

Figure 4.1. Closed-loop control block diagram.

Figure 4.1 shows a block diagram for the observer-based ACS that was used for active control of combustion instabilities using modulated fuel injection. The bold lines indicate the fuel flow path, and the thin lines indicate electrical signals. There are two control loops: the "AC" control loop on the right incorporates the observer and provides a control signal with the same frequency as the unstable pressure oscillations in the combustor. The mean flow control ("DC") loop on the left is necessary to provide a constant mean flow rate of fuel through the actuator. The "mean flow controller" block is a classical proportional-integral (PI) controller tuned to provide a constant flow rate of fuel through the actuator. This mean flow control loop is required in order to compensate for thermal expansion of the magnetostrictive actuator and to compensate for "overdriving" the reed valve, as described in Appendix C.

The high frequency (AC) control loop consists of a sensor, an observer, and a controller. The controller output is added to the mean flow (DC) controller output, and the resulting signal is used to drive the fuel injector actuator (FIA). During operation, the

sensor continuously measures the combustor pressure and sends the measured signal to the observer. The observer analyzes the measured pressure and determines the amplitudes, frequencies and phases of the most unstable combustor modes in real time. The controller then uses these data to generate a control signal for the FIA. Specifically, the controller uses data describing the open loop response of the control system, which has been previously determined in offline tests to determine the gain and phase of the control signal for optimum damping. Once the control parameters for optimum damping are identified, these parameters are stored in a lookup table for reference by the controller. During an active control session, the observer determines the frequency of the most unstable mode, and the control signal's phase and gain are obtained from this table.

Previous studies have demonstrated that this ACS could rapidly and effectively damp large amplitude instabilities. Figure 4.2 illustrates the effectiveness of this observer-based active controller when used to control instabilities in a gas rocket at Georgia Tech, see [58]. The pressure oscillations were damped within 40msec, and the dominant mode of the instability (400Hz) was damped by approximately 30dB. While this ACS is highly effective, its application required the determination of the open loop response of the system in separate tests. The need for offline open loop response tests would be eliminated if the ACS determined the optimum control parameters in the course of operation. To be effective, this system should be capable of controlling instabilities in different combustors over wide ranges of operating conditions.

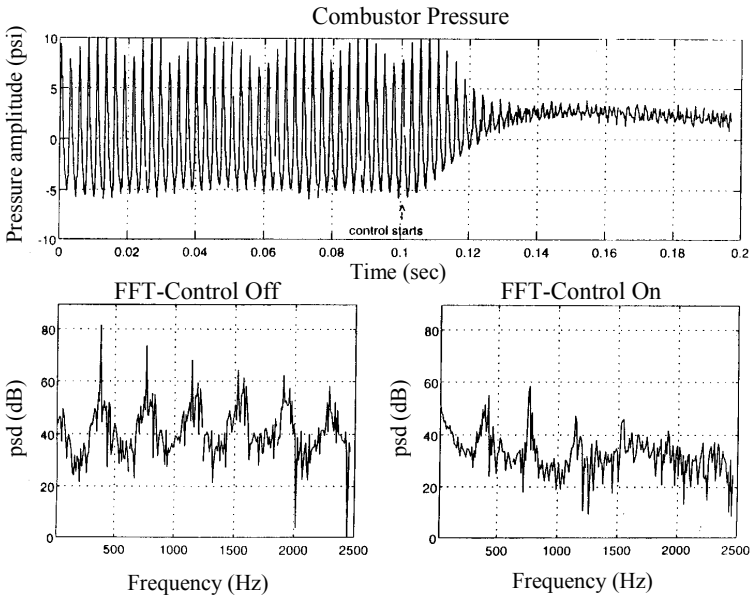

Figure 4.2. Demonstration of fixed-parameter ACS on Georgia Tech gas rocket.

Section 4.2 discusses the control parameters required for effective control of pressure oscillations in a combustor and a method of offline testing that was used in previous ACS studies, as well as limitations on controllability. Section 4.3 describes a concept for online identification of the optimum control phase, which was developed to be coupled with the observer-based ACS to allow rapid and effective control of unstable combustors without any *a priori* knowledge of the dynamic response of the system. Section 4.4 gives a detailed explanation of the how the algorithm works and shows results from a van der Pol oscillator simulation used to investigate the algorithm performance. Section 4.5 shows results from experiments that demonstrate the effectiveness of the algorithm. As will be explained in Section 4.6, this ACS with online identification does not constitute a fully adaptive controller. However, the concepts explained in this chapter lay the groundwork for the adaptive controller that is described in Chapter 5.

4.2 Determination of Active Control Parameters

One approach for effective control of pressure oscillations in an unstable combustor with a closed-loop ACS is to provide an oscillatory combustion process that is out of phase with the unstable pressure oscillations. To accomplish this objective, the adaptive controller must determine the proper phase for the control modulation of the fuel injection rate, and the control amplitude or gain required to damp the unstable oscillations.

4.2.1 Effect of Time Delays on Control Phase

In accordance with Rayleigh's criterion, the ACS would damp pressure oscillations by generating heat release oscillations that are out-of-phase with the combustor dynamic pressure. To provide these out-of-phase oscillations, it is first necessary to determine the optimum control phase. This optimum control phase varies from combustor to combustor because the feedback mechanisms and the control dynamics can vary significantly from one system to another. Furthermore, this optimum control phase can vary with time due to changes in operating conditions such as power output, ambient temperature, fuel composition, an so on. Figure 4.3 describes some of the factors that influence the phase of the control signal that provide maximum damping of the pressure oscillations in the combustor. This diagram does not represent a comprehensive model of combustor dynamics nor the active control feedback loop; it indicates, however, some of the time delays that are inherent to most actively controlled combustors.

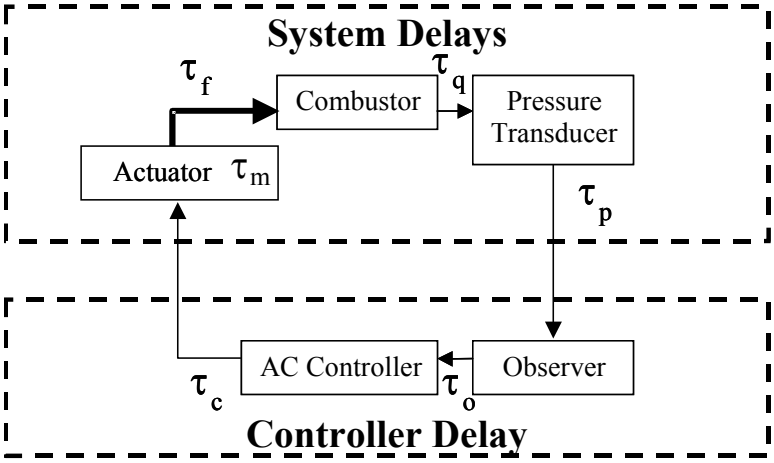

Figure 4.3. Closed loop feedback time delays.

Each block in Fig. 4.3 represents a transfer function that includes a frequency dependent gain and phase. Additionally, there are time delays τ that represent the time required for the signal to travel from one block to the next. For example, the time required for the control signal to reach the actuator τ_c should be very short. There is a certain amount of mechanical delay associated with the actuator's response to the control signal τ_m. The transfer function associated with the actuator can be determined experimentally. The time required for the fuel flow rate oscillations to reach the combustor τ_f depends upon the length of the fuel supply line and the speed of sound in the fuel. The "combustor" transfer function includes sub-blocks, such as the transfer function of the fuel nozzle and the flame transfer function, each containing its own time delays that may vary with operating conditions. For example, at high load the fuel flow rate is higher, which means higher injection pressure and thus shorter time delay associated with fuel injection. The time required for heat release oscillations to generate measured pressure oscillations at the pressure transducer is given by τ_q. Ideally, the controller could act instantly based upon the measured pressure oscillations, but there is some time required to measure and process the signals, given by τ_p and τ_o.

4.2.2 Effect of time delays on system stability and controllability

Rayleigh's criterion indicates that the optimum attenuation of pressure oscillations will occur when the phase of control fuel injection rate modulations produces heat release oscillations 180 degrees out of phase with respect to the unstable combustor pressure oscillations. In order to accomplish this objective, it is necessary to account for all of the combustion system delays and the controller time delay shown above. Figure 4.4 illustrates the effect of time delays on the determination of the proper phase for the control signal with a simplified example of the time delays between the observer input (pressure signal) and the control effect (heat release). The goal is to choose a control signal delay $\tau_{control}$ that produces heat release oscillations out of phase with respect to the pressure oscillations. Figure 4.4 shows a simple example where the system time delays are short. In this case, the delays for fuel delivery (second curve) and combustion (third curve) provide phase lags of $\pi/2$ and $\pi/4$, respectively. By adding a control phase of $\pi/4$, the sum of the three phase lags is equal to π. In this manner, the controller generates heat release oscillations (bottom curve) that are out-of-phase with the pressure oscillations (top curve), using an optimum control delay for maximum damping of $\pi/4$.

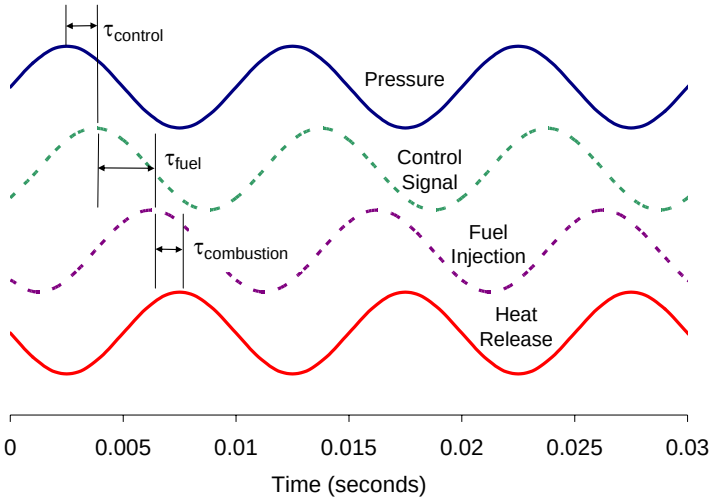

Figure 4.4. Time delays in control injection sequence.

Note that $\tau_{control}$ is a frequency dependent variable. More commonly, the control delay is given as a phase delay rather than a time delay, i.e.,

$$\phi_{control}(f) = 2\pi f * \tau_{control}(f) \tag{4.1}$$

where f is the frequency of the unstable oscillations. In general, the control phase delay for optimum damping will vary for different frequencies, depending upon the system response of the combustor pressure oscillations at those frequencies.

In many cases, the (fixed) system time delays will be long enough that the resulting phase delay between the controlled heat release and the unstable pressure oscillations is greater than π, even if the controller time delay is very small. In these cases, it is necessary to adjust the controller's time delay to produce a total phase shift of 180 degrees between the pressure and control process heat release oscillations. In some cases, this will result in a total delay that is equivalent to 3π, 5π, 7π… for optimized control. However, increasing the control loop time delay diminishes the overall performance of the controller. This reduced controller effectiveness is due to reduced gain margin that is available to control the system in a stable manner for large time

delays. In other words, there is a limited range of control system feedback gain that can be used to damp instabilities. For very high feedback gain, the control signal tends to destabilize the system. To demonstrate this phenomenon, an experiment was performed with a modification of the acoustic feedback setup described in Chapter 2. Using the computer, an artificial time delay was inserted into the control loop, to delay the response of the observer and controller, as shown in Fig. 4.5.

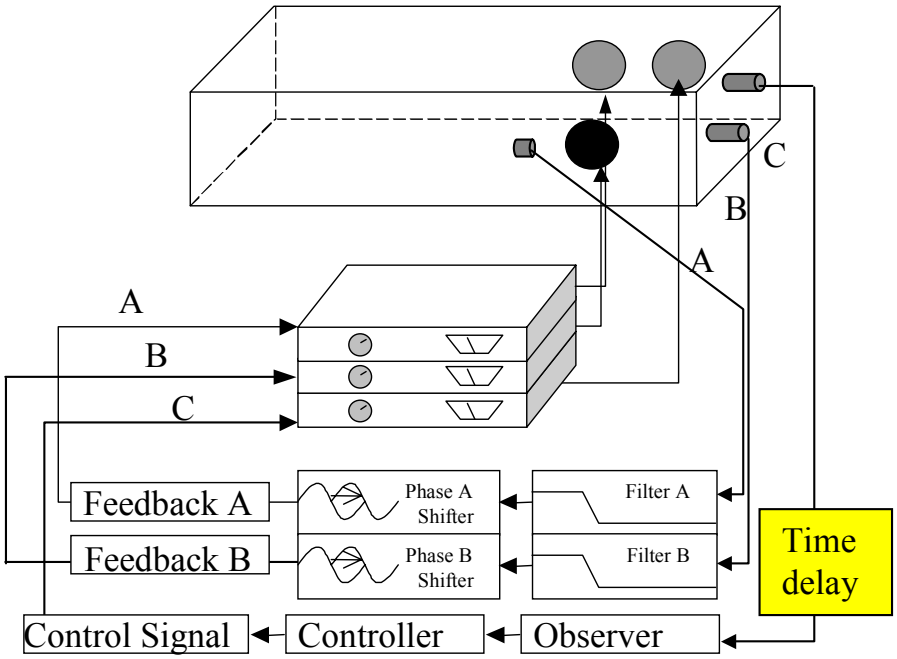

Figure 4.5. Experimental setup for determining effects of time delays on closed-loop feedback control

After inserting the time delay, feedback loop "B" was tuned to provide a limit cycle instability. The controller was then tuned to the optimum control phase that provided maximum damping for the given time delay. Next, the gain of the controller was gradually increased to maximize the attenuation of the pressure oscillations. At some point the "gain limit" was reached, where further increases in the control gain did not provide additional attenuation of the pressure oscillations. When this gain limit was exceeded, the controller became unstable and drove large amplitude oscillations in the

acoustic feedback setup. As shown in Fig. 4.6, the maximum allowable gain decreases rapidly when the control loop time delay, τ_{delay}, exceeds one oscillation period, τ_0. For more information on the effect of time delays on controller effectiveness, see Chapter 6.

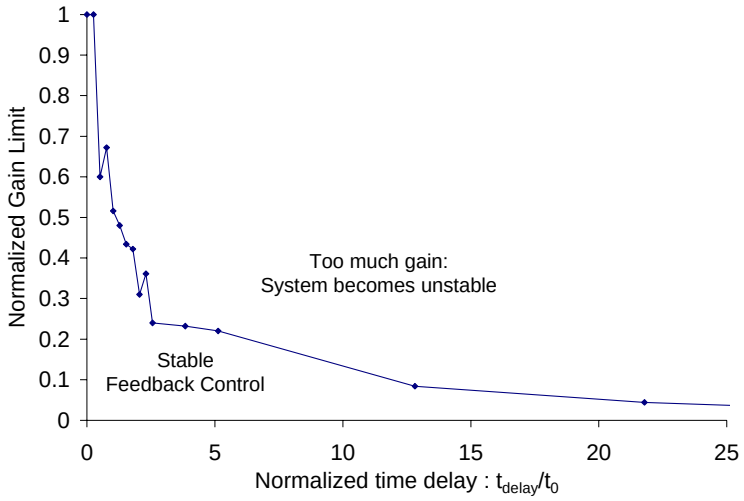

Figure 4.6. Effect of control loop time delays on the maximum allowable gain to damp pressure oscillations in the acoustic feedback setup.

4.2.3 Offline determination of the time delays and control phase

Though some investigators have attempted to model all of the processes that affect time delays in a laboratory setup, it is generally difficult to accurately model all of these processes. A conventional way to assess the global time delays in the system is to perform offline tests that determine the amplitude and phase of pressure oscillations with respect to the actuator control signal in a particular combustor. One way to determine the proper control phase for maximum damping is to experimentally determine the dependence of the effectiveness of the controller upon the control signal phase, which is gradually varied during the experiment. Once the optimal phase was determined, the gain was adjusted to provide the maximum damping for the least control effort and to prevent destabilizing the system. Another way to obtain such data is to drive heat release oscillations in the combustor using the actuator and to measure the combustor pressure

response to the control input, as is discussed in Chapter 3 in connection with the DLN combustor simulator. Figure 4.7 shows frequency response data that was obtained during such tests in a full-scale gas turbine combustor [59]. These data indicate a strong response of the combustor acoustic pressure to fuel flow modulations below 100Hz, with a rapid drop of the response at higher frequencies. There is also rapid change in phase as a function of frequency, indicating that an ACS must have precise control of the phase for the targeted frequency. These data provide the frequency response of the combustor to open loop forcing, which can be utilized by a fixed-phase ACS to the best control phase for damping oscillations at various frequencies. The coherence data gives an indication of what frequencies may be controllable using this particular actuator arrangement in this combustor. Low coherence indicates poor control authority, i.e., the combustor dynamic pressure does not respond well to the control actuation.

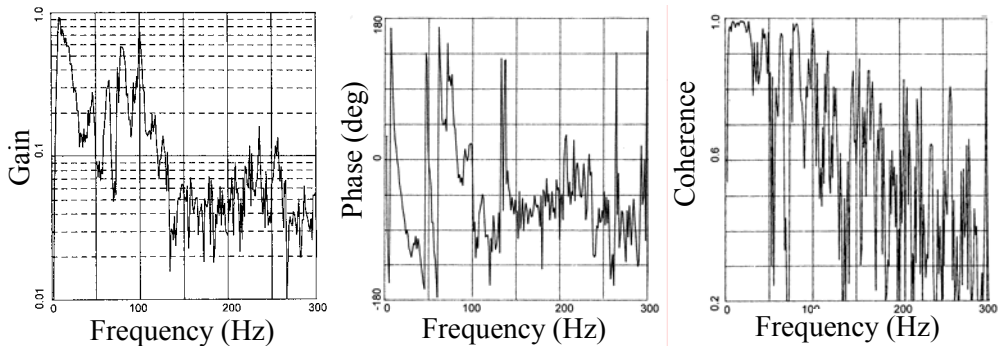

Figure 4.7. Open-loop frequency response data acquired in offline testing.

Because changes in operating conditions can affect the time delays of the various processes that affect the system response to active control, the offline determination of control parameters is practical only for a specific operating condition. The online identification procedure that is described in the following sections provides a method for rapidly determining the proper control parameters should the operating conditions change. The theory developed in the following sections will also be used by the adaptive controller that is described in Chapter 5.

4.3 Online Identification Concept

This section qualitatively discusses the investigated control approach. To provide the developed ACS with adaptive control capabilities, it was necessary to develop an approach that would allow the ACS to identify the optimum phase of the control signal during an online active control session, i.e., "online identification." In an adaptive ACS, control phase and gain are initially assumed and then adjusted based on the system's response to the control action. The identification scheme described herein determines the initial control phase by systematically changing the phase of the control signal and using the observer to determine the real-time response of the unstable oscillations to the continuously varying control signal. The measured response data is then analyzed to determine the optimum initial control parameters.

Figure 4.8 provides an overview of the online identification process. First, the observer identifies the frequency of the most unstable mode. When the identification process is initiated, a small control signal is sent to the actuator with the frequency of the most unstable mode and an arbitrary phase. Because the phase is arbitrary, the resulting fuel flow rate modulations by the ACS may increase or decrease the amplitude of the instability (or have no effect) when control is applied, depending on whether the generated combustion process heat addition oscillations are in or out of phase with respect to the combustor pressure oscillations. Next, the amplitude of the control signal is fixed, and the phase of the control signal is progressively changed by 360 degrees from its initial value, while the observer measures the amplitude response of the combustor pressure oscillations. The measured combustor response is then correlated with the control signal parameters to determine the optimum phase. Once determined, this optimum control phase is applied by the ACS to damp the instability.

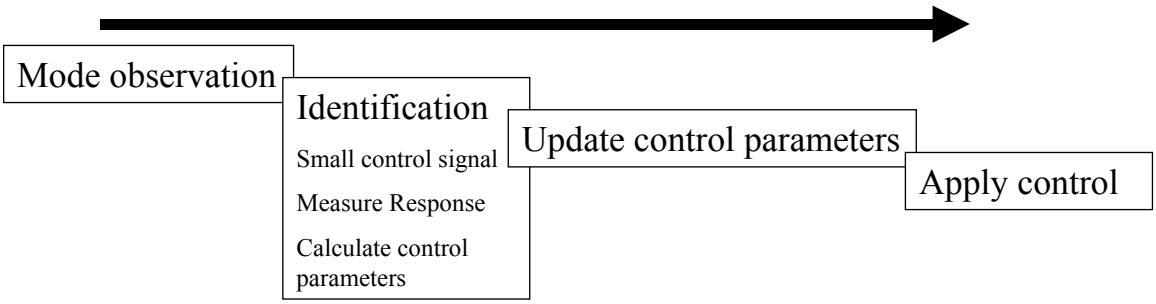

Figure 4.8. Open-loop frequency response data acquired in offline testing.

Figure 4.9 shows the variation in the amplitude of simulated combustor pressure oscillations in response to slowly varying the control signal phase over a 0-360 degree range. As the phase of the control signal changes, the amplitude of the combustor limit cycle oscillations continuously increases and decreases in response to the control signal phase variations. In this case, the control is most effective, i.e., the pressure oscillations are minimized, when the control phase is equal to 180 degrees. By correlating the amplitude of the limit cycle oscillations with this phase it should be possible to effectively determine the optimum control signal phase; i.e., the one that produces minimum limit cycle amplitudes. It is expected, however, that if the identification sweep frequency is increased, time delays inherent in the system will induce a phase lag as well as a decrease in the amplitude of the response. Figure 4.10 illustrates this concept. Note that the amplitude of the modulations decreases significantly for the faster phase sweep. Note also that the phase where the amplitude is minimized appears to occur at approximately 270 degrees, even though the actual "optimum" control phase is approximately 180 degrees, see Fig. 4.9. This phase lag occurs due to the acoustic response of the unstable system, i.e., it depends on whether the system has second-order response, third-order response, and so on.

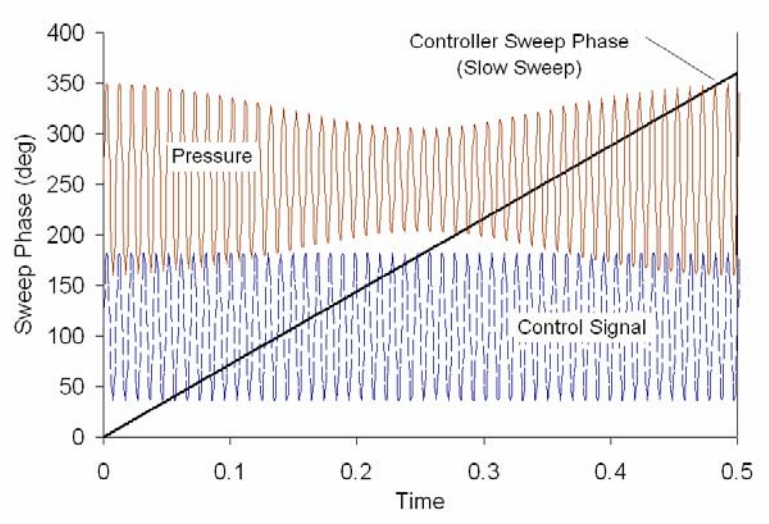

Figure 4.9. Slow identification phase sweep.

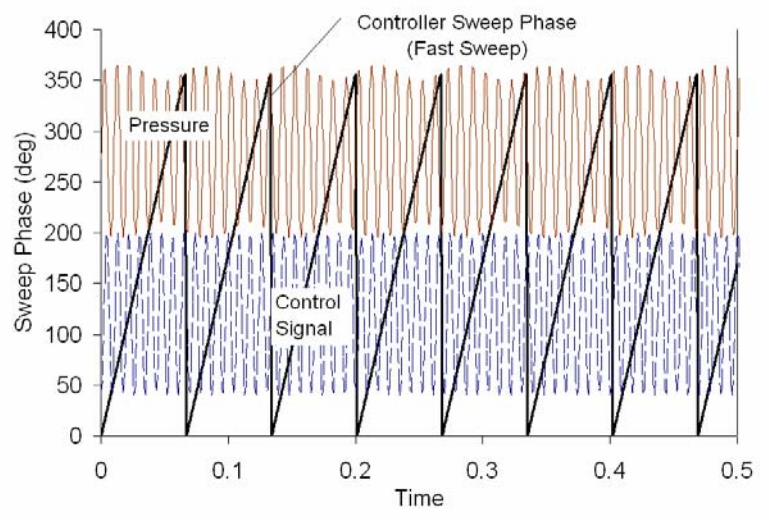

Figure 4.10. Fast identification phase sweep.

4.4 Online Identification Algorithm and Simulation

In this section, the investigated online identification algorithm will be discussed by describing its predicted performance when it is applied to a van der Pol oscillator, which was chosen for this study because its behavior is described by a nonlinear, second order, ordinary differential equation that is similar to the equations describing combustion instabilities.

4.4.1 The van der Pol Oscillator

The van der Pol oscillator model produces limit cycle oscillations that are similar to limit cycle oscillations in an unstable combustor, see Fig. 4.11. In general, the van der Pol oscillator itself may not accurately model the physics of a particular unstable combustion system, but it does provide the capability to model the effects of an ACS on a system similar to a combustor, which has a nonlinear feedback mechanism that results in limit cycle oscillations.

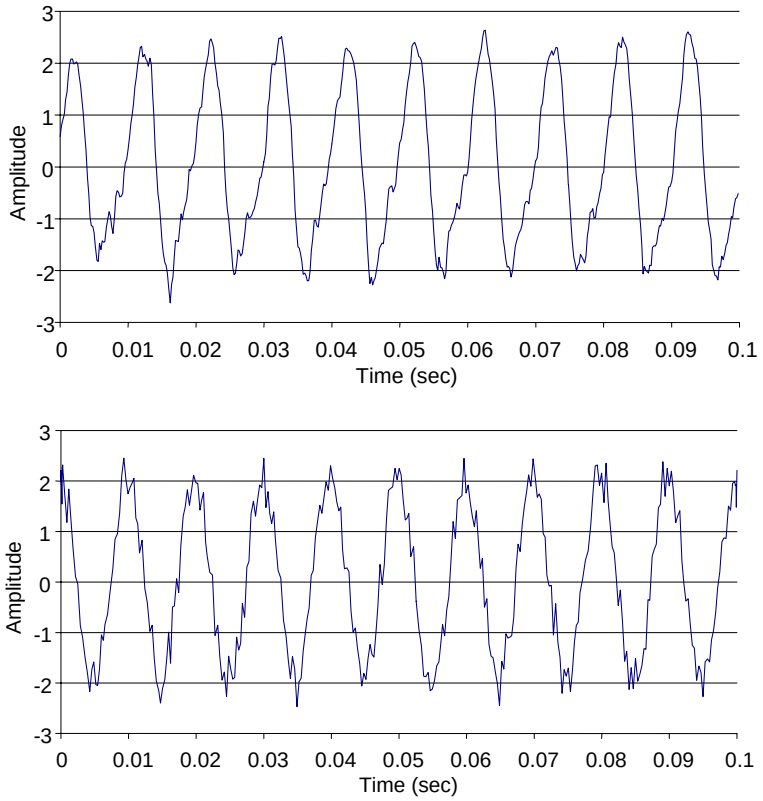

Figure 4.11. Limit cycle oscillations in a) an unstable combustor, b) a van der Pol oscillator simulation.

It will be shown that the results from the van der Pol model agree reasonably well with data obtained in the DLN combustor simulator and the acoustic feedback simulator, both of which can be modeled by a second order nonlinear system. The van der Pol equation is given by:

$$\frac{d^2 p}{dt^2} - \varepsilon(1 - p^2)\frac{dp}{dt} + \omega^2 p = 0 \tag{4.2}$$

where ω corresponds to the natural unstable frequency (i.e., the frequency of the limit cycle oscillations) in rad/sec and ε corresponds to the damping in the oscillator. The second term in the van der Pol oscillator is critical to understanding the limit cycle behavior of such an oscillator. For $|p|<1$, the quantity $(1-p^2)$ is positive, driving the signal

toward a higher amplitude while the growth rate of the signal is controlled by ε. For |p|>1, the quantity $(1-p^2)$ is negative, and the second term in Eq. 4.2 damps oscillations toward a lower amplitude. As the driving and damping forces are balanced, the oscillator settles into limit cycles oscillations. For limit cycle conditions, the oscillator pressure is approximately given by:

$$p = P_0 \cos(2\pi f t) \tag{4.3}$$

During an active control session, the observer determines the amplitude, P_0, and frequency, f, of the dominant mode of the limit cycle pressure oscillations. Once these parameters are known, the control signal, U, is expressed in the following form:

$$U = K_c P_0 \cos(2\pi f t + \phi_c) \tag{4.4}$$

where ϕ_c and K_c are the control phase and gain, which are applied in order to damp the pressure oscillations. To provide the best damping of the pressure oscillations, the optimum control phase is chosen, i.e., $\phi_c = \phi_{optimum}$.

4.4.2 Modeling the Online Identification Process

The developed online identification scheme first detects and characterizes the unstable combustor mode, and then identifies the optimum control phase without *a priori* knowledge of the combustor response. Using the developed ACS, the system is forced with a sinusoidal signal characterized by a constant amplitude $K_{ident,}$ the unstable frequency of the system f, and an arbitrary phase ϕ_i. Applying this forcing function to the van der Pol equation yields:

$$\frac{d^2 p}{dt^2} - \varepsilon(1 - p^2)\frac{dp}{dt} + \omega^2 p = K_{ident} \sin(\omega t + \phi_{ident}) \tag{4.5}$$

The term on the right hand side of the equation represents the forcing of the unstable system with identification amplitude K_{ident} and identification phase ϕ_{ident}. The system response to this forcing depends on both identification parameters. If the identification phase is equal to the optimum control phase, i.e., $\phi_i = \phi_{optimum}$, the instability will be damped. On the other hand, if ϕ_i is out of phase with respect to the optimum control phase, i.e., $\phi_i = \phi_{optimum} + 180$deg, the instability amplitude will be increased. As the identification phase is varied between damping and driving conditions, the effect of forcing is reduced, becoming zero at $\phi_i = \phi_{optimum} \pm 90$ degrees.

If the identification phase is varied slowly, the forcing causes the amplitude of the limit cycle oscillations of the unstable system to vary periodically, attaining minimum and maximum values when $\phi_i = \phi_{optimum}$ and $\phi_i = \phi_{optimum} + 180$ degrees, respectively. Figure 4.12 illustrates the response of the oscillator's pressure during an identification phase sweep. The top plot shows the online identification control phase sweep, along with a dotted line indicating the optimum control phase equal to 180 degrees. When the identification sweep passes the optimum control phase, the oscillator's pressure amplitude is minimized.

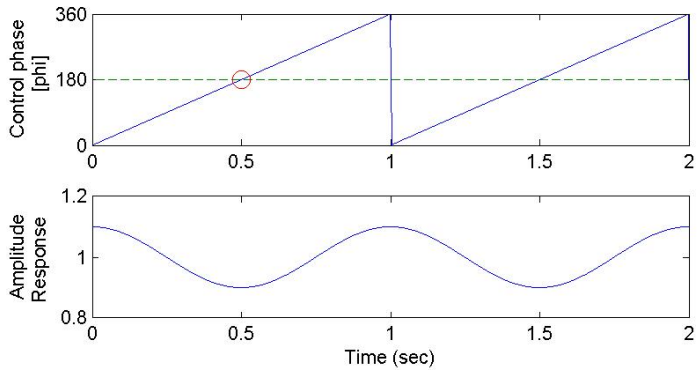

Figure 4.12: Demonstration of the online identification process. In this case, the optimum control phase is 180 degrees, where the amplitude response curve has a minimum.

Recognizing the relationship between the control phase input and the amplitude response of the unstable system, what is needed is a method to calculate the optimum control phase based upon the amplitude response of the combustor to the control system forcing during the identification sweep. To do this calculation, the orthogonal sine and cosine functions are utilized. Figure 4.13 shows the sine and cosine of the control phase during the online identification sweep. By correlating the amplitude response to the sine and cosine functions, the phase at which the minimum amplitude occurs can be calculated. This correlation is derived below.

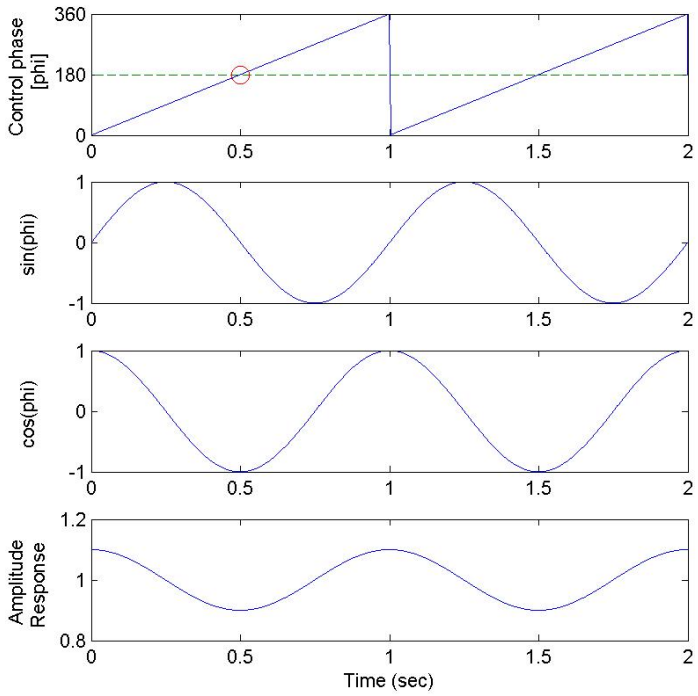

Figure 4.13: Sine and cosine of the control phase

To determine the optimum control phase $\phi_{optimum}$, the phase difference between the amplitude response of the limit cycle oscillations and the sine and cosine functions of

the sweeping phase is calculated. The optimum control phase, $\phi_i = \phi_{optimum}$ is calculated as follows:

$$\sigma_{ident} = \frac{1}{T_{ident}} \int_0^{T_{ident}} (|A(t)| - \overline{A}) \sin(2\pi f_{ident} t) dt \tag{4.6}$$

$$\chi_{ident} = \frac{1}{T_{ident}} \int_0^{T_{ident}} (|A(t)| - \overline{A}) \cos(2\pi f_{ident} t) dt \tag{4.7}$$

$$\phi_{optimum} = \arctan 2(-\sigma, -\chi) \tag{4.8}$$

where f_{ident} is the frequency of the identification sweep, T_{ident} is the duration of the identification sweep, |A(t)| is the pressure amplitude determined by the observer, and $\overline{\mathbf{A}}$ is the mean pressure amplitude when the controller is not active. Equations 4.6 and 4.7 are used to calculate the sine (σ_{ident}) and cosine (χ_{ident}) correlation functions. In this case, the amplitude response is orthogonal to the sine function, so $\sigma_{ident} = 0$ and $\chi_{ident} = 1.0$. Using Eq. 4.8 , the optimum control phase is calculated using the quadrant-specific arctangent function. In this example, $\phi_{optimum}$ = arctan2(0,-1) = 180 degrees. Once the optimum control phase is determined, the phase correction is made, and the amplitude of the pressure oscillations is quickly minimized.

For very slow sweep rates, the above equations hold. However, as the sweep rate is increased, the time delays associated with the unstable system will cause a phase lag in the calculated control phase. Figure 4.10 illustrates this phase lag effect as the frequency is increased. Figure 4.14 shows how this phase lag affects the correlation of the amplitude response control signal input. In the middle plot, the amplitude response is instantaneous (phase lag = 0), and the amplitude response is minimized at the optimum control phase (180 degrees). However, in the bottom plot, the amplitude response is delayed by a phase lag, so the amplitude appears to be minimized when the control phase is zero, thus introducing an error of 180 degrees into the calculation. In other words,

using Eq. 4.8 to calculate the optimum control phase introduces an error in the phase calculation if no account is taken for the phase lag.

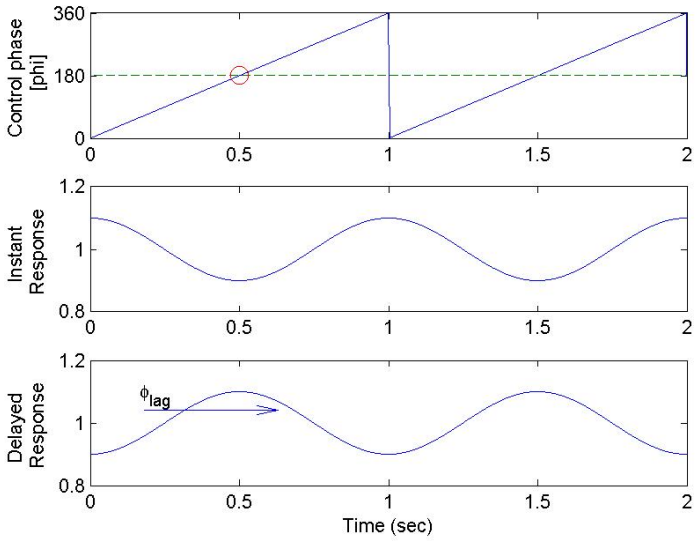

Figure 4.14. Demonstration of online identification process with 180 degree phase lag.

The dependence of this phase lag upon the sweep frequency and the damping coefficient ε has been investigated using the second order van der Pol oscillator, and the results show that this phase lag tends toward –180 degrees as the sweep rate is increased, see Fig. 4.15. For lightly damped systems, this asymptotic approach to –180 degrees is very rapid as the sweep frequency is increased. However, as the system damping is increased, this phase lag parameter changes much more slowly.

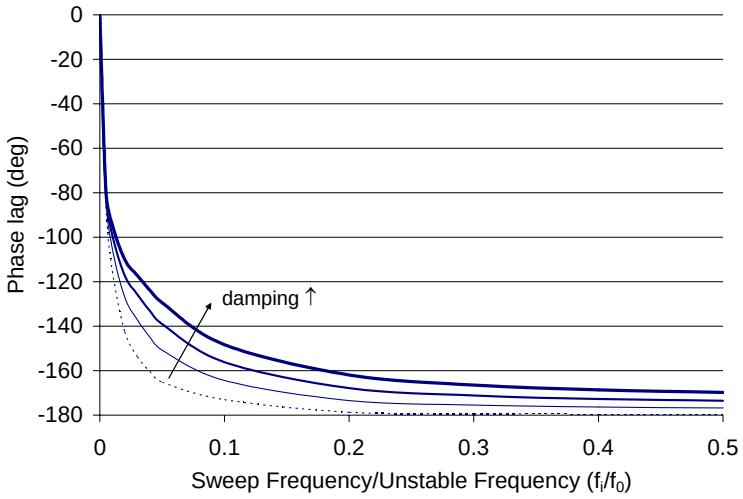

Figure 4.15. Identification phase dependence on sweep frequency.

To compensate for this phase lag, a phase correction factor, ϕ_{corr}, is added to the phase given in Eq. (4.8) to yield the following phase expression:

$$\phi_{optimum} = \arctan 2(-\sigma,-\chi) + \phi_{corr}(f_{ident}) \tag{4.9}$$

A comparison of experimentally determined phase lags to the van der Pol model results is discussed in the next section. For now, it has been assumed that the phase correction applicable to van der Pol oscillations qualitatively describes the phase correction in unstable combustors, and can be obtained at each sweep frequency f_{ident} from Fig.4.15, i.e.,

$$\phi_{corr}(f_{ident}) = -\phi_{lag} \tag{4.10}$$

where ϕ_{lag} describes the phase lag observed in Fig. 4.15 at the identification sweep frequency f_{ident}.

Because the phase correction rapidly varies with frequency as $f_{ident} \rightarrow 0$ and because a rapid identification scheme is desired, it is recommended that the sweep frequency be high enough to set the correction factor approximately equal to 180 degrees.

This approximation holds for lightly damped systems when the sweep rate is "large", i.e., $f/f_0 > 0.1$. However, as the damping increases, the validity of this approximation deteriorates as the asymptotic approach of the phase lag toward –180deg is much slower.

4.4.3 Measuring confidence in the identification result

The disadvantage of increasing the sweep frequency is that the amplitude of the system response to the constant amplitude forcing decreases. As the system response decreases, the signal-to-noise ratio also decreases, thus decreasing the confidence in the calculated control phase. If the confidence in the control phase is too low, the identification parameters (K_{ident}, f_{ident}) need to be changed to increase the magnitude of the system response and, thus, yield the proper control phase (after another identification sweep). If the algorithm is unable to converge to a control phase with a suitable confidence level, the combustor may not be controllable using this scheme. Thus, a calculation of the confidence level is required. For this purpose, Pearson's product moment correlation coefficient [60] was used. This correlation factor, also called a linear correlation, is given by:

$$r = \frac{\sum_j (x_j - \bar{x})(y_j - \bar{y})}{\sqrt{\sum_j (x_j - \bar{x})^2}\sqrt{\sum_j (y_j - \bar{y})^2}}, \; j : 1 \rightarrow j_{\max} \tag{4.11}$$

In this application, the input function x_j is the cosine of the phase of the identification input signal, i.e.,

$$x_j = \cos(2\pi f_i \frac{j}{j_{\max}}), \; j : 1 \rightarrow j_{\max} \tag{4.12}$$

and the response function y_j is the slowly varying amplitude of the combustor oscillations in response to the slowly varying identification input signal; i.e.,

$$y_j = \cos(2\pi f_i \frac{j}{j_{\max}} - \phi),\ j:1 \rightarrow j_{\max} \tag{4.13}$$

In the above equations, j is the index of the instantaneous identification measurement, and j_{max} is the total number of measurements, which equals the product of the number of sweep cycles and the number of measurements per cycle. For two perfectly correlated signals, i.e., two sinusoids that are in phase, this correlation factor is equal to 1.0. However, if there is a phase offset between the two sinusoids, then this correlation varies between 1.0 and –1.0, depending upon the phase difference between the input and response signals. For the example shown in Fig. 4.16, the correlation factor equals -1.0 because the two signals are out of phase.

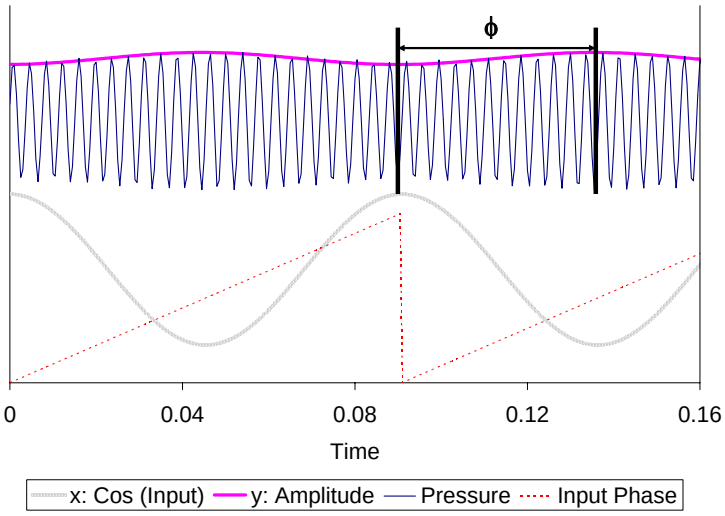

Figure 4.16. Determination of correlation factor.

During online identification, this phase difference depends upon the sweep frequency f_{ident}, and equals zero at low f_{ident} and 180 degrees at high f_{ident}. Because this phase difference depends upon the identification sweep frequency f_{ident} and not the physics of the process controlling the unstable oscillations, its effect upon the correlation coefficient evaluated in Eq. (4.11) should be eliminated. This is accomplished by

subtracting this phase, see Eq. (4.10), from the phase of the input signal, see Eq. (4.12), thus yielding the following expression for the input signal for Eq. (4.11):

$$x_j = \cos(2\pi f_i \frac{j}{j_{\max}} - \phi_{corr}),\ j:1 \to j_{\max} \tag{4.14}$$

With the addition of this phase correction, the correlation coefficient now takes on values between 0.0 and 1.0 regardless of the phase difference between the input and response curves. When "good" correlation exists between the input signal in Eq. (4.14) and output signal in Eq. (4.13), the correlation coefficient calculated by Eq. (4.11) should be close to one. If the correlation coefficient is close to zero, the combustor pressure response to the identification process is negligible. This may occur if, for example, the combustor pressure signal is dominated by random noise or if the identification forcing is too small for the combustor to respond. A small correlation coefficient may also indicate a problem with the control system, e.g., a damaged actuator that is no longer capable of supplying the necessary control amplitude to the system.

To increase the confidence level in the identified control parameters, a second correlation coefficient is also calculated for the identification process. This "mean square" correlation is given by the following expression:

$$R = \frac{\sqrt{\sigma_{ident}^{\ 2} + \chi_{ident}^{\ 2}}}{C} \tag{4.15}$$

where σ_{ident} and χ_{ident} are the sine and cosine correlation functions given in Eqs. (4.6) and (4.7) and C is the variation in the limit cycle amplitude during an identification cycle, given by:

$$C = \frac{A_{\max} - A_{\min}}{2T_{ident}} \tag{4.16}$$

where A_{max} and A_{min} are the maximum and minimum amplitudes A(t) of the combustor oscillations during the period of the integration (T_{ident}) used to calculate σ_{ident} and χ_{ident}, see Eqs. (4.6)-(4.8). As with the Pearson's product moment correlation, the mean square

correlation varies between zero and one, with large correlation values indicating a reasonable confidence in the phase calculation and small correlation values indicating little confidence that the calculated control phase is accurate. If the correlation coefficient is small, it indicates that there may be a problem with the control system or that larger identification amplitude is required to determine an accurate value for the optimum control phase.

4.4.4 Filtering to improve accuracy

In order to improve the accuracy of the online identification process, especially at high rates of identification, calculations for multiple identification sweeps are averaged together. In order to accomplish this averaging, a low-pass filter is applied to the sine and cosine components of the phase calculation (see eqs. 4.6 and 4.7). With the filter applied, equations 4.6 and 4.7 become

$$\sigma_{filtered} = \sigma_{filtered} + \eta(\sigma - \sigma_{filtered}) \tag{4.17}$$

$$\chi_{filtered} = \chi_{filtered} + \eta(\chi - \chi_{filtered}) \tag{4.18}$$

where η is the filter constant, whose range is typically 0.3-0.5. Higher values of η result in negligible filtering, and lower values of η result in very slow response. A low pass filter is used in lieu of a linear average because it is found that subsequent identification sweeps usually provided more accurate results than the initial identification sweeps. The low-pass filter thus gives more weight to recent data than does a linear average. The phase shift is then given as

$$\phi_{optimum,filtered} = \arctan 2(-\sigma_{filtered}, -\chi_{filtered}) + \phi_{corr}(f_i) \tag{4.19}$$

4.5 Experiments

This section describes experiments that are performed to investigate the performance of the online identification algorithm. The experimental setups for all of the

experiments are described in Chapter 2. Experimental setups used in this study are the acoustic feedback setup (Section 2.1) and the DLN combustor simulator setup (Section 2.2). The first set of experiments was designed to understand the effects of changing the online identification sweep frequency and amplitude for determining the proper control phase. The second set of experiments simulated a realistic scenario in which the online identification algorithm was used to determine the proper control phase, and then active control is applied to damp the pressure oscillations.

4.5.1 Phase lag and correlation coefficient determination

For the first set of experiments, the acoustic feedback facility was used. Limit cycle pressure oscillations were driven in the facility by appropriate tuning of the filter/phase shifter combination and by increasing the feedback gain. Twenty identification cycles were performed for each identification sweep frequency. After each set of twenty identification sweeps, the phase lag and the two correlation coefficients were calculated. Also, the amplitude of the pressure response was measured to determine the relation between the amplitude response and the correlation coefficient. This process was performed once for all sweep frequencies, and then repeated. The sweep frequency was varied between a minimum value of 0.1Hz and a maximum value of 70Hz, which is slightly less than 30 percent of the unstable natural frequency of 247Hz.

Data measured in the acoustic feedback setup suggests that the van der Pol oscillator adequately describes the oscillations in this setup. Figure 4.17 compares the phase lag measured in this setup at different sweep rates with those predicted for the van der Pol oscillator, see Figure 4.15. It shows that the differences between the measured and predicted phase decreases as the sweep frequency increases. This is a welcome result as it indicates that the phase correction predicted by the van der Pol oscillator could be applied to the measured data at the high sweep frequencies at which the identification process will be performed to reduce the identification time. In the data from the two

experiments shown, the damping is increased from experiment 1 to experiment 2 by lowering the feedback gain on the acoustic setup.

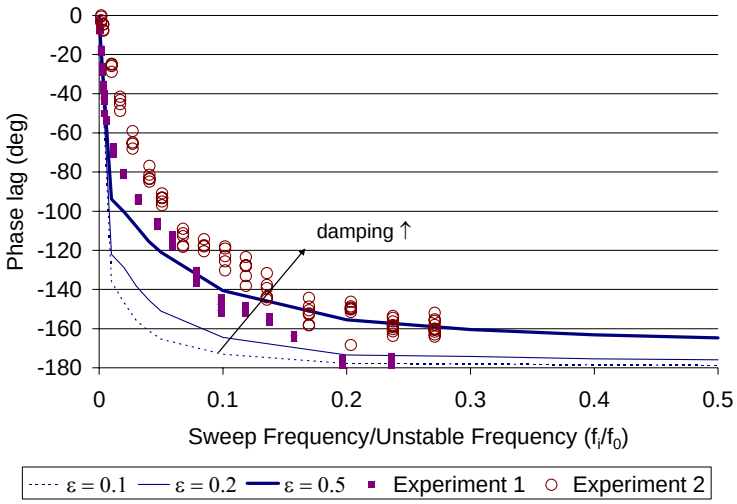

Figure 4.17. Comparison of the frequency dependence of the phase lags measured in the acoustic setup and predicted for the van der Pol oscillator.

Once the control phase is identified, the controller must be able to determine the confidence in the identified phase. Figure 4.18 shows the dependence of the two confidence coefficients on sweep frequency for fixed identification amplitude. As expected, for slow identification sweep frequencies there is a high level of confidence, as indicated by both coefficients. Also shown in Figure 4.18 is the dependence of the amplitude of the system response, measured as percentage of the mean limit cycle amplitude, on varying sweep rate. For high sweep frequencies, the amplitude response is approximately 1.0 percent of the mean pressure amplitude in the unstable system. Figure 4.19 gives an illustration of how the correlation coefficients are related to the amplitude of the system response. As expected, for higher system response amplitude, these two measures of confidence exhibit the same trends. Both of these correlation coefficients can be used to determine whether the identified phase should be trusted or the identification process should be run again. The nominal cutoff value for the confidence level is

approximately 0.6. If the correlation coefficient is higher than this value, the identified optimum control phase is considered valid.

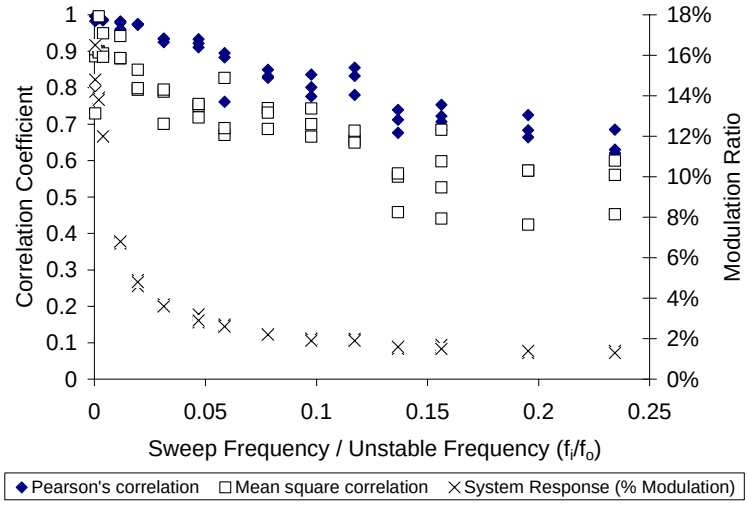

Figure 4.18. Dependence of confidence correlation on sweep frequency.

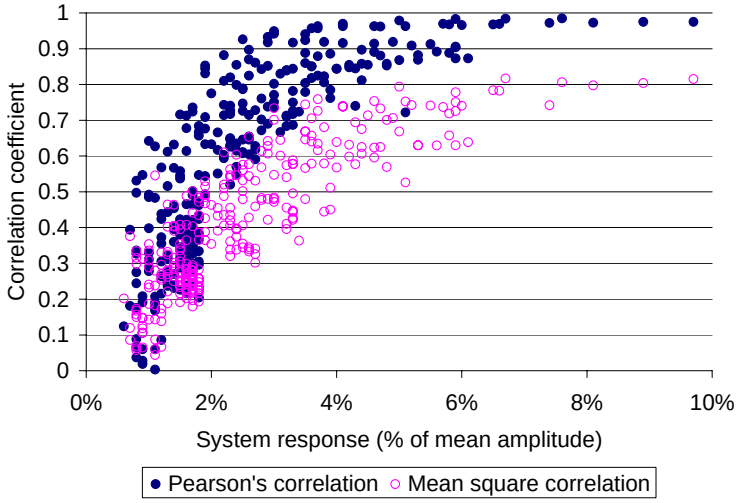

Figure 4.19. Experimental comparison of correlation coefficients obtained by the two correlation approaches as a function of the amplitude of the combustor response.

4.5.2 Demonstration of Online Identification Algorithm

The second set of experiments was designed to investigate the performance of the online identification algorithm. Experiments were performed on both the acoustic feedback setup and the DLN combustor simulator. Typical test data measured in both test facilities when the controller was switched off are shown below. After some time, the online identification process was manually initiated. During this process, the sweep-to-sweep fluctuations in pressure amplitude are observed. After several cycles, the controller determined the optimum control phase. The identification process was completed, and the controller began damping the pressure oscillations with the newly determined control phase.

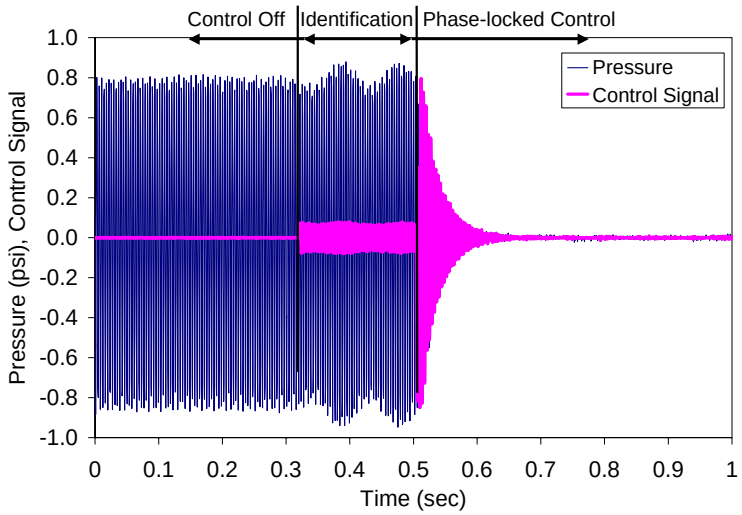

Figure 4.20: Time trace of unstable pressure oscillations in the acoustic feedback simulator, followed by an identification sequence and then active control with the identified optimum control phase.

Figure 4.20 shows active control of the acoustic positive feedback instability in the setup described in Section 2.1 after the system identification has been completed. Because the noise level in this system was low, the online identification algorithm was

able to rapidly determine the proper control phase, using only two iterations of the identification sweep. Also, since it was relatively easy to control the acoustic feedback system (once the proper control phase is identified), the instability was completely damped 0.1 seconds after completing the system identification.

A closer inspection of the identification process during the same experiment in Fig. 4.21 shows how the control signal is shifted with respect to the pressure oscillation during the identification phase sweep. During the identification sweep process, the phase between the control signal and the unstable pressure oscillations is continually varied. At t = 0.38 sec, the two signals are nearly out-of-phase, and the amplitude of the pressure oscillations is maximized. At t = 0.43 sec, the signals are nearly in-phase, and the amplitude of the oscillations is minimized. At t = 0.48 sec, the signals are nearly out-of-phase again, and the amplitude is again maximized.

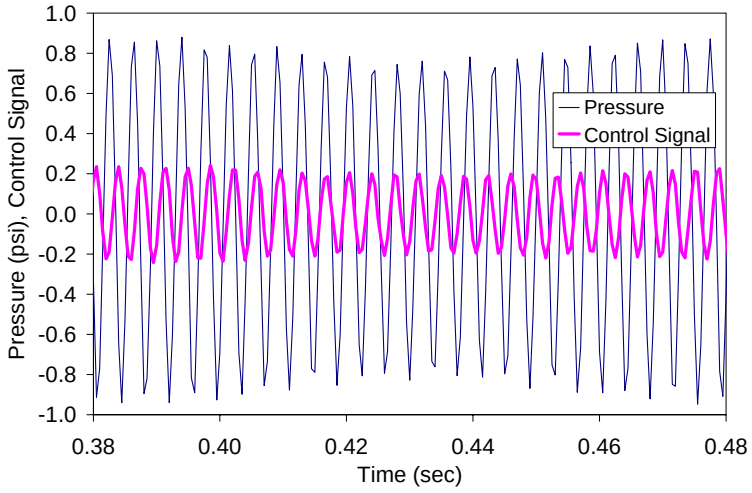

Figure 4.21: Time trace of unstable pressure oscillations and the identification sweep signal during the online identification process. As time progresses, the control signal's phase is changing with respect to the acoustic pressure trace.

Performance of the identification algorithm when applied to the DLN combustor simulator is described in Fig. 4.22. Comparison of the identified phase with phases measured in open loop tests shows that the developed identification algorithm correctly

determines the proper phase for control. Comparison of the control system performance in the combustor and acoustic setup shows that the control authority required to stabilize the acoustic simulator is higher than that in the combustor. In other words, it is easier to damp the unstable oscillations in the acoustic feedback facility. Also, the identification time used in the combustor experiment is purposefully made longer than required to better demonstrate the identification scheme. Similar performance is achieved with as few as five identification sweeps, although a minimum of ten identification sweeps is recommended for the noisy combustion environment.

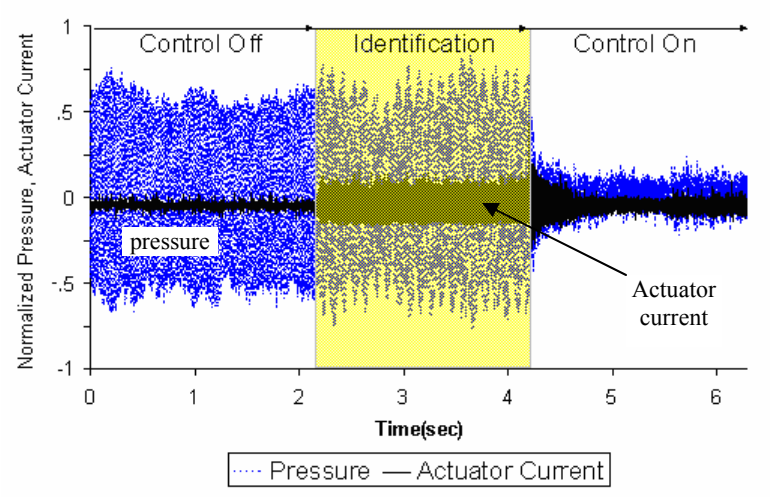

Figure 4.22: Time trace of unstable pressure oscillations in the DLN combustor simulator, followed by an identification sequence and then active control with the identified optimum control phase.

4.6 Summary

This chapter describes an online identification algorithm that is capable of rapidly and effectively determining the optimum control phase with a few caveats. First, this identification process will only work when the combustor is already unstable and operating at its limit cycle. During the online identification process, the ACS is not actively controlling with a predetermined optimum control phase. Therefore, the pressure oscillations cannot be significantly attenuated while the process is running.

Second, it is only capable of determining the control phase for the present operating condition. If the operating conditions should change, the identification process would need to be repeated. Third, the identification process does require a small amount of amplification of the limit cycle amplitude, as can be seen in Figs. 4.20-4.22. Finally, this chapter has shown that the online identification algorithm can be used to effectively identify the optimum control phase, *provided that the proper phase lag correction factor has already been identified through modeling or a separate set of experiments*. Requiring a separate set of offline experiments to determine this phase lag parameter means that this algorithm is not suitable for a fully automatic system. However, if a rapid method can be used to determine this phase lag correction, the offline testing procedures could be minimized, and the online identification procedure can rapidly determine the proper control phase for a given operating condition, provided that the above caveats are resolved.

The online identification algorithm described in this chapter serves as a building block in the development of the fully adaptive control algorithm that is described in the next chapter. The guiding principles in the development of the adaptive control algorithm are the same as for the online identification algorithm, but several refinements are added in order to overcome the shortcomings of the online identification algorithm. In principle, the online identification algorithm can be used in order to rapidly identify a change in the optimum control phase due to, e.g., an abrupt change in operating conditions. However, the developed adaptive controller utilizes similar principles and offers similarly fast performance without the shortcomings of the online identification scheme.

CHAPTER 5

ADAPTIVE CONTROLLER

An adaptive control algorithm was developed to rapidly and continually adjust the control parameters to damp pressure oscillations in an unstable combustor. This chapter discusses the adaptive control algorithm development and experimental results demonstrating its performance.

5.1 Introduction

Chapter 4 introduced a method for online identification of the optimum control phase and showed that while this algorithm could effectively determine the optimal phase for damping combustion instabilities, it had several limitations. The two most significant limitations were that: 1) it was a one-time optimization of the control phase rather than a continual adaptation method, and 2) it required a phase lag parameter in order to identify the proper control phase. The continually adapting control algorithm presented in this chapter overcomes both of these limitations while rapidly converging to the optimum control parameters.

The developed adaptive controller was based upon the same principle as the online identification algorithm, i.e., the system response to small perturbations in the control signal yields information about the behavior of the unstable system and the optimum parameters for damping the unstable pressure oscillations. This information is used to adjust the present control parameters and, thus, improve the damping performance

5.2 Adaptive Controller Concept

This new method for adaptive control of combustion instabilities was developed utilizing the correlation analyses derived in Chapter 4. The adaptive controller also utilizes the observer algorithm discussed in previous chapters. The concept is somewhat similar to the online identification process described in Chapter 4. The algorithm details are described below.

The observer rapidly and continually updates the observed frequency and amplitude of the dominant mode(s) of the instability. The controller then generates a sinusoidal control output having the same frequency as the unstable oscillations. Initially, the controller assigns arbitrary phase to the control signal. The oscillations will be damped if the "proper" control phase is chosen; however, a poor choice of control phase will tend to amplify the combustor pressure oscillations, which may have damaging effects on the combustor or other system components. When the adaptive control algorithm is activated, it searches for the phase that provides the maximum damping of the pressure oscillations. As long as the adaptive controller is active, it continues to search for the optimum control phase. It will be shown later that while this continuous adaptation results in slightly lower damping of the pressure oscillations when compared with a fixed-phase controller with optimized control parameters, this performance degradation is compensated by the ability of the ACS to quickly adapt to changes in operating conditions. Furthermore, the adaptive controller saves a significant amount of time and the expense associated with offline testing and calibration of the fixed-phase controller.

The online identification algorithm described in Chapter 4 uses a full 360-degree sweep of the input control phase to determine the optimum control phase (see Fig. 5.1). Several sweeps are normally performed to improve the accuracy of the calculation and a

filtered average is used to determine the new control phase. The controller then changes to the new control phase in a single step, and control is applied.

The adaptive control algorithm improves the above discussed approach by continually incrementing the control phase in small steps. During an adaptation cycle, the instantaneous control phase is equal to the mean control phase plus a modulated component, i.e., $\phi_{c,inst} = \phi_{c,mean} + \phi_{c,mod}$. At the end of an adaptation cycle, a control phase adjustment is calculated by correlating the input and response functions. This control phase adjustment is added to the mean control phase value, and the process is repeated. Unlike the online identification algorithm, the adaptive controller is not attempting to calculate the optimum control phase so that a single phase adjustment can be applied; instead, it is continually determining whether the mean control phase should be increased or decreased to improve the damping performance. During an adaptation step, the controller makes only a small adjustment to improve the control phase, and successive adaptation cycles result in a closer approximation to the optimum control phase (see Fig. 5.2). In this manner, the adaptive controller can continually track the optimum control phase, which may change due to variations in operating conditions. Although the control phase adjustments are small, they are performed in rapid succession so that the overall speed of the adaptive algorithm is high in comparison with the online identification algorithm.

Figures 5.1-5.2 show the difference between the online identification and adaptive controller with cartoons illustrating the concepts. Figure 5.1 shows that the minimum pressure in this illustration occurs at a control phase of 120 degrees. At the end of the online identification cycle, the control phase is set to 120 degrees. During the online identification process, relatively large amplitude fluctuations are created by sweeping the control phase across all possible values. As seen in Fig. 5.2, the adaptive controller continually modulates the control phase and calculates small corrections to the control phase, in the direction that minimizes the pressure amplitude. The adaptive controller

continually searches for a "better" phase by calculating whether a positive or negative phase adjustment is required to reduce the pressure amplitude. In this example, an increase in the control phase is accompanied by a decrease in the pressure amplitude, signifying that the optimum control phase is at a value higher than the current mean phase value. At the end of each adaptation cycle, the mean phase value is incremented toward the optimum control phase, thus reducing the mean amplitude level after each adaptation step until the optimum control phase is achieved. The next section provides the algorithm details.

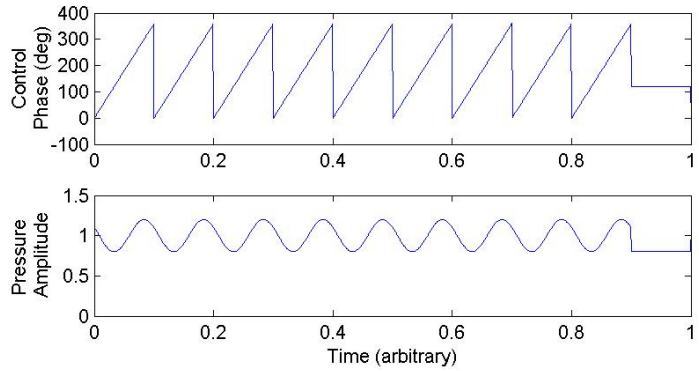

Figure 5.1. Illustration of the online identification technique

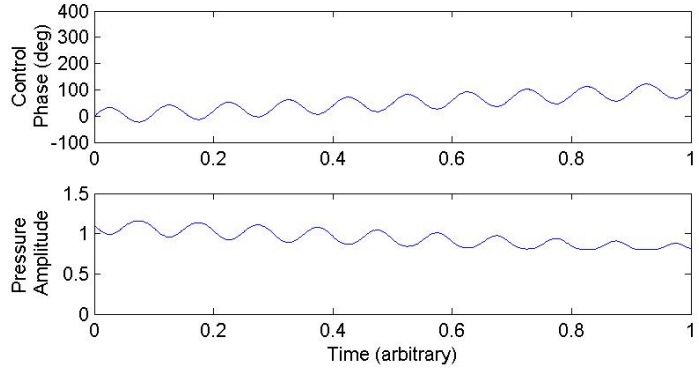

Figure 5.2. Illustration of the continuous adaptive control technique

5.3 Adaptive Controller Algorithm

5.3.1 Adaptive Controller Development

In this section, the development of the adaptive controller algorithm is discussed. The adaptive controller modulates the control phase (the phase between the pressure oscillations and the control signal) as follows:

$$\begin{aligned} \phi_{c,inst} &= \phi_{c,mean} + \theta \sin(2\pi f_{mod} t_{mod}) \\ &= \phi_{c,mean} + \phi_{c,\mathrm{mod}} \end{aligned} \tag{5.1}$$

where θ is the amplitude of the control phase modulation. $\phi_{c,inst}$ is the instantaneous control phase, and $\phi_{c,mean}$, and $\phi_{c,mod}$ are the mean and modulated parts of the control phase, respectively. From Fig. 5.2, we see that as the control phase approaches the optimum control phase, the calculated amplitude of the pressure oscillations decreases. The following equation approximately describes this response:

$$A_{inst} \sim A_{mean} - K \cos(\phi_{c,inst} - \phi_{optimum}) \tag{5.2}$$

where A_{mean} is the mean amplitude value over all possible phase values, $\phi_{c,inst}$ is the control phase, and $\phi_{optimum}$ is the phase at which the adaptive controller provides the optimum damping of the unstable system. A_{inst} is the instantaneous pressure amplitude. When $\phi_{c,mean} = \phi_{optimum}$, the amplitude of the pressure oscillations is minimized, and when $\phi_{c,mean} - \phi_{optimum} = 180$ degrees, the amplitude of the oscillations is maximized. However, nonlinearities in system response often result in the maximum amplitude condition at a phase where $\phi_{c,mean} - \phi_{optimum} \neq 180$ degrees. Figure 5.3 illustrates the amplitude response for both a linear model and a nonlinear van der Pol model as the mean control phase is swept through the full range of all possible phases. During a sweep of the mean control phase, the instantaneous control phase is modulated about the mean phase value to simulate the response of the unstable system to the adaptive controller forcing. The amplitude response shows a "compression" of the amplitude response where both the

minimum and maximum amplitudes are observed; in this case, the amplitude minima occur at $\phi_{rel,mean} = \phi_c - \phi_{optimum} = 0$ degrees (t = 0, 9, 18 sec). For the linear model, the amplitude maxima occur at $\phi_{rel,mean} = 180$ degrees (t = 4.5, 13.5 sec), while for the nonlinear model these maxima occur at $\phi_{rel,mean} = 120$ degrees (t = 3, 12 sec).

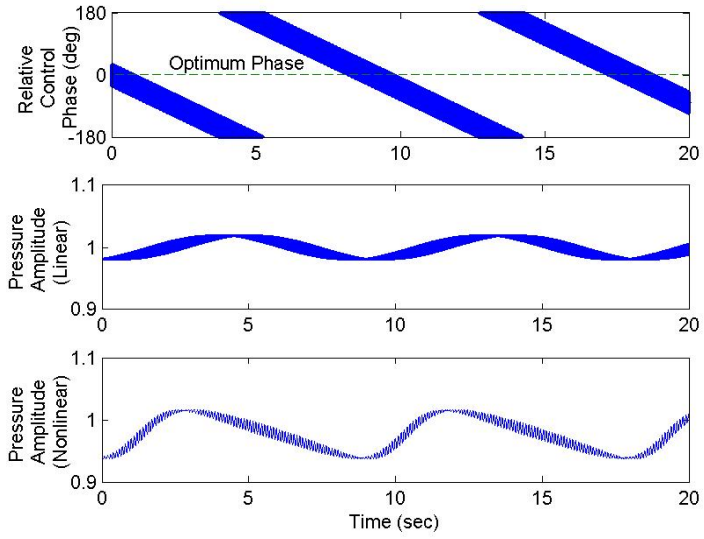

Figure 5.3. (Top) The mean control phase is swept linearly, while the instantaneous phase is modulated about the mean; (Middle) Linear amplitude response to phase modulation while mean phase is swept; (Bottom) Nonlinear amplitude response to phase modulation.

Substituting eq. 5.1 into eq. 5.2 yields the following:

$$\begin{aligned} A_{inst} &\sim A_{mean} - K\cos(\phi_{c,mean} - \phi_{optimum} + \phi_{c,\mathrm{mod}}) \\ &= A_{mean} - K\cos(\phi_{rel,mean} + \phi_{c,\mathrm{mod}}) \end{aligned} \tag{5.3}$$

where the relative mean phase, $\phi_{rel,mean}$ is defined as the difference between the mean control phase and the optimum control phase. Figure 5.3 also shows that the pressure amplitude is minimized when the relative mean phase, $\phi_{rel,mean} = \phi_{c,mean} - \phi_{optimum} = 0$. At this phase, the variation in pressure amplitude is very small (the response band is very narrow), showing that modulating the phase near the optimum phase has little effect. However, as the control phase is moved away from the optimum phase, the "response

band" widens, indicating maximum response to phase modulations when $\phi_{rel,mean} \sim 90$, 270 degrees, … For further illustration of this point, the dependence of the derivative of the amplitude function upon the relative phase, $\phi_{rel,mean}$, is described in Fig. 5.4. When $dA_{inst}/dt = 0$, the combustor pressure oscillation amplitude does not change as the control phase is modulated; when this derivative function is maximized (at $\phi_{rel,mean} = 90$, 270deg), the largest response to control phase modulations is observed.

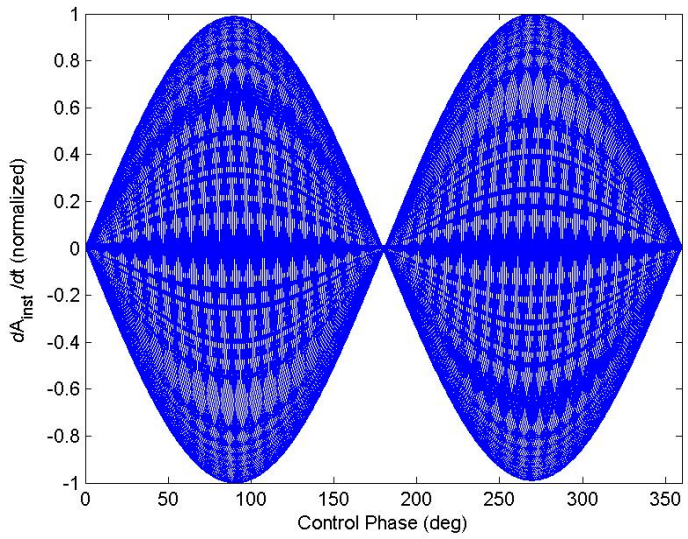

Figure 5.4: First derivative of the amplitude response to phase modulation during a mean phase sweep

Figure 5.4 also shows that there is little response to phase modulations at both the optimum control phase ($\phi_{rel} = 0$) and the phase where the pressure amplitude is maximized ($\phi_{rel} = 180$deg). In Fig. 5.5 these regions are described as regions of "driving" and "damping". The diminished response in these regions where $dA_{inst}/dt \sim 0$ will be discussed later in the chapter.

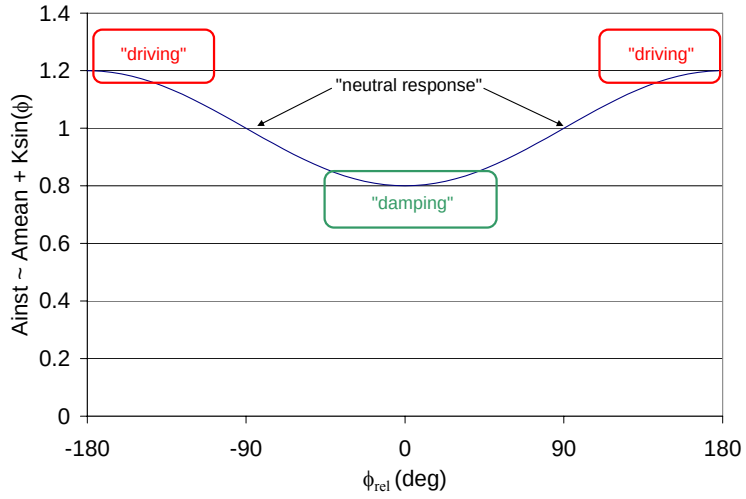

Figure 5.5. Relationship between ϕ_{rel} and the driving, damping, and neutral response regions

For now, the discussion will focus on the regions where the pressure amplitude response to phase modulations is maximized, i.e., $\phi_{rel,mean} = \phi_c - \phi_{optimum} \sim 90, 270\text{deg},\ldots$ In Fig. 5.5, these regions are described as "neutral" response regions. They have been designated as such because applying active control here does not yield an appreciable change in the mean amplitude of the pressure oscillations. However, the neutral response region provides the maximum change in response during an adaptive modulation cycle, as seen in Fig. 5.3. For the linear model in Eq. 5.3, neutral response occurs when $\phi_{rel,mean} \sim 90$ degrees; the amplitude response at this relative mean phase is given by:

$$\begin{aligned} A_{inst} &\sim A_{mean} - K\cos\left(\frac{\pi}{2} + \phi_{c,\mathrm{mod}}\right) \\ &= A_{mean} + K\sin(\phi_{c,\mathrm{mod}}) \\ &= A_{mean} + K\sin(\theta\sin(2\pi f_{\mathrm{mod}} t_{\mathrm{mod}})) \end{aligned} \tag{5.4}$$

Therefore, the modulated part of the amplitude response function in Eq. 5.4 is given by:

$$A_{\text{mod}} = K\sin(\theta\sin(2\pi f_{\text{mod}} t_{\text{mod}})) = K\sin(\phi_{c,\text{mod}}) \tag{5.5}$$

where θ is the angle of adaptation and K is the amplitude of the combustor pressure response function. Equation 5.5 describes the fluctuating part of the combustor pressure amplitude in response to a constant amplitude control signal whose phase is modulated sinusoidally. In the limit as $u \to 0$, $\sin(u) \to u$. Therefore, for small θ, if u is defined as $u = \theta\sin f(2\pi f_{\text{mod}} t_{\text{mod}})$, and Eq. 5.5 reduces to:

$$A_{\text{mod}} \sim K\theta\sin(2\pi f_{\text{mod}} t_{\text{mod}}) \tag{5.6}$$

Figure 5.6 describes the behavior of Eq. 5.5. It shows that the system response to a "small" sinusoidal modulation of the control phase is sinusoidal, with a period equal to $T_{\text{mod}} = 1/f_{\text{mod}}$, as long as $\phi_{\text{rel,mean}} \sim 90$ degrees. The limitations imposed by the "small" θ assumption are discussed in Section 5.3. Figure 5.6 also shows the phase lag, ϕ_{lag}, which was discussed in Chapter 4 and will be treated later in this chapter. For the present discussion, the phase lag is assumed to be zero.

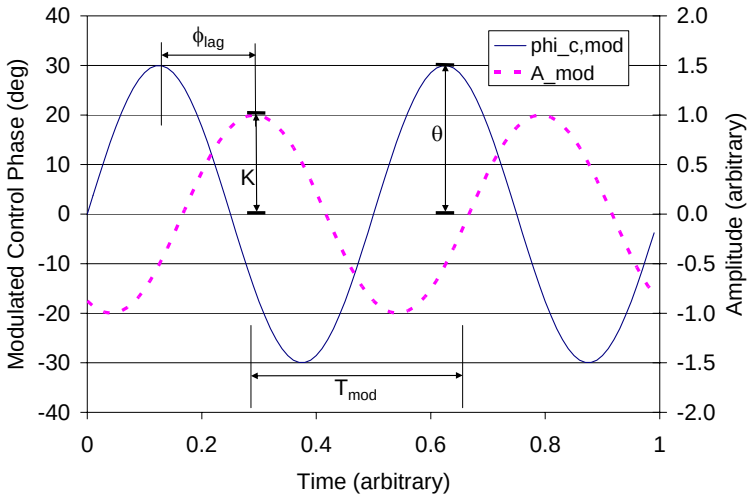

Figure 5.6. Linear response of pressure oscillation amplitude to small sinusoidal control phase modulations. Two adaptation cycles are shown. In this case, no corrective action is taken due to the adaptive learning.

After one adaptation cycle is complete, the system's amplitude response is correlated with the input control phase. The adaptive controller then calculates a phase correction factor from the modulated phase and amplitude in a manner similar to the one used in the online identification algorithm, i.e.,

$$\sigma_{\text{mod}} = \frac{1}{T_{\text{mod}}} \int_0^T (A_{\text{mod}}) \sin(2\pi f_{\text{mod}} t) dt \tag{5.7}$$

$$\chi_{\text{mod}} = \frac{1}{T_{\text{mod}}} \int_0^T (A_{\text{mod}}) \cos(2\pi f_{\text{mod}} t) dt \tag{5.8}$$

$$\phi_{corr} = \arctan 2(-\sigma_{\text{mod}}, -\chi_{\text{mod}}) \tag{5.9}$$

where ϕ_{corr} is the phase correction factor and arctan2 is the quadrant-specific arctangent function. Equation 5.9 shows that when the amplitude response function is in-phase with the adaptive phase modulations (i.e., the relative mean phase is positive), the phase correction factor ϕ_{corr} = -90 degrees. Figure 5.7 shows that this in-phase behavior is observed when the relative phase $\phi_{\text{rel}} > 0$. As long as $\phi_{\text{rel}} > 0$, an increase in the relative phase drives an in-phase increase in the pressure amplitude. In this example, an in-phase response occurs because the phase lag is equal to zero.

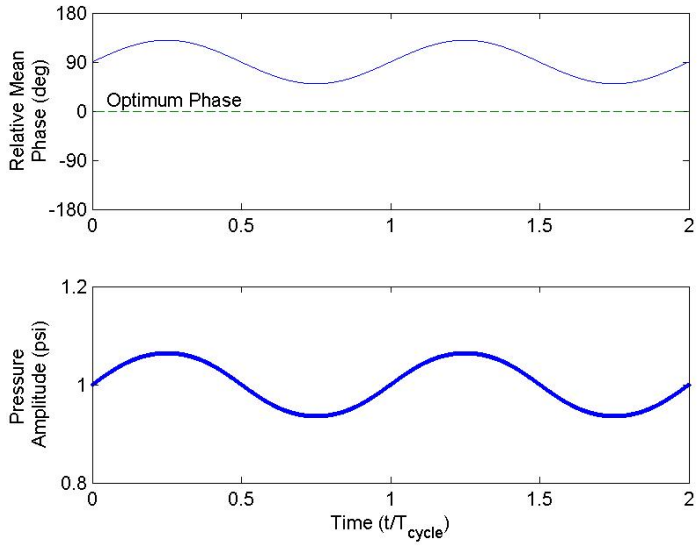

Figure 5.7. In-phase response of pressure amplitude to control phase modulations when $\phi_{rel} > 0$ and $\phi_{lag} = 0$.

Unlike the online identification algorithm, this phase correction factor is not immediately applied to the control phase. Instead, this phase correction factor simply determines whether the mean control phase value should be increased or decreased. This increase or decrease is accomplished by adjusting the control phase by a fixed positive or negative amount, e.g., ±5 degrees, depending upon the sign of ϕ_{corr}. The maximum adaptation step size, $\Delta\phi_{max}$ determines the size of this control step, and the sign of the phase correction factor is applied to $\Delta\phi_{max}$ to determine the direction of adaptation. Adjustments to the size of the control step are discussed later in the chapter.

A key point in understanding the adaptive control algorithm is that the controller does *not* calculate the correct control phase during its adaptation cycle. The equations for the calculation performed by the adaptive controller and the online identification algorithm are identical. However, the domain of the adaptive controller for a single adaptation cycle is limited to the range of phase modulation: $-\theta < \phi_{c,mod} < \theta$, where $\theta < 90$ degrees.. The result of this domain constraint is that the controller can only determine the *direction* of maximum damping, rather than the optimum phase. To illustrate the

response of the system to these control phase modulations, Fig. 5.8 simulates a test sequence in which the mean control phase is swept linearly over all possible control phases, while the instant control phase is modulated about the mean. This kind of test, discussed later in this chapter, was used to evaluate the performance of the adaptive controller. In this example, Fig. 5.8 shows the response of a simulated linear system to such a test. The mean control phase sweep results in changes to the mean pressure amplitude, while the control phase modulation about the mean results in oscillations about the mean amplitude. These oscillations of the pressure response are correlated with the control phase modulations to calculate the calculated phase correction factor, which is shown in the bottom plot of Fig. 5.8. It is seen that the phase correction factor is equal to +90 degrees when the relative phase is less than zero, and –90 when the relative phase is greater than zero.

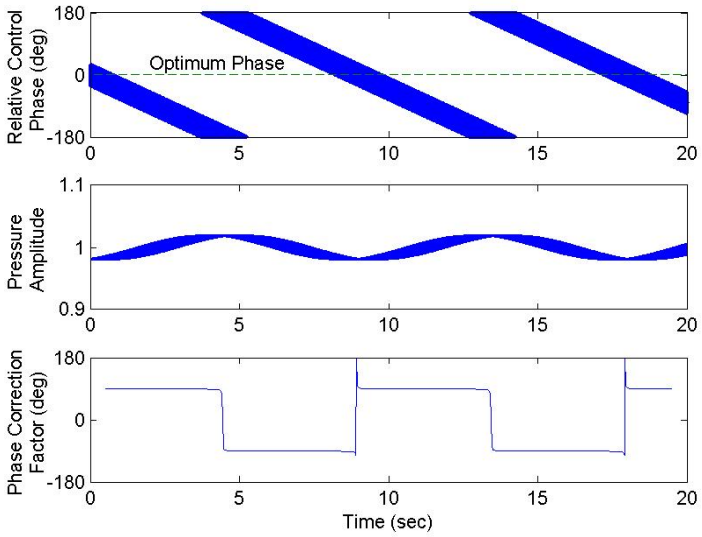

Figure 5.8. Calculated phase correction factor as mean relative control phase is varied

5.3.2 Phase Lag Effect

Chapter 4 showed that a phase lag develops as the sweep frequency increases, to a maximum of –180 degrees for a second order system. This phase lag also occurs during the adaptive modulation algorithm. As a phase lag develops by increasing the modulation frequency, the modulated response is delayed, which results in a change in the phase correction factor, ϕ_{corr}. The effect of this phase lag is to lower the phase correction curve in Fig. 5.8 by the angle of phase lag. As the modulation frequency increases, the phase lag is "lowered" by 180 degrees, which effectively inverts the phase correction curve in Fig. 5.8. Thus, the phase correction calculation from Eq. 4.8 becomes:

$$\phi_{corr} = \arctan 2(\sigma_{\mathrm{mod}}, \chi_{\mathrm{mod}}) \tag{5.10}$$

Figure 5.9 illustrates the phase relation between the input control phase modulations and the amplitude response signal from the acoustic feedback system, where the 180 degree phase lag is observed due to the high modulation frequency. The mean "relative" phase values are given in degrees relative to the optimum control phase: $\phi_{rel,mean} = \phi_{c,mean} - \phi_{optimum.}$ As the mean relative phase moves from +120 degrees to + 30 degrees, the amplitude response function remains out-of-phase with the control phase modulations. As long as the mean relative control phase is positive, this out-of-phase response is observed, and the phase correction factor as calculated by Eq. 5.10 is –90 degrees. When the mean relative phase becomes negative (e.g., -30 degrees or -120 degrees), the amplitude response is in-phase, and the phase correction is calculated to be +90 degrees. The model presented in Fig. 5.8 shows that the phase relation between the input and response functions is constant for a range of mean phase values; this relationship is confirmed by the data shown in Fig. 5.9. As long as the mean relative control phase is positive the two signals are consistently out-of-phase and the controller

requires a negative phase correction; as long as the mean relative control phase is negative, the two signals are consistently in-phase and the controller requires a positive phase correction. This figure also shows that the mean amplitude of the response diminishes as the relative phase approaches zero. This diminished amplitude response will be discussed in more detail later in this chapter.

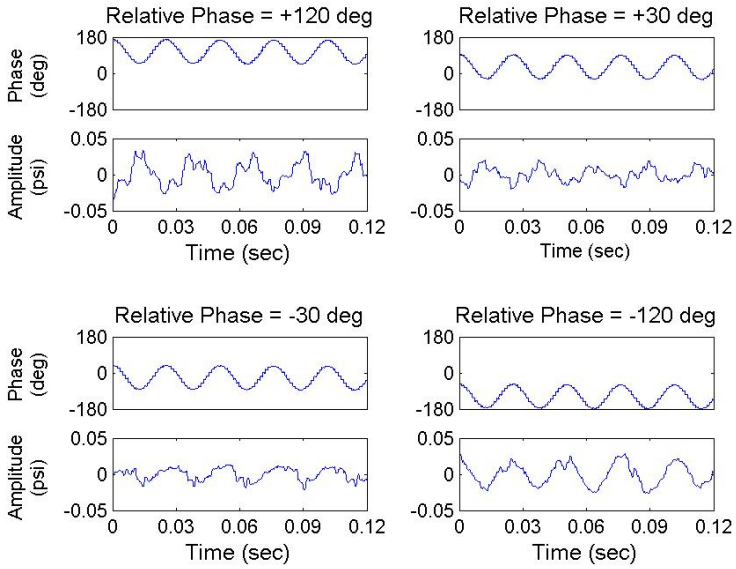

Figure 5.9. Response of pressure oscillation amplitude to sinusoidal phase variation in acoustic facility with varying mean phase angles relative to the optimum control phase

The developed adaptive control approach has several advantages. First, the adaptive control parameters can be tuned to allow greater flexibility in the speed and accuracy of the active controller. Second, since the exact determination of the optimum control phase is not critical, the controller is less susceptible to flow noise or other disturbances that can increase errors in the online identification approach. To overcome this issue with the online identification algorithm, multiple control phase sweeps are performed; the resulting phase correction factor is calculated by a weighted average of the multiple identification sweeps. As an additional measure of confidence, a correlation

coefficient is calculated to determine how well the input and response functions are correlated. However, depending upon the nature of the disturbance and its amplitude, the error in the calculated control phase can be substantial when using the online identification algorithm, which may have a significant impact on the damping effect of the active control if the wrong control phase is calculated. On the other hand, encountering a similar disturbance during an adaptation cycle of the current approach causes a momentary phase correction in the wrong direction. The result of such misdirection is a slight delay in achieving the optimum control phase, which is normally corrected during the subsequent adaptation step. If the step size chosen is small enough, the momentary disruption in the adaptation process will have little effect.

Both of these advantages are improvements over the online identification algorithm; however, the main advantage of the adaptive controller is that it eliminates the need to predetermine the phase lag correction factor. This change addresses one of the major shortcomings of the online identification algorithm. In Chapter 4, it was shown that for second order systems, the phase lag correction factor approaches –180 degrees as the frequency of the phase sweep is increased. However, unknown system damping affects the slope of this curve, making it difficult to precisely determine the phase lag. Thus, this phase lag uncertainty introduces some error into the online identification algorithm. The same phase lag correction factor also applies to the adaptive controller; however, *it is not necessary to precisely identify this parameter in the adaptive control algorithm*. Figure 5.9 demonstrates that the response of the unstable system to control phase modulation is nearly identical over a range of mean phase values. The adaptive controller calculates the phase of this response function, and determines whether to increase or decrease the control phase from this calculation. If the phase lag is *approximately* known, the adaptive controller works as intended.

It was shown in Chapter 4 that for a lightly damped system, the phase lag parameter asymptotically approaches –180 degrees very rapidly as the sweep rate was increased. The same phase lag applies to the adaptive modulation rate: as the modulation rate is increased, the phase lag approaches –180 degrees. For systems with higher damping, it was shown that the asymptotic limit was approached more slowly, so that the phase lag assumption of –180 degrees results in a larger error.

For example, if there is an error of 60 degrees in the lag compensation, the phase signal is shifted by 60 degrees, as shown in Fig. 5.10. The result of this error is that Eq. 5.10 yields a phase correction factor of +150 degrees when the relative mean control phase is negative and –30 degrees when the control phase is positive. However, in the adaptive control procedure, only the sign of the phase correction factor is considered when making the phase adjustment. As long as the phase lag error is less than 90 degrees, the adaptive controller calculates the proper direction for the phase adjustment. If the modulation frequency is very low, it is possible to increase this phase error beyond 90 degrees, which results in the adaptive controller seeking the maximum pressure amplitude, rather than the minimum pressure amplitude. However, this problem can be avoided by using a modulation frequency that is sufficiently high (e.g., $f_{mod} > 0.1*f_0$).

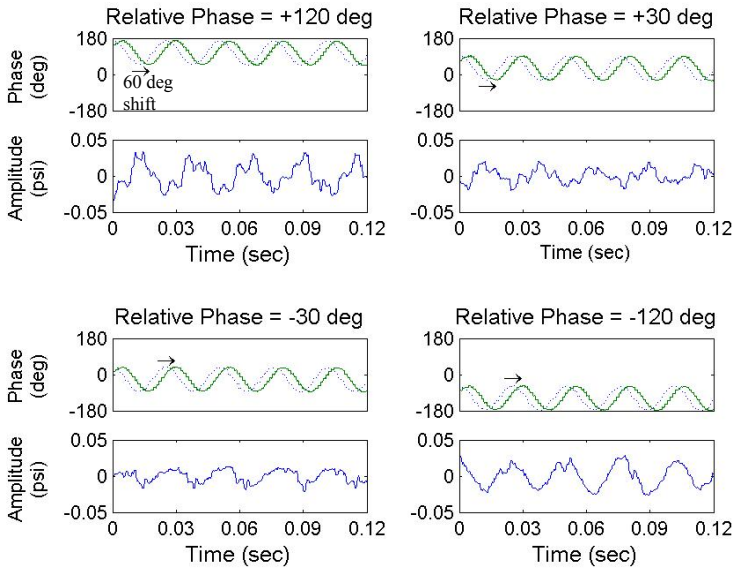

Figure 5.10. Response of pressure oscillation amplitude to sinusoidal phase variation in control phase, with phase lag compensation error of 60 degrees.

5.3.3 Nonlinear van der Pol model of Phase Response

Earlier, the phase response of a simple linear system was shown to yield phase correction factors of +/- 90 degrees as the mean phase was swept across a range of values. To get a better picture of what happens in a nonlinear system with damping, the van der Pol model was employed again. The van der Pol equation used in this analysis has a slightly modified forcing function compared with the equation used in Chapter 4:

$$\frac{d^2p}{dt^2} - \varepsilon(1-p^2)\frac{dp}{dt} + \omega^2 p = K_{adapt}\sin(\omega t + \phi_{c,mean} + \phi_{c,\mathrm{mod}}) \tag{5.11}$$

where K_{adapt} is the amplitude of the control signal, $\phi_{c,mean}$ is the mean control phase, and $\phi_{c,mod}$ is the modulated component of the control phase. Figure 5.11 shows the response of the van der Pol solution to the forcing function in Eq. 5.11. In this case, the mean control phase is varied linearly with time, i.e., $\phi_{c,mean} = 2\pi f_{sweep}t$, and the modulated part of the control phase is given by $\phi_{c,mod} = \theta\sin(2\pi f_{mod}t)$. This sweep of the mean control

phase is done slowly to provide a quasi-steady mean phase for the purposes of evaluating the effects of $\phi_{c,mod}$. The modulating phase amplitude θ is set to 40 degrees, and the modulation rate, f_{mod} is set to 40Hz. The natural frequency for the modeled van der Pol oscillator is 200Hz.

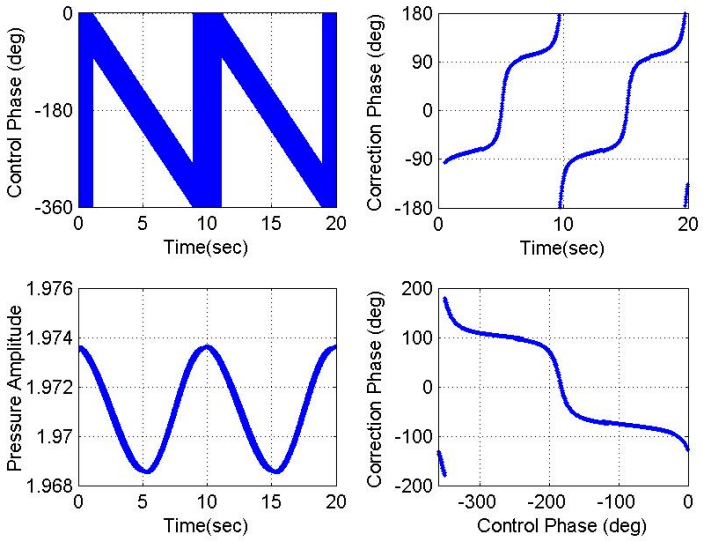

Figure 5.11. Response of van der Pol oscillator to control phase modulations as the mean relative control phase is swept

The plot on the bottom-right shows the phase correction factor as a function of the mean relative control phase. This plot illustrates that the phase correction factor crosses zero at a relative control phase of zero, i.e., where the mean control phase is equal to the optimum control phase. There are three main features to note in Fig. 5.11:

1) The phase correction factor curve is sloped slightly when compared with the linear model presented in Fig. 5.8.
2) The phase correction factor is slightly above the +/-90 degree values predicted by the linear model.
3) The phase correction factor crosses zero at the same time that the pressure amplitude is minimized.

Figure 5.12 shows two important features that vary as the modulation frequency is changed. The first is the average value of the phase correction factor, which depends upon the phase lag. When the modulation frequency is high, the average phase correction factor during a phase sweep approaches +/-90 degrees, depending upon whether $\phi_{rel,mean}$ is greater than or less than zero. For lower modulation frequencies, the phase lag correction of –180 degrees is no longer valid, and a phase lag error occurs, as shown in Fig. 5.10. The effect of this phase lag error is to push the phase correction factor curve upward by an amount equivalent to the phase lag error. For example, if the phase lag error is 60 degrees, the aveyrage phase correction factor is no longer +/-90 degrees but +150 degrees / -30 degrees.

The second feature to notice is the slope of the phase correction factor. As the modulation frequency is increased, the slope of the phase correction factor increases, due to the increased nonlinearity of the amplitude response to control phase modulations. This increase in nonlinear response is due to a reduction in the effective damping of the system response when the modulation frequency is increased.

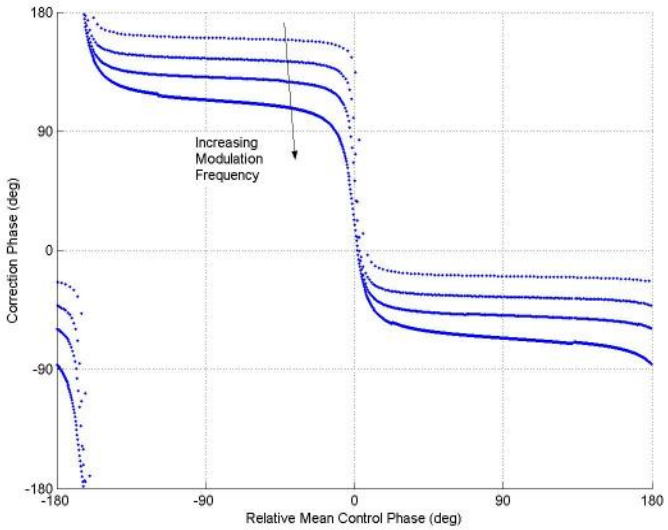

Figure 5.12. Effect of increasing the modulation frequency on the phase correction factor for the van der Pol simulation with high system damping

Another parameter that can change the system response to adaptive phase modulations is its damping. Figure 5.13 shows the effect of increasing the modulation frequency for a system with less damping than the one shown in Fig. 5.12. The first key difference in this plot is that the phase correction factor curve has a greater slope. Also, the plot is "pushed" downward, closer to the +/-90 degree breakpoints. The increased slope is similar to what is observed as the modulation frequency is increased. The key feature to note is the asymmetry of the phase correction function. For a heavily damped system, the phase of maximum driving is approximately equal to +/- 180 degrees from the optimum control phase. However, the nonlinearity of a lightly damped system introduces asymmetry into this function that shifts the phase of maximum driving to occur at a different mean phase value. On the phase correction factor plot, this phase occurs where the correction phase asymptotically approaches +/-180 degrees. In Fig. 5.13, the phase of maximum driving occurs at a relative mean control phase of –90 degrees. In Fig. 5.12, the phase of maximum driving was approximately –160 degrees.

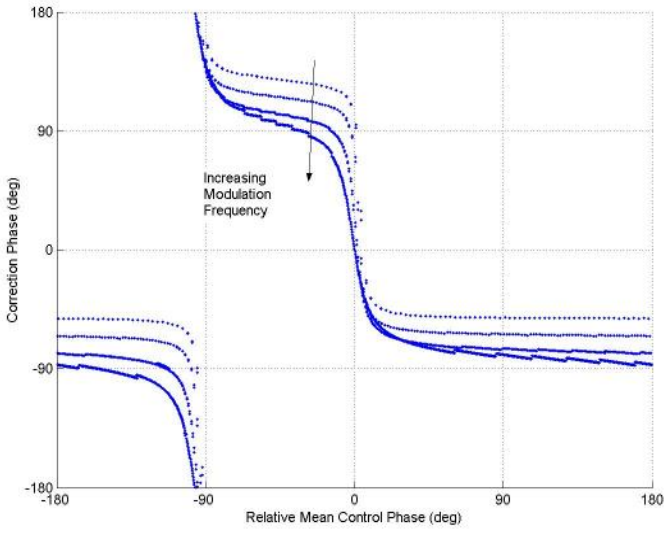

Figure 5.13. Effect of increasing the modulation frequency on the phase correction factor for the van der Pol simulation with low system damping

5.3.4 Limits on adaptation rate

To improve the response time of the adaptive control algorithm to changes in operating conditions, the adaptive controller was developed without an averaging scheme like the one used in the online identification algorithm. Unfortunately, the lack of such an averaging scheme makes the adaptive controller more susceptible to system noise. In order to mitigate this problem, the adaptive controller makes small corrections to the control phase during each adaptation cycle.

Further restriction is placed on the control phase correction by a scaling factor that is calculated during the adaptation cycle. This scaling factor provides additional restrictions on the impact of system noise by reducing the importance of a weakly correlated system response to control phase modulations. The scaling factor also limits controller "wandering" due to continuous control adjustments after the control phase has already been set to its optimum value. To improve reliability in noisy environments and to minimize this "wandering", control phase adjustments are scaled by the "mean square" correlation factor that was defined in Chapter 4, i.e.,

$$\begin{aligned} R &= C\sqrt{\sigma^2 + \chi^2} \\ C &= \frac{A_{\max} - A_{\min}}{2T_{ident}} \end{aligned} \tag{5.12}$$

Using this correlation factor, the adaptive controller correction to the mean control phase is given by:

$$\Delta\phi = R\Delta\phi_{\max}\frac{\phi_{corr}}{|\phi_{corr}|} \tag{5.13}$$

where $\Delta\phi_{max}$ is the maximum adaptation step size and R is the correlation coefficient, which varies between 0 and 1. Using the correlation coefficient, R, has two effects:

1) For very noisy systems, the correlation coefficient is generally smaller, which results in smaller adaptation steps and thus slower adaptation.

2) As the controller nears the optimum control phase, the amplitude of the response function diminishes, thus lowering the correlation coefficient and slowing the adaptation process.

5.3.5 Algorithm sensitivity

The preceding discussion of the adaptive control algorithm was based on the assumption that a sinusoidal modulation of the control phase results in a sinusoidal response of the pressure amplitude at the same frequency, see Eq. 5.6. This behavior is only observed when the instantaneous control phase is "small" and the response is linear. In the limit of the control phase approaching zero (i.e., "small" mean control phase), the assumption that sin(x) = x is valid. Table 5.2 shows that the error of assuming sin(x) = x is less than 10 percent for $\theta < 0.8$.

Table 5.2: Error of estimating sin(θ) = θ

x	sin(x)	Error
0.00	0.00	0%
0.10	0.10	0%
0.20	0.20	1%
0.30	0.30	1%
0.40	0.39	3%
0.50	0.48	4%
0.60	0.56	6%
0.70	0.64	8%
0.80	0.72	10%
0.90	0.78	13%
1.00	0.84	16%

To determine the effect of a 10 percent error in θ, Figure 5.14 shows the time dependence of $\phi_{c,mod} = \theta\sin(2\pi f_{mod} t_{mod})$ and $A_{mod} = K\sin(\theta\sin(2\pi f_{mod} t_{mod}))$ for $\theta = 0.8$. Note that both of these quantities are normalized by their respective maxima. Figure 5.14 shows that the control phase modulation is perfectly sinusoidal, and that correlation between the two plots is high in spite of the fact that the normalized amplitude response is not perfectly sinusoidal.

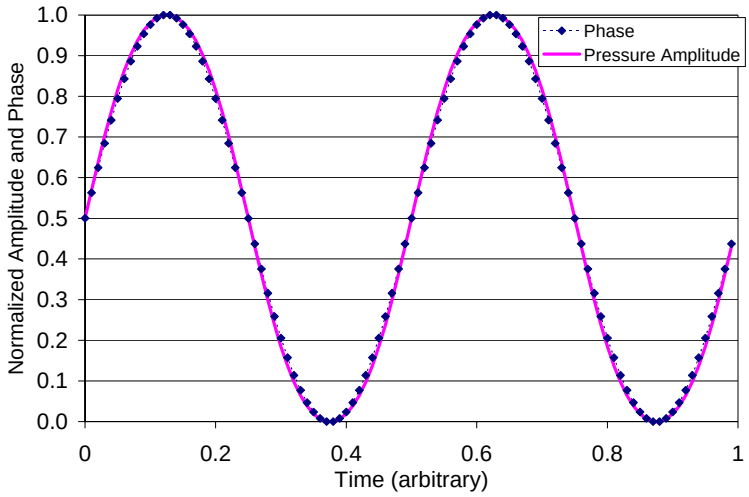

Figure 5.14: Time dependence of the normalized control phase modulation and the resulting normalized amplitude response of the combustor pressure oscillations for θ=0.8 (45 degrees).

To assess the level of correlation between the control phase and the pressure amplitude response, the mean square correlation factor, which gives a time-lag independent correlation between the two signals (Eq. 5.12) was used. For $\theta = 0.8$, the mean square correlation factor between the modulation phase and the system response is 0.9996, indicating nearly perfect correlation between the two signals.

It has been previously shown that for "small" phase modulations, the pressure response in an "ideal" linear system is sinusoidal and well correlated with the control phase modulations. On the other hand, for larger control phase modulations, i.e., as $\theta \rightarrow \pi/2$, the amplitude response becomes saturated, as shown in Fig. 5.15.

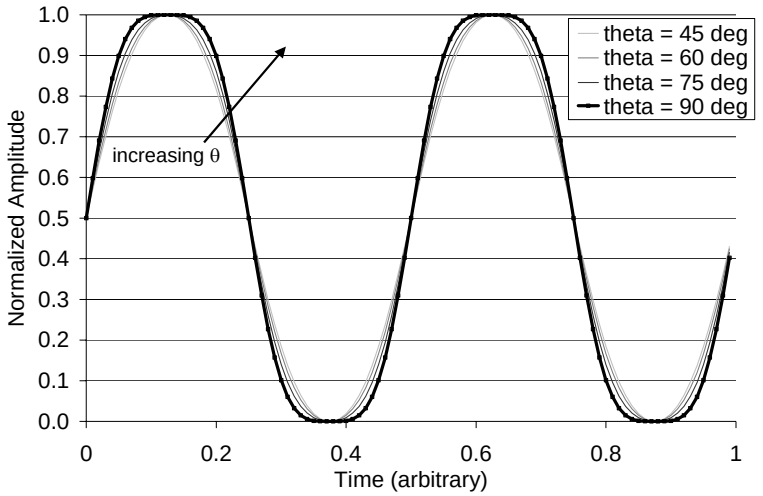

Figure 5.15: Time dependence of the normalized control phase modulation and the resulting normalized amplitude response of the combustor pressure oscillations for varying the modulation angles: i.e., $\pi/4 < \theta < \pi/2$.

This saturation response is due to the presence of higher harmonics in the amplitude response function, as demonstrated by the Taylor series expansion of the expression in Eq. 5.5:

$$\begin{aligned} A_{mod} &= K\sin(\theta\sin(2\pi f_{mod}(t_{mod}-\tau_{delay}))) \\ &= K\left[\sin(\theta\sin(u))\right] \\ &\approx K\left[\theta\sin(u)-\frac{(\theta\sin(u))^3}{3!}+\frac{(\theta\sin(u))^5}{5!}\cdots\right] \\ &= K\left[\theta\sin(u)-\frac{\theta^3}{4}\frac{3\sin(u)-\sin(3u)}{3!}+\frac{\theta^5}{16}\frac{10\sin(u)-\sin(3u)-\sin(5u)}{5!}\cdots\right] \end{aligned} \tag{5.14}$$

where $u = 2\pi f_{mod}(t_{mod} - \tau_{delay})$. For small values of θ, the higher order terms diminish rapidly. However, as the phase modulation amplitude θ increases, these terms become more dominant. For example, when $\theta = \pi/2$, the Taylor series expansion shows that the second harmonic of the modulation frequency ($3*f_{mod}$) accounts for roughly 13 percent of

the pressure amplitude signal content. In this case, the mean square correlation factor (without signal noise) is still very high at 0.9927, indicating that the correlation between the sinusoidal phase modulations and the pressure amplitude fluctuations can be used to calculate the phase correction factor with a high level of confidence. As the modulation amplitude θ is increased further, the second harmonic becomes larger than the driven modulation frequency, and the correlation factor between the control phase modulation and the amplitude response drops off substantially. For values of $\theta < \pi/2$, the expected amplitude response to a sinusoidal modulation of the control phase should be a highly correlated, near-sinusoidal function of f_{mod}. For values of $\theta > \pi/2$, the correlation with the fundamental modulation frequency diminishes.

Up to this point, the discussion of the system response to control phase modulations has focused on the response of the combustor pressure amplitude when the mean relative control phase $\phi_{rel,mean} = \pi/2$. Next, we examine the more general case, where $\phi_{rel,mean} \neq \pi/2$. Referring to Eq.5.3, the modulated component of the pressure amplitude is given by Eq. 5.14.

$$\begin{aligned} A_{\text{mod}} &= -K\cos(\phi_{rel} + \phi_{c,\text{mod}}) \\ &= -K[\cos(\phi_{rel})\cos(\phi_{c,\text{mod}}) - \sin(\phi_{rel})\sin(\phi_{c,\text{mod}})] \end{aligned} \tag{5.15}$$

Inspection of the case where $\phi_{rel,mean} = \phi_{c,mean} - \phi_{optimum} \rightarrow \pi/2$ shows that the first term in Eq. 5.15 vanishes, and the amplitude function is approximated by $K\sin(\phi_{c,mod}) = K\sin(\theta\sin(u))$, which is the previously derived result. This result leads to the conclusion than the response is linear for small θ, as was previously assumed. Note that $\sin(\theta\sin(u))$ is an odd function of u.

For other values of ϕ_{rel}, the amplitude function is a combination of both terms in Eq. 5.15. As $\phi_{rel,mean} \rightarrow 0$, the second term vanishes, and the amplitude function is

approximated by -cos(θsin(u)), which is an even function of u. The Taylor series approximation of this function is given by:

$$\begin{aligned} A_{\text{mod}} &= -K\cos(\theta\sin(2\pi f_{\text{mod}}(t_{\text{mod}} - \tau_{delay}))) \\ &= -K\left[\cos(\theta\sin(u))\right] \\ &\approx -K\left[1 - \frac{(\theta\sin(u))^2}{2!} + \frac{(\theta\sin(u))^4}{4!}\cdots\right] \\ &= -K\left[1 - \frac{\theta^2}{2}\frac{1-\cos(2u)}{2!} + \frac{\theta^4}{8}\frac{3-4\cos(2u)+\cos(4u)}{4!}\cdots\right] \end{aligned} \tag{5.16}$$

In the limit as $\theta \to 0$ the modulated amplitude function approaches the constant value $A_{mod} \to -K$ for $\phi_{rel,mean} = 0$ (for $\phi_{rel,mean} = \pi$, $A_{mod} \to +K$). As the amplitude of the control phase modulation θ increases, the higher order terms become important, introducing even harmonics of the fundamental modulation frequency, f_{mod}, into the response according to Eq. 5.16. Note that the fundamental frequency, $u = 2\pi f_{mod}$ vanishes when $\phi_{rel,mean} = 0$.

To understand the physical meaning of these equations, we examine what happens when θ equals zero (no control phase modulation) and $\phi_{rel,mean}$ is varied. For the case where $\phi_{rel,mean} = \pm \pi/2$, the mean amplitude is not affected by the control signal, as described by the curve "neutral response" in Fig. 5.5. As $\phi_{rel,mean}$ approaches $\pm\pi$, the amplitude of the pressure oscillations is increased, indicating driving in-phase oscillations with the control input. On the other hand, as $\phi_{rel,mean}$ approaches 0, the amplitude of the oscillations is decreased. When $\phi_{rel,mean}$ equals 0, the maximum damping has been achieved, a condition which, by definition, corresponds to the optimum control phase.

5.3.6 Fundamental and Harmonic Response

Thus far, it has been shown that for small values of θ and $\phi_{rel,mean} \sim \pi/2$, the amplitude function varies sinusoidally with the modulating frequency f_{mod}, see Eq. 5.5. As θ is increased, higher harmonics of f_{mod} appear, but their amplitude is very small for values of θ < 1.0. The characteristics of these higher harmonics are described as follows:

$$\text{As } \phi_{rel} \to \pm\pi/2, \qquad A_{mod} \to -K\left[\boldsymbol{\theta \sin(u)} - \frac{\theta^3}{4}\frac{3\sin(u)-\sin(3u)}{3!} + \cdots\right] \tag{5.17}$$

$$\text{As } \phi_{rel} \to \pi, \qquad A_{mod} \to K\left[(1-\frac{\theta^2}{4}) + \boldsymbol{\frac{\theta^2}{4}\cos(2u)} + \cdots\right] \tag{5.18}$$

$$\text{As } \phi_{rel} \to 0, \qquad A_{mod} \to -K\left[(1-\frac{\theta^2}{4}) + \boldsymbol{\frac{\theta^2}{4}\cos(2u)} + \cdots\right] \tag{5.19}$$

The above equations represent three conditions: a) "neutral" response (Eq. 5.17), where the mean control signal has no effect on the combustor pressure oscillations, and the mean pressure amplitude is the same as in the uncontrolled case; b) "driving" response (Eq. 5.18), where the combustor pressure oscillations are augmented by the control signal, and the mean pressure amplitude in the combustor is thus higher than in the uncontrolled case; c) "damping" response (Eq. 5.19), where the control actuation damps the pressure oscillations in the combustor, resulting in a mean pressure amplitude that is lower than the amplitude of the uncontrolled pressure oscillations. These equations show that when the controller is in a neutral condition ($\phi_{rel} = \pm\pi/2$), the system should respond very strongly to control phase modulations, varying as ~Kθsin(u). Physically, this means that the system responds strongly to control phase modulations. As the mean control phase is adapted toward the optimum damping condition, i.e., $\phi_{rel,mean} = 0$, the response of the system will tend to favor the first harmonic over the

fundamental frequency. However, as the system response approaches the perfect driving or perfect damping conditions, the response varies as $K*(\theta^2/4)*\cos(2u)$, indicating that the first harmonic response is very small for $\theta < 1.0$ and may not be very useful for determining optimum control parameters.

An analysis of the frequency response of the system for the fundamental and first harmonics of the control modulation frequency is presented below. The goal of this analysis is to determine the value of $\phi_{rel,mean}$ for which the system response to the first harmonic of the modulation frequency becomes dominant over the system response to the fundamental modulation frequency. Figure 5.16 shows the how the amplitude response of the linear model given in Eq. 5.16 varies with changes in the relative mean control phase ϕ_{rel} and the control phase modulation amplitude θ. This plot shows the ratio between the first harmonic (bold term in Eqs. 5.18-5.19) to the fundamental mode (bold term in Eq. 5.17) of the amplitude of the system response. Figure 5.16 shows the ratio of these two terms, as $\phi_{rel,mean}$ and θ are varied. For $\phi_{rel,mean} \sim \pi/2$, the fundamental term dominates (the ratio is less than 1.0), but as $\phi_{rel,mean}$ approaches 0, the first harmonic begins to dominate (ratio is greater than 1.0). The importance of the first harmonic is amplified as θ becomes larger. For a nominal phase modulation amplitude of $\theta = 0.70$ (40 degrees), the first harmonic becomes dominant when $\phi_{rel,mean} < 20$ degrees (1.22 radians), i.e., when the relative control phase is within 20 degrees of the optimum control phase.

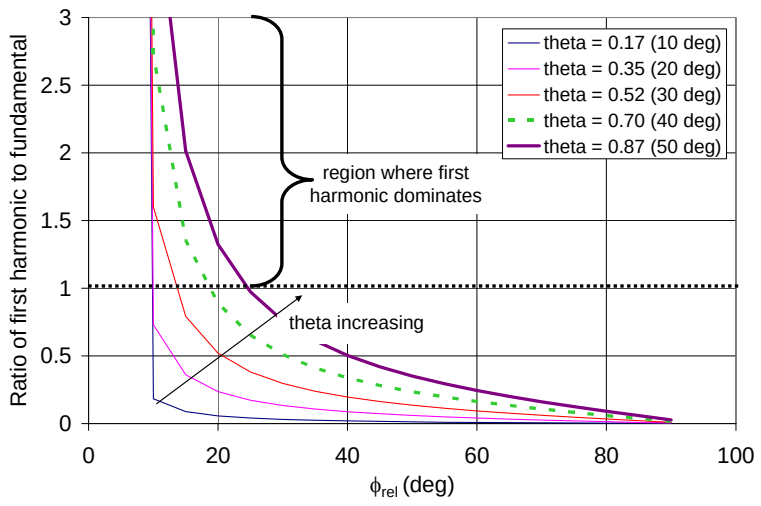

Figure 5.16. Ratio of amplitude of first harmonic to amplitude of fundamental response at the frequency of control phase modulation. As $\phi_{rel} \rightarrow 0$ degrees, the first harmonic begins to dominate, resulting in a "double-frequency" beating.

5.4 Experimental Results

Several types of experiments were performed to assess the performance of the adaptive control algorithm. Most of these experiments utilized the modified experimental setup, shown in Fig. 4.1. In this setup, an electronic phase shifter was inserted into the signal line between the pressure transducer (with charge amplifier) and the control computer. This phase shifter controls the phase between the actual pressure signal and signal read by the computer. The input phase to the control computer (containing the observer and controller) can be offset by as much as 150 degrees using the phase shifter. In doing so, it is possible to test whether the ACS can converge on the optimum control phase and evaluate the performance of the ACS. When the phase offset is zero, the "system phase" and the "control phase" are equal. However, as the phase offset is changed, the controller must compensate for this offset in order to keep the system phase constant and thus maintain control of the system.

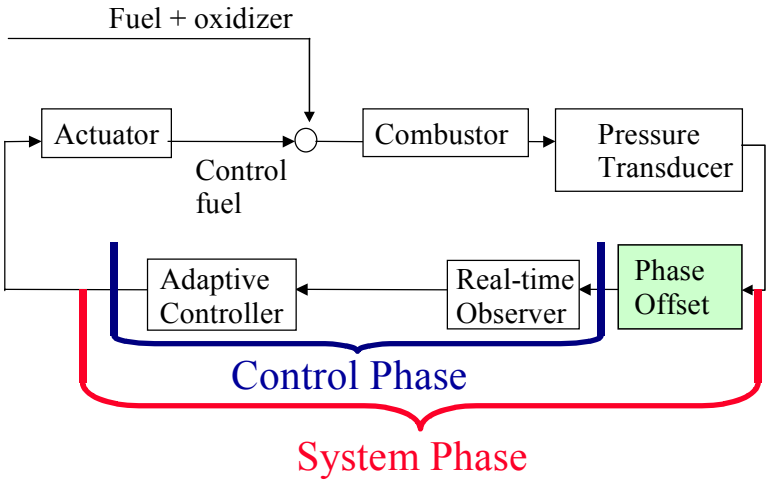

Figure 5.17. Closed-loop control block diagram with manual phase offset.

5.4.1 Liquid Fuel Combustor Adaptive Control Experiments

The first set of experiments was performed on the liquid fuel combustor to determine whether the adaptive control algorithm converged to the optimal control phase in a combustion test. In these tests, the combustor was operated at an equivalence ratio of 0.97 and exhibited instabilities with RMS amplitude of 1.4 psi at its quarter wave mode of 400 Hz (note that the 1.4psi oscillations equal almost 10 percent of the mean pressure in this atmospheric combustor). The test started with an identification process in which the phase of the control signal was swept in a slow, continuous manner at a constant rate of 36 degrees/sec. The effect of the phase sweep was manifested as a periodic variation of the pressure amplitude indicating the presence of an optimum phase at which the amplitude of the oscillations was at its minimum. After performing several slow sweeps, the identification process was stopped, and the adaptive control scheme was activated. It should be noted that the adaptive control scheme was not provided with any information obtained during the slow identification process. It was expected that, if the adaptive scheme operated properly, it should converge to the optimal phase that was determined in the slow identification process. Figure 5.18 describes the variation of the combustor

pressure amplitude during the slow phase sweep and then the response of the combustor pressure to the application of the adaptive control scheme. For an equivalence ratio of 0.97, the identification process demonstrated two successive combustor pressure minima when the control phase equaled 280 degrees, thus identifying this as the optimal control phase. Figure 5.18 also shows that when adaptive control was applied, the controller converged rapidly to the optimal control phase and maintained control at this phase with small variations of +/- 20 degrees. The attained pressure attenuation was generally consistent with that obtained during the slow phase sweep when the control phase was approximately 280 degrees. The adaptive controller required approximately one second to converge to the optimal control phase. The mean square correlation scale factor was not implemented during these tests. Its use would most likely have caused the controller to "settle" on the optimum control without much "wandering," thus minimizing the amplitude of the pressure oscillations even further.

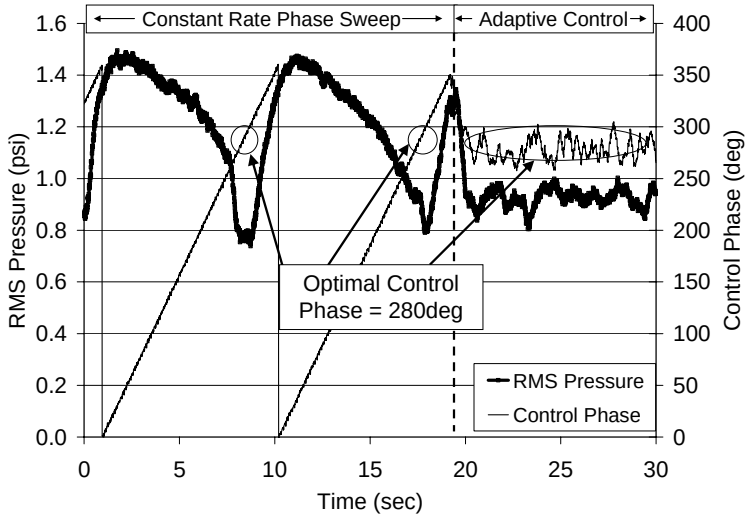

Figure 5.18. Off-line identification of the optimal control phase followed by its determination by the adaptive controller.

The second set of experiments was designed to test the convergence rate of the adaptive controller by determining its response to sudden changes in the required control

phase. This was accomplished by introducing a phase offset by an auxiliary variable phase shifter that was placed in series with the pressure transducer, see Fig. 4.1. By turning a knob on the phase shifter, the overall phase in the forward loop was altered, and the adaptive controller was expected to compensate for this "phase disturbance" by changing the control phase. Such a change in the phase offset allows performance assessment of the adaptive controller without changing operating conditions in the combustor. It is important to note that when a sudden phase offset larger than 90 degrees is introduced, the controller temporarily increases the amplitude of the oscillations rather than damp them. To restore control over the system, the adaptive controller must respond rapidly to the abrupt phase offset.

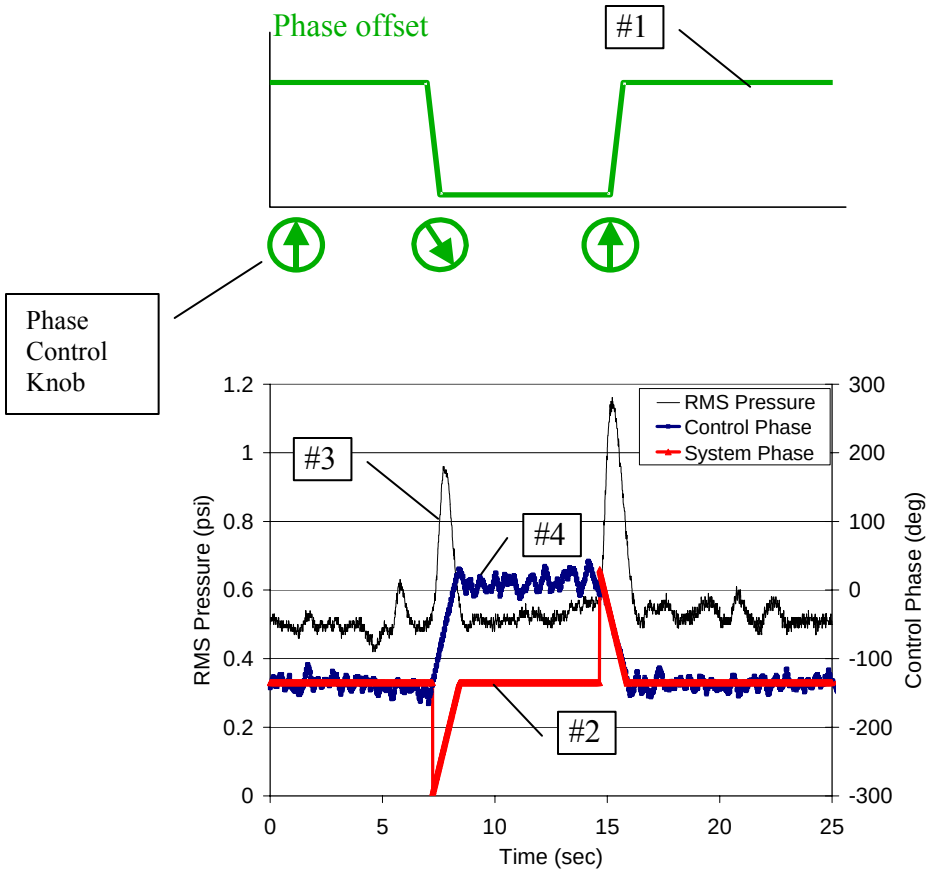

Figure 5.19: Adaptive system pressure and phase response to step changes in the control phase produced by the phase shift offset.

Figure 5.19 shows the response of the adaptive controller to positive and negative step-like changes of 150 degrees in the phase offset (the knob on the variable phase shifter was turned as fast as possible from minimum to maximum and back) while the combustor was operated at an equivalence ratio of 0.85. The following sequence of events is shown in Fig. 5.19. (To aid the discussion, each curve is numbered (#1 - #4) and referenced as needed.) At t = 7 sec, the phase shifter knob abruptly changed the phase of the pressure signal input (#1) to the controller by 150 degrees. This caused a sudden change in the "system phase" (#2), which caused a rapid increase in the pressure amplitude (#3). Immediately, the adaptive controller began increasing the control phase (#4) to compensate for the change in the system phase (#2). As the control phase (#4) was increased, the system phase (#2) was restored to the optimum state, and the pressure amplitude (#3) was reduced to its minimum value. The optimum control phase (#4) is now +150deg from its initial phase. At t = 15 sec, the phase shifter knob was abruptly turned the other direction, thus causing the phase of the pressure signal (#1) to return to its original state. This time, the system phase (#2) was increased by 150 degrees, which caused the pressure amplitude (#3) to increase substantially. The controller immediately began adjusting the control phase (#4) back to the original control phase and the pressure amplitude (#3) was reduced. For both abrupt phase changes, the controller adjusted the phase at a rate of 150 degrees/sec. Several similar tests were performed with different phase step changes, and the convergence rate in all cases was approximately 150 degrees/sec. This convergence rate is dependent upon the selected adaptation parameters, which will be discussed later in this chapter.

In the third set of experiments, the performance of the adaptive controller at various combustor operating conditions was investigated. It was noted in previous tests with this combustor that when the equivalence ratio was increased from lean to near stoichiometric operating conditions, the amplitude of the instability increased. It was also noted in these experiments that the increase the stoichiometry of the system was

accompanied by a significant degradation in the system's controllability. These trends are demonstrated in Figs. 5.20-a,b, which show the control system effectiveness under lean and near-stoichiometric operating conditions, respectively.

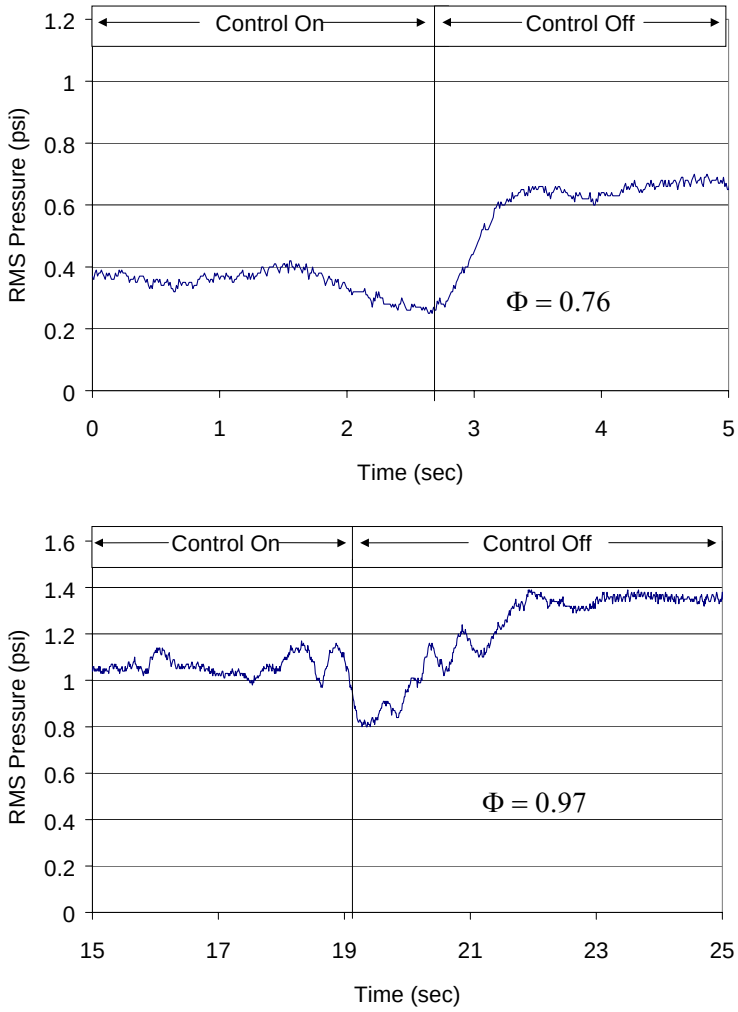

Figure 5.20: System pressure under active control and uncontrolled operating conditions for a) lean operation, b) stoichiometric operation.

Figure 5.20-a shows that when control was turned off during lean operation (i.e., $\Phi = 0.76$), the RMS pressure nearly doubled to 0.7 psi. When this test was repeated with an equivalence ratio of 0.97, the pressure amplitude increased from 1.05 to 1.35 psi. These results indicate that the investigated ACS is capable of almost 50 percent attenuation at lean operating conditions, but only 25-30 percent attenuation at near

stoichiometric operating conditions. These steady-state control results suggest the controller performance limits that can be expected during transient events.

There are two contributing factors for the limited controllability at stoichiometric conditions in this liquid fueled ramjet simulator: a) mechanical limitation of fuel flow modulation rate, and b) heat release fluctuations as a function of equivalence ratio.

The first factor limiting the controllability is related to the mechanical operation of the injector's pintle. As shown in 5.21 (and also Fig. 2.4), the rate of fuel flow in the fuel injector actuator is controlled by the vertical position of the pintle in relation to the conical housing. As the pintle moves down, a gap is created between the two cones, allowing fuel to enter the plenum. For low fuel flow rates, the pintle moves down slightly into the conical section, and for high fuel flow rates the pintle moves down further. At some distance, the distance between the two cones is large enough that it no longer restricts the fuel flow; instead, the flow becomes restricted by the geometry of the flow passage inside the pintle. At that point, the fuel flow rate cannot be increased by opening the plenum any further, i.e., the fuel flow rate is saturated at its maximum value.

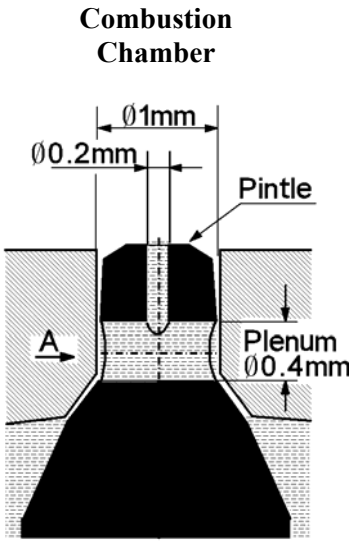

Figure 5.21: Liquid Fuel Ramjet Simulator Pintle Nozzle

This fuel flow saturation effect is illustrated in Fig. 5.22. At low mean flow rates, modulation of the pintle position (solid line at bottom) results in modulation of the fuel flow (solid line at top) over the whole range of the pintle movement. However, at high fuel flow rates (marked line at bottom), this modulation results in saturation of the fuel flow (marked line at top). The effect of this saturation is a reduction in the total modulation of the fuel flow. (Saturation also introduces nonlinearities which may affect the damping or possibly destabilize other modes.)

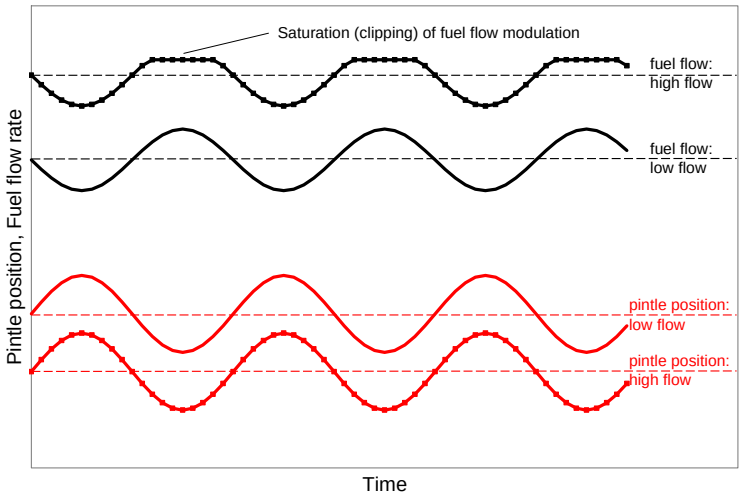

Figure 5.22: Illustration of saturation effect at high fuel flow rates

The second explanation for the controllability limitations is related to the amplitude of the reaction rate fluctuations in response to modulating as the equivalence ratio increases. As discussed by Lieuwen and shown in Fig. 5.23, the magnitude of the heat release fluctuations changes as a function of mean equivalence ratio. In Fig. 5.23, the mean equivalence ratio starts at 1.0, with equivalence ratio fluctuations of approximately +/-0.2. At stoichiometric conditions, the resulting reaction rate (heat release) fluctuations is minimal. As the mean equivalence ratio is reduced (moving to the right), the reaction rate fluctuations increase. Lieuwen used this figure to help explain the tendency for lean premixed combustors to become more unstable at low equivalence

ratios. In the current application of active control to the liquid fuel combustor, the figure indicates that forced modulation of the fuel flow (equivalence ratio) can produce large fluctuations in heat release at low equivalence ratios. Thus, modulating the pintle position provides a robust method for adding energy out of phase with the combustion instability. However, as the equivalence ratio approaches 1.0, the same level of ACS fuel flow modulation results in less control authority because the fuel flow modulation does not produce a significant change in the reaction rate in the system.

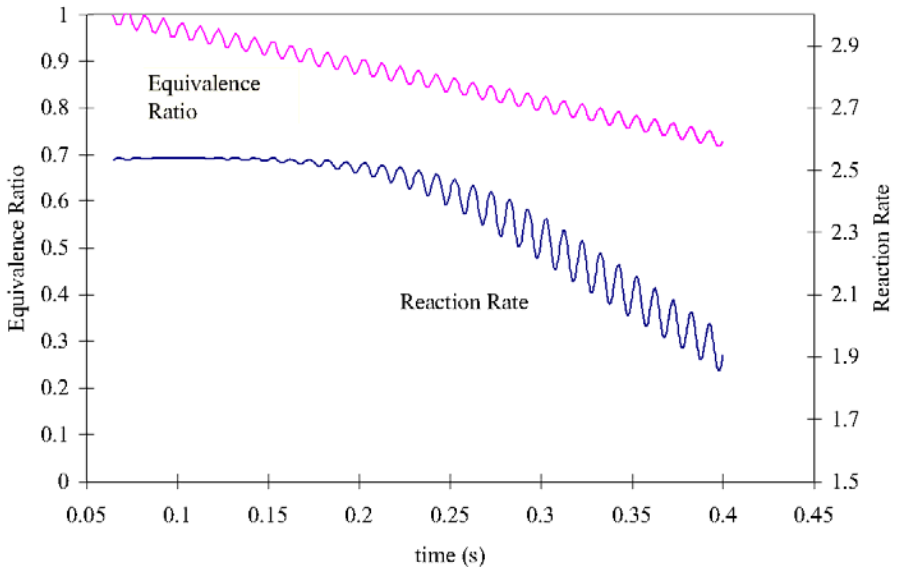

Figure 5.23: Dependence of the response of the reaction rate to equivalence ratio perturbations upon the mean equivalence ratio. [4]

The next test was designed to investigate the ability of the adaptive controller to continuously compensate for changes in operating conditions by observing how it responded to small changes in equivalence ratio. Figure **5.24** shows the time trace of the equivalence ratio along with the adapted control phase. It clearly shows that the adapted phase continuously adjusts to changing equivalence ratio. These results together with those showing that the adaptive controller rapidly converges to the proper control phase, see Figs. 5.18 and 5.19, indicate that the developed adaptive algorithm is capable of providing the necessary adjustments in control phase for stabilizing a combustor.

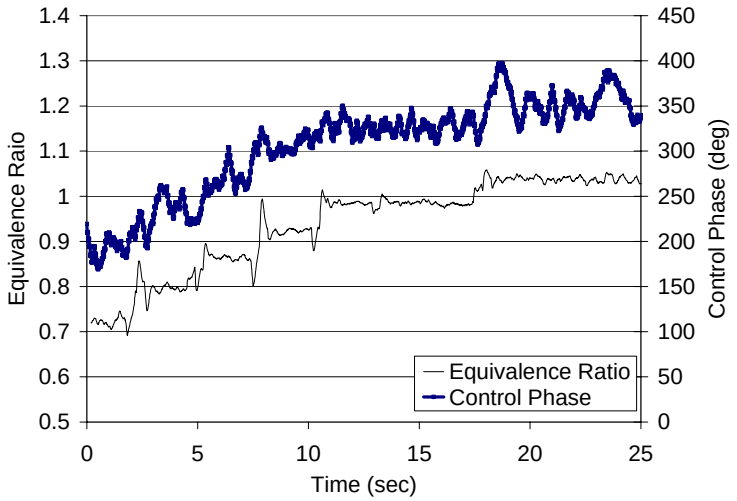

Figure 5.24: Time trace of control phase and equivalence ratio when fuel flow is increased incrementally.

The results of these tests were also used to determine the dependence of the adapted phase upon the equivalence ratio for this combustor. Figure 5.25 indicates that the total variation in control phase for the investigated range of equivalence ratios is approximately 140 degrees. A fixed-phase controller would not be able to handle this phase change over the described operating conditions; for this application, the dependence of the phase upon the equivalence ratio would have to be determined in separate experiments and/or analysis. Consequently, an adaptive controller that can rapidly vary the phase of this range is should significantly outperform a fixed phase controller for this system.

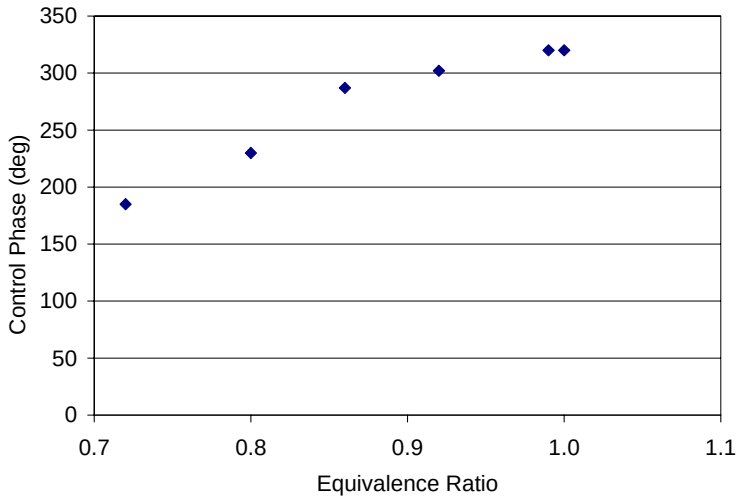

Figure 5.25: Control phase dependence on equivalence ratio.

In the final set of experiments, the adaptive controller attenuated instabilities in the combustor while the fuel supply to the combustor was varied rapidly. This test was designed to represent missile maneuvering using rapid changes in the fuel flow rate, thus providing information about the performance of the adaptive controller in practice. This type of transient event represents a significant challenge for an adaptive algorithm and requires that it respond quickly to changes in operating conditions without destabilizing the combustor during the transient. First, the fuel flow rate was increased rapidly from 0.65g/s ($\Phi = 0.76$) to 0.89 g/s ($\Phi = 1.04$) without active control. The experiment was then repeated with adaptive control applied. Figure 5.26 shows that the adaptive control system is capable of handling this transient, providing attenuation of 40 percent and 25 percent before and after occurrence of the transient, respectively. During the transient event, the pressure spike is attenuated by approximately 20 percent. The reduced controllability at higher flow rates is consistent with the data presented in Fig. 5.20. It is significant to note that the controller was well behaved during the transient event, i.e., it did not further destabilize the combustor. It should be also noted that the control phase

difference between the low and high fuel flow rates is approximately 120 degrees, thus necessitating a rapidly converging adaptive controller.

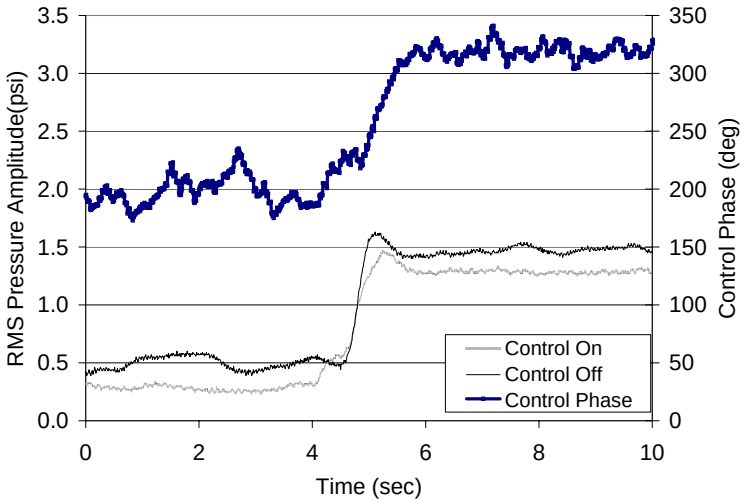

Figure 5.26: Adaptive controller response to transient fuel flow rate input.

5.4.2 Acoustic Feedback Setup Adaptive Control Experiments

The above experiments in the liquid fuel combustor represent a realistic operating condition with significant random noise levels that limit controller effectiveness and make it difficult to assess the impact of various input parameters on controller performance. The next set of experiments was performed in the acoustic feedback facility to determine some of the attributes of the adaptive controller in a less noisy environment. This facility is not subject to high intensity turbulence as is found in a typical combustor. While it may be argued that this facility does not represent a realistic operating environment, it does provide the opportunity to evaluate the adaptive controller performance as different control parameters are varied, thus providing a method for determining the optimum set of input parameters for adaptive control.

Several different tests were made with the acoustic test box to determine how the effectiveness of the adaptive controller depends upon its control parameters. The results of the experiments are compared with the findings of the theoretical analysis presented earlier in this chapter. Also, limitations of the adaptive control approach are described, and the control parameters are varied to determine the optimum controller configuration. The following parameters were studied in order to determine an optimal configuration for controlling combustion instabilities.

Modulation Frequency (f_{mod}): The frequency at which the control phase is modulated in order to determine the system response to the control input.

Modulation Amplitude (θ): The angle of maximum phase modulation for an adaptation cycle. The instantaneous control phase, ϕ_{inst} is equal to the mean control phase ϕ_{mean} plus an offset that oscillates sinusoidally between $\phi_{inst} = \phi_{mean} \pm \theta\sin(2\pi f_{mod})$.

Maximum Adaptation Step Size ($\Delta\phi_{max}$): The nominal step size for adaptive correction to the mean control phase after an adaptation cycle is complete. This value is multiplied by the correlation coefficient (R) and the sign of the phase correction factor (ϕ_{corr}) to determine the exact step size.

5.4.2.1 Adaptive controller characterization

The first set of tests was conducted to examine the response of the dynamic pressure in the acoustic facility to modulations about a quasi-steady mean phase. In particular, this set of tests was conducted to investigate two characteristics of the system response:

- Presence (or lack thereof) of the first harmonic of the modulation frequency

- The characteristics of the phase correction factor compared to the van der Pol model

Overview of Procedure

For these tests, the mean phase value was swept at a rate of 40 degrees/sec, thus requiring a total of 9 seconds to make a complete sweep of all possible mean phase values. This sweep rate is equivalent to an online identification rate of 0.11Hz. With an unstable frequency in the acoustic test facility of 247Hz, the ratio of the sweep rate to the unstable frequency is 4.5e-4, which means that the phase lag effect of the mean phase sweep rate should be infinitesimal (see Chapter 4).

The frequency of modulation was varied in different tests, but the nominal frequency of modulation for most tests was 40Hz, corresponding to a modulation period of 0.025 sec. Using the mean sweep rate of 40deg/sec, the mean phase variation during a single modulation cycle was 1 degree. The mean phase variation of 1 degree per adaptation cycle is considered quasi-steady since this variation is very small in comparison with the phase modulations that are used during the adaptation process. Also, this quasi-steady characterization is valid because the effect of a 1 degree variation in control phase is imperceptible when compared to the effects of, e.g., random noise in the combustor.

Measurement of fundamental and first harmonic

As shown in Fig. 5.16, the first harmonic of the modulation frequency should appear in the system response as the mean relative control phase approaches the optimum control phase. The next experiment was designed to study this effect. Figure 5.27 shows data measured during a 60 second period from a typical experiment. The top plot shows

the mean control phase, ϕ_{mean}, and the instantaneous control phase, ϕ_{inst}, which is sinusoidally modulated about ϕ_{mean} with an amplitude in this case of $\theta = 80$deg. The mean control phase is the straight line, and the instantaneous control phase appears as a wide band above and below the mean control phase. The middle plot shows the dynamic pressure in the acoustic box as it responds to the control phase modulations, and the bottom plot shows the amplitude of the phase modulations as calculated by the real-time observer. In this figure, the large-scale changes in the amplitude of the pressure oscillations in response to the slow modulation sweep rate are readily observed. The next figure (5.28) shows the same data for the time period $15 < t < 16$. This figure shows the modulation of the control phase and the small-scale response of the pressure oscillations to changes in both the modulation phase and the quasi-steady mean control phase. It indicates that the response to the control phase modulations is very small, less than 5 percent of the mean amplitude of the dynamic pressure.

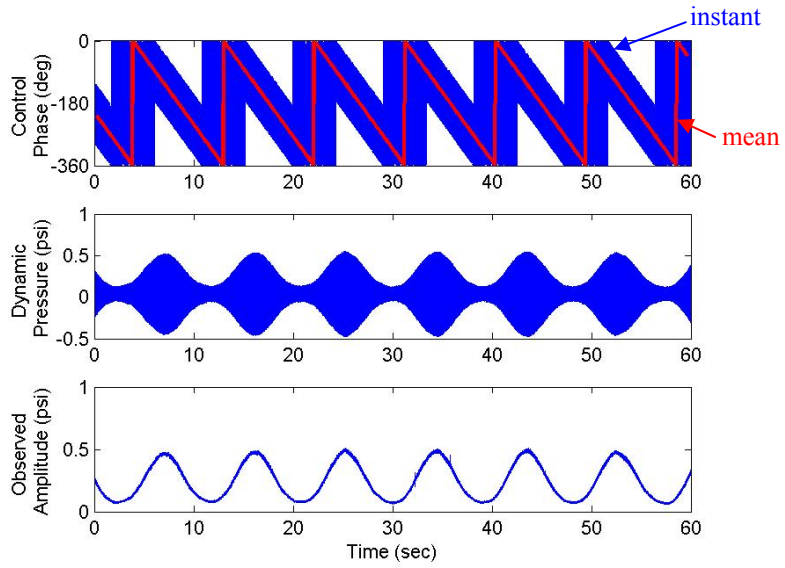

Figure 5.27: 60-second sweep of the mean control phase while simultaneously modulating the instantaneous control phase

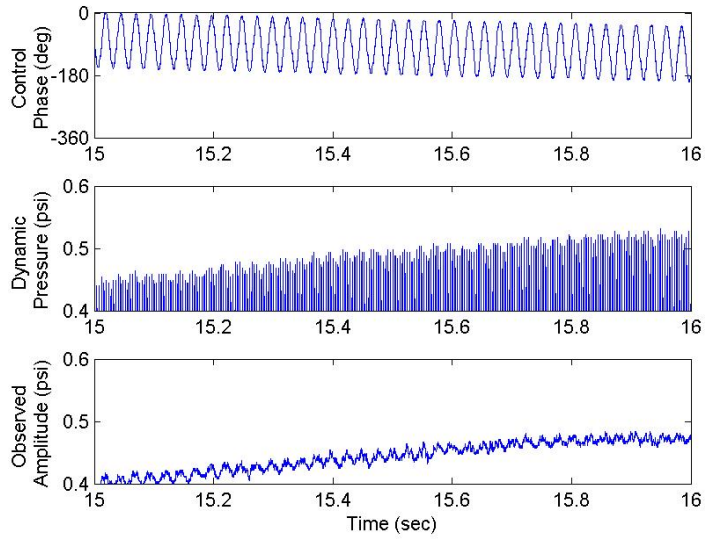

Figure 5.28: Modulation of the control phase about a quasi-steady mean control phase produces fluctuations in the dynamic pressure.

The primary goal of these phase sweep experiments was to understand the relationship between the fundamental frequency of modulation and the first harmonic. As described previously, when the adaptive controller approaches the optimum control phase, the amplitude of the first harmonic increases, and the amplitude of the fundamental decreases. Depending upon the control phase modulation amplitude, θ, the magnitude of the first harmonic may become larger than the amplitude of the fundamental frequency of modulation as the dominant response frequency in the observed amplitude. To investigate this behavior, the time dependence of the spectrum frequency content of the amplitude response function was investigated. Specifically, the amplitude of the fundamental and first harmonic were determined using an FFT of the observed amplitude. This "modulation amplitude" response is shown on the bottom of Fig. 5.29 for the time period $59.4 < t < 59.8$. The peak value in "band 1" represents the fundamental response, and the peak value in "band 2" represents the response of the first harmonic. The low frequency peak represents the change in mean amplitude of the signal, i.e., the DC response.

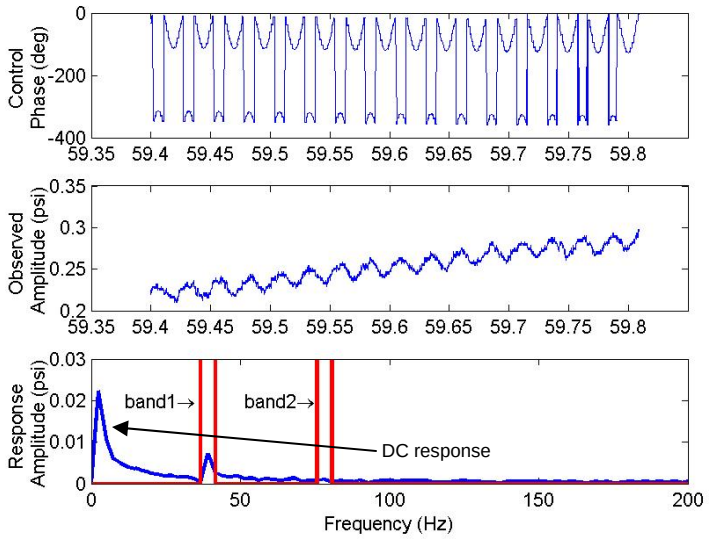

Figure 5.29: Investigation of fundamental and first harmonic response amplitude

Figure 5.30 shows the FFTs of the amplitude response at different points in the slow mean phase sweep cycle. When the control phase is equal to the optimum control phase of –300 degrees, the amplitude of the response at the fundamental frequency (peak 1) is very low. Similarly, the amplitude response at the fundamental frequency is low when the maximum driving condition is obtained at $\phi_{c,mean}$ = -120 degrees. However, when the control phase is in the "neutral response" condition of –30 and –210 degrees, the amplitude of the fundamental response is much higher. The first harmonic response (peak 2) increases slightly for the maximum driving and maximum damping conditions, but its amplitude is still smaller than that of the fundamental mode for this experiment. It is also interesting to note that the DC amplitude is much higher for the "neutral response" cases (-30 and -210 degrees), which is caused by the rapid change in mean amplitude response as the mean control phase is changed. This high DC response indicates that adapting the mean control phase has a strong impact on the amplitude response in this range of mean control phases. In contrast, when the mean control phase is equal to the optimum control phase (-300 degrees), the DC response is very small, indicating that a

small change in the mean control phase has very little impact on the amplitude of the pressure oscillations.

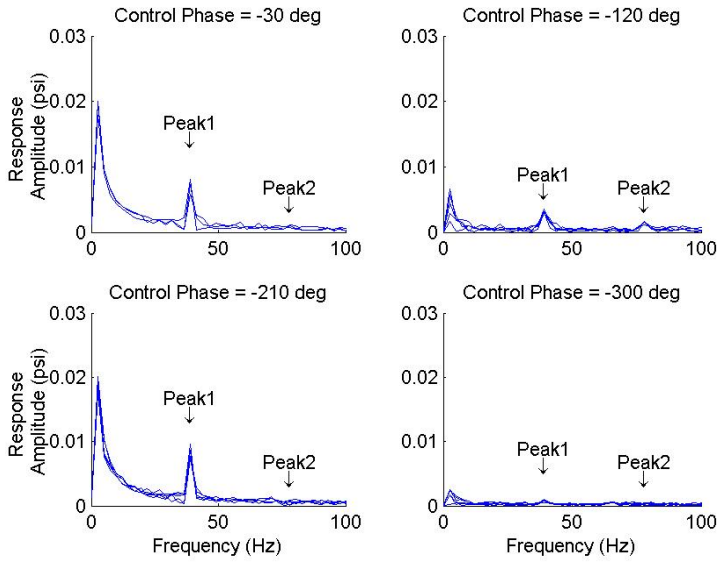

Figure 5.30: FFT of the amplitude response for different mean control phases

Figure 5.31 shows the time dependence of the dynamic pressure and the amplitude response of the fundamental (peak 1) and first harmonic (peak 2) of the modulation frequency. The values of peak 1 and peak 2 in the middle plot are normalized by the mean amplitude of the dynamic pressure. The ratio of the two peak values is shown on the bottom plot. This ratio approaches 1.0 at the optimum control phase and the maximum driving phase, but never exceeds 1.0 in this particular experiment. The amplitude of the fundamental response decreases dramatically as the mean control phase approaches the optimum control phase, but there is very little change in the response of the first harmonic. Therefore, the change in amplitude ratio for this experiment is driven primarily by changes in the fundamental frequency response. Figure 5.32 shows the variation of the amplitude ratio as a function of the mean control phase.

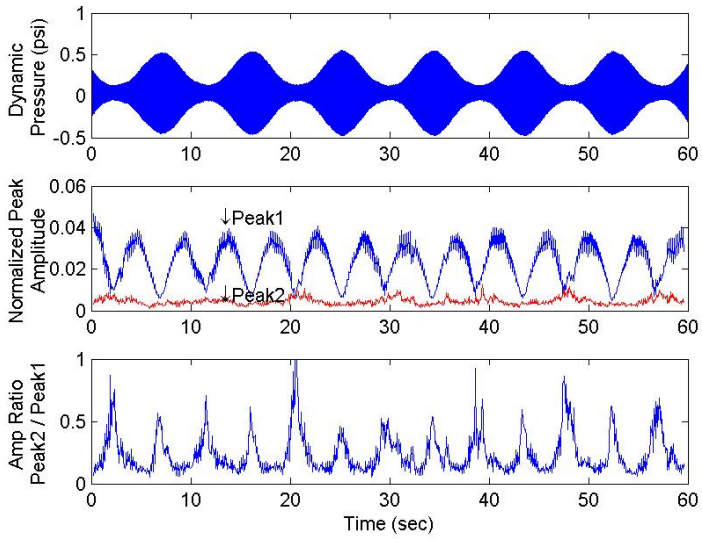

Figure 5.31: Variation of fundamental and first harmonic as the mean control phase changes

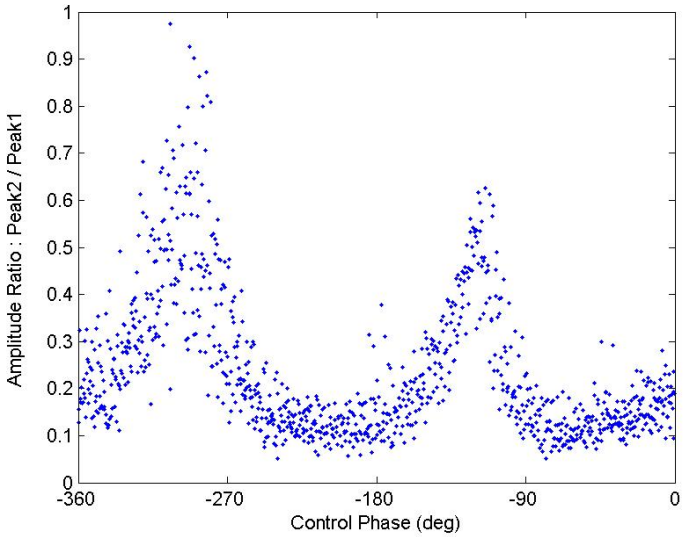

Figure 5.32: Ratio of the first harmonic to the fundamental as a function of mean control phase; in this case, the optimum control phase is –300 degrees.

To get the amplitude of the fundamental and first harmonic as a function of time, test data from the 60-second experiment was divided into 1000 samples that were then analyzed by FFT. Each sample represents a 2048-point FFT, with a sampling frequency of 5000Hz. Thus, the bin-width for the FFT equaled 5000/2048 = 2.44Hz, and the

sampling period equaled 2048/5000 = 0.4096 sec. Note that the FFT shown in Fig. 5.29 was made by post-processing the data that was acquired during the experiment. It should not be confused with the real-time observer that was used to calculate the amplitude of the pressure oscillations during the test.

To improve the frequency resolution of the FFT, it is necessary to increase the number of points per sample, at the expense of lower time resolution, which in this case means that the mean control phase variation over the sample time increases. This, in turn, increases the magnitude of the error produced by assuming a quasi-steady mean control phase over the sample period. There are two ways to resolve this problem: 1) lower the sweep rate, or 2) increase the sampling frequency. If the sweep rate is lowered, then the quasi-steady assumption holds over a longer period of time. However, this means that during a 60-second test, there will be fewer full sweep cycles, which reduces the number of sweeps over which the results are averaged. If the sampling frequency is increased, then the larger number of data points collected per test becomes difficult to manage. Using the existing data acquisition parameters, a 60-second experiments generates 300,000 data points. If the sampling frequency is doubled, this number grows to 600,000. The above discussion centers upon a tradeoff between needing a high sampling rate to measure rapidly fluctuating data (pressure oscillations with natural frequencies above 200Hz), and trying to measure over a long period of time to capture events that occur on a much slower time scale (mean control phase sweep rate of 0.11Hz).

Measurement of Correlation Coefficient

One of the key calculations in the adaptive control algorithm is the correlation coefficient, described in Eq. 5.12. This correlation coefficient describes the strength of the correlation between input phase modulations and output pressure amplitude

fluctuations of the *fundamental* frequency of the phase modulations. No correlation is calculated for the first harmonic. As discussed earlier, this correlation coefficient can be used to modify the adaptation step so that the correction of the mean control phase is proportional to the confidence of the calculation. The effect of this modification is to slow down the adaptive process as the controller approaches the optimum control phase, thus preventing excessive "wandering" of the control phase during the adaptation process. Figure 5.12 shows the variation of the correlation coefficient as the mean control phase is varied during a typical experiment. As the control phase is varied, the correlation coefficient between the control phase input and the amplitude response is calculated. The correlation coefficient is at its maximum in the "neutral response" zones, and at its minimum for maximum damping (optimum control phase) or maximum driving (worst control phase). Figure 5.33 shows the dependence of the correlation coefficient as the mean control phase is varied during a typical experiment. As the control phase is varied, the correlation coefficient is calculated between the control phase input and the amplitude response. The correlation coefficient is highest in the "neutral response" zones, and lowest for maximum damping (optimum control phase) or maximum driving (worst control phase). Figure 5.34 shows the correlation coefficient as a function ofupon the mean control phase. For this set of control parameters, the correlation coefficient at the optimum control phase is approximately 0.4. At the neutral response phase, the correlation coefficient is approximately 0.9. Using the correlation coefficient as a multiplier for the adaptation step size, the adaptation rate for the adaptive controller will be slowed by more than 50 percent when approaching the optimum control phase, thus minimizing "wandering" about the optimum control phase.

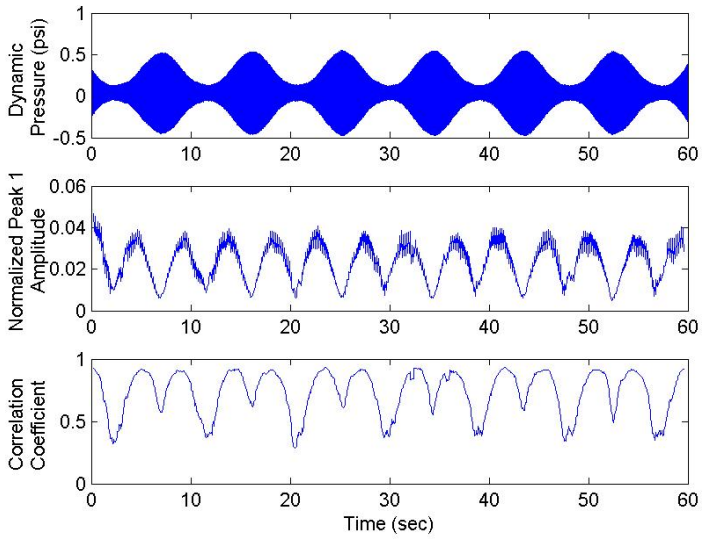

Figure 5.33: Varying the control phase causes changes in the amplitude response of a) dynamic pressure, b) fundamental peak amplitude, c) correlation coefficient

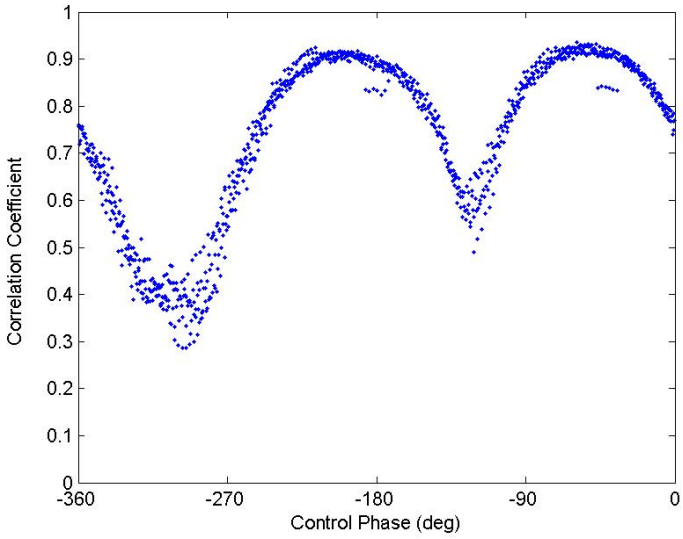

Figure 5.34: Correlation coefficient as a function of mean control phase; in this case, the optimum control phase is –300 degrees.

Thus far, it has been shown that the amplitude ratio between the first harmonic and the fundamental of the phase modulation frequency is minimum in the "neutral response" zone where $\phi_{c,mean} - \phi_{optimum} \sim n\pi/2$, and has peaks at both the optimum control phase where the pressure amplitude is minimized and at the phase where the maximum

driving occurs. It has also been shown that the correlation coefficient approaches 1.0 in the "neutral response" zone and is minimized for optimum control phase and the maximum driving phase. Next, we will examine how varying adaptive control parameters affects the amplitude ratio and the correlation coefficient.

Response of Fundamental and First Harmonic

Several "sweep" experiments were performed in the same manner described above in the acoustic feedback setup, where the mean control phase was swept continuously and the instantaneous control phase was modulated sinusoidally. Two control parameters were varied in the experiments: a) control phase modulation frequency (f_{mod}), and b) control phase modulation amplitude (θ). The results of these experiments are described below.

First, the dependence of the amplitude ratio of the first harmonic and the fundamental upon the phase modulation frequency was studied. For these experiments, the phase modulation amplitude was held constant at $\theta = 80$ degrees. Figure 5.35 shows that for a modulation frequency of 20Hz, the amplitude ratio exceeds 1.0 for a range of phases near the optimum control phase of –300 degrees, indicating that the first harmonic response is actually higher than the fundamental response. However, as the modulation frequency exceeded 20Hz, the amplitude ratio significantly decreased. The main reason for the change in the amplitude ratio is that as the modulation frequency is increased, the amplitude of the modulated response A_{mod} is much lower, for both the fundamental and the first harmonic response.

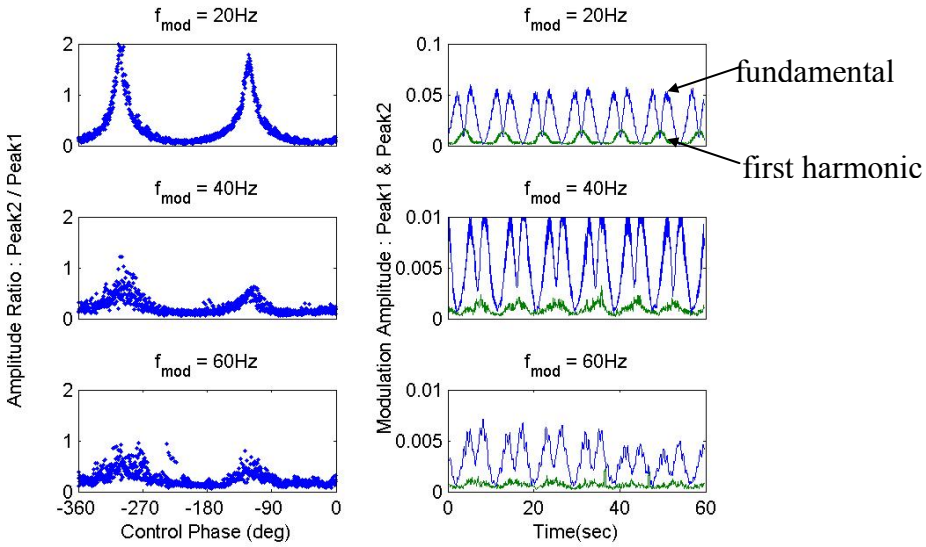

Figure 5.35: Effect of phase modulation frequency on the amplitude ratio, and on the amplitude of the fundamental and first harmonic

The following figures show what happened as the modulation frequency was held constant and the phase modulation amplitude was increased. Figures 5.36 and 5.37 show the response of the amplitude as the phase modulation amplitude is increased from 20 degrees to 80 degrees with the modulation frequency held constant at 20Hz. Increasing the phase modulation amplitude increases the resulting amplitude response to the control phase modulations. Equation 5.16 shows that the amplitude response at the fundamental frequency of the control phase modulations varies as θ, and that the first harmonic varies as θ^2. Thus, as the phase modulation amplitude θ increases, the response of the first harmonic increases faster than the response of the fundamental oscillation. In Fig. 5.35 it was shown that the amplitude ratio and the modulation amplitude both increased as the frequency of the modulations was lowered. Similarly, Figs. 5.36 and 5.37 show that both the amplitude ratio and the modulation amplitude increased as the modulation phase θ was increased. In other words, both studies show that the control parameters that cause an increase in modulation amplitude also cause an increase in the amplitude ratio between the first harmonic and the fundamental. Interestingly, Figs. 5.35 and 5.37 show

that the first harmonic response is much larger for the optimum control phase than for the phase of maximum driving.

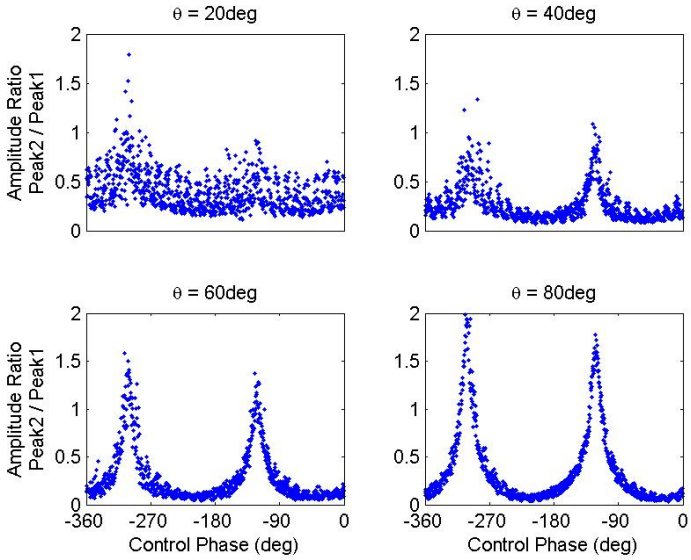

Figure 5.36: Effect of phase modulation amplitude, θ, on the amplitude ratio.

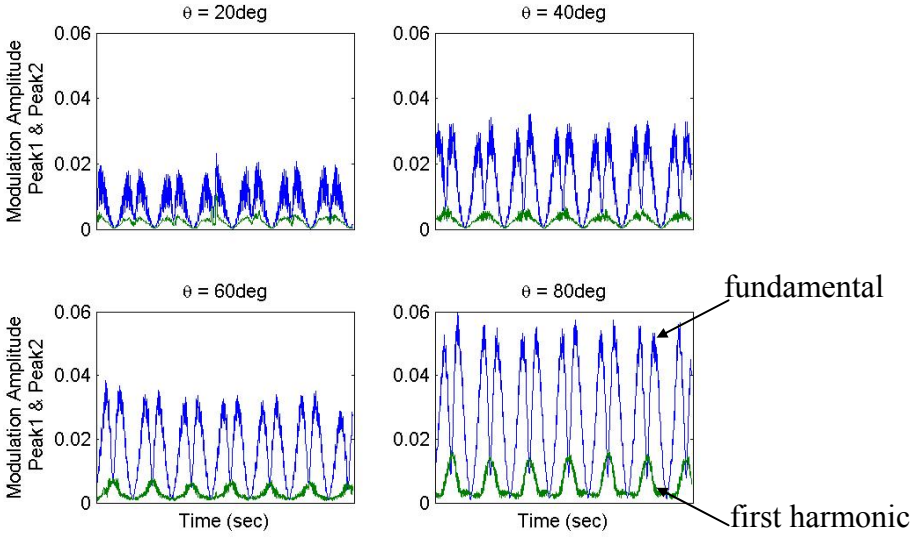

Figure 5.37: Effect of phase modulation amplitude, θ, on the amplitude response of the fundamental and the first harmonic.

Response of the Correlation Coefficient

Figure 5.38 shows that the correlation coefficient also decreases as the modulation frequency is increased. The correlation coefficients in this figure are for different phase modulation frequencies and a constant phase modulation amplitude of 80 degrees. The lower correlation coefficient at higher modulation frequencies is mainly due to the lower amplitude response at higher modulation frequencies. Thus, the signal-to-noise ratio is lower; consequently, the amplitude response is not as well correlated with the control phase modulations.

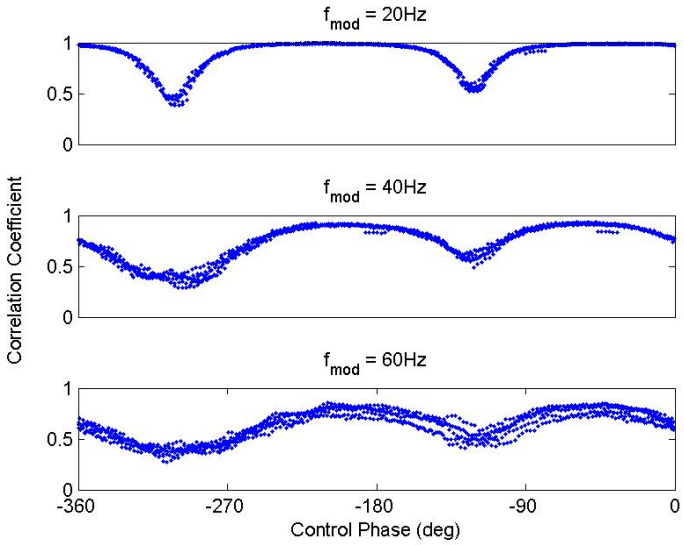

Figure 5.38: Effect of phase modulation frequency on the correlation coefficient

Figure 5.39 shows the effect of increasing the modulation amplitude on the correlation coefficient, with the modulation frequency held constant at 20Hz. As with the previous data, increasing the phase modulation amplitude increases the amplitude of the response function at the fundamental modulation frequency and, thus, the correlation coefficient. The net result of varying the phase modulation frequency or the phase modulation amplitude is the same, i.e., increasing the amplitude of the system response to phase modulations causes an increase in the amplitude ratio and in the correlation

coefficient, both of which result in a higher confidence of convergence to the optimum control phase.

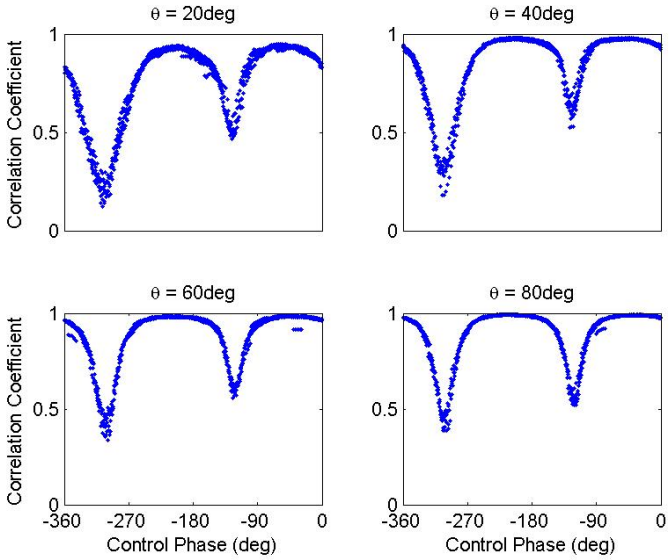

Figure 5.39: Effect of phase modulation amplitude, θ, on the correlation coefficient.

Phase Correlation Factor Response

As discussed previously, the correlation coefficient can be used to modify the adaptation step size. Also, the ratio of the amplitudes of the fundamental and the first harmonic can be used to determine how close the mean control phase is to the optimum control phase. However, the most important calculated parameter in the adaptive controller algorithm is the phase correction factor. The behavior of this function was described previously in the discussion of the van der Pol model. The same analysis will now be used to examine the data from the phase sweep experiments.

First, the phase modulation amplitude was held constant at 80 degrees, and the phase modulation frequency was varied from 20Hz to 60Hz. The measured data shown in Fig. 5.40 are very similar to the results predicted with the van der Pol model (see Fig. 5.13); i.e.,

1) For low modulation frequency, the curve is relatively flat, with a sharp transition from positive to negative at the optimum control phase.

2) As the modulation frequency is increased, the overall slope of the curve increases, and the transition near $\phi_{c,mean} = \phi_{optimum}$ is more gradual.

3) As the modulation frequency is increased, the nominal value of the phase correction factor approaches +/- 90 degrees. This occurs as the phase lag approaches the assumed value of –180 degrees,

4) The phase correction factor always crosses zero at the optimum control phase (-300 degrees), regardless of the modulation frequency.

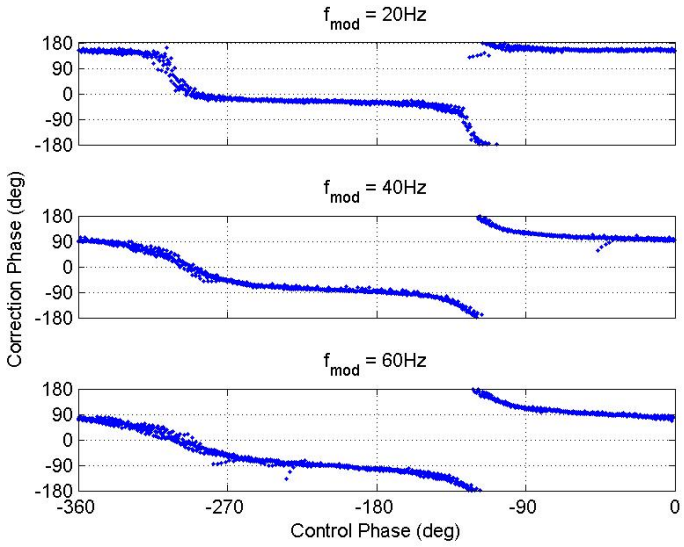

Figure 5.40: Effect of phase modulation frequency, f_{mod}, on the phase correction factor

Figure 5.41 shows the effect of the phase modulation amplitude θ on the phase correction factor for a phase modulation frequency f_{mod} = 20Hz. It shows that the phase modulation amplitude has no effect on the overall shape of the curve, although for small phase modulation values, there is increased uncertainty in the calculation, which is responsible for the increased scatter on the plot.

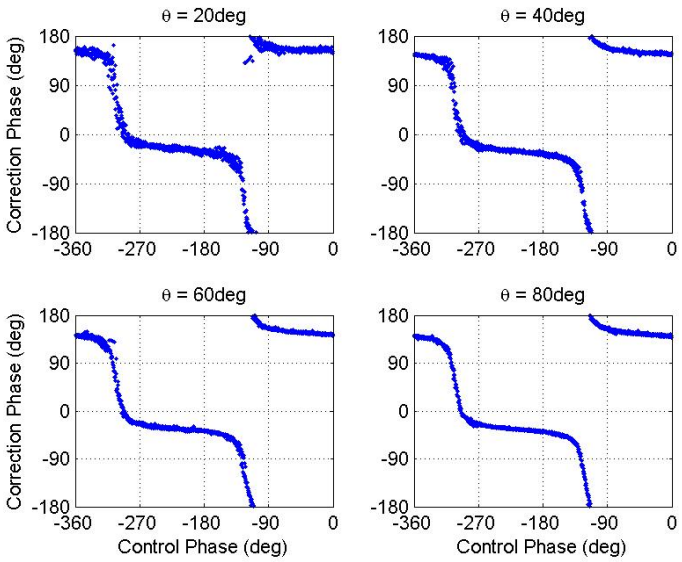

Figure 5.41: Effect of phase modulation amplitude, θ, on the phase correction factor

The following statements summarize the results of the adaptive controller characterization:

1) As the adaptive controller approaches the optimum control phase, the dominant amplitude response transitions from the fundamental to the first harmonic. This effect is more pronounced when the amplitude response to modulation is high. The amplitude of the modulation response can be increased by lowering the modulation frequency (f_{mod}) or by increasing the phase modulation amplitude (θ).

2) The correlation coefficient, which is a measure of confidence in the phase correction factor calculation, increases as the amplitude response increases (again) due to lowering of the phase modulation frequency or by increasing the phase modulation amplitude. The correlation coefficient is a minimum at the optimum control phase. The correlation coefficient can be used as a multiplier to slow down the adaptation process as the mean control phase approaches the optimum control phase.

3) The phase correction factor depends upon the phase modulation frequency. As the phase modulation frequency increases, the phase lag correction approaches –180 degrees. Also, the phase correction factor is equal to zero when the control phase equals the optimum phase. Finally, the phase correction factor does not depend upon the phase modulation amplitude, θ.

The above results indicate that the confidence in the control phase calculation would increase if the control parameters were chosen to maximize the amplitude of the response function, i.e., the phase modulation frequency should be as low as possible and the modulation amplitude should be as high as possible. However, a modulation frequency that is too low results in a phase lag correction that may not be close to –180deg. The next section discusses the performance of the adaptive controller in terms of its dependence upon the factors that were studied in this section.

5.4.2.2 Adaptive Controller Performance

There are several ways in which the performance of the adaptive controller can be evaluated. The most important measure is whether it ultimately converges to the optimum control phase. The experiments described in the characterization section have indicated that the developed adaptive controller correctly determines the direction of a phase adjustment in order to ultimately reach the optimal control phase. The next consideration is how quickly the optimum control phase is attained after a rapid change in operating conditions. Another consideration is the stability of the controller during a transient event. Finally, the adaptive controller must be compared to its fixed-phase counterpart to determine how well the pressure oscillations are damped, once it converges to the optimum control phase.

Overview of Experiments

In the first set of experiments that evaluated the performance of the adaptive controller, a phase shifter was added into the control loop, as discussed previously. This phase shifter allowed for a rapid change in the optimum control phase. In a typical "phase-shifter" experiment, the optimum control phase was abruptly changed by quickly rotating a knob on the analog phase shifter, thus adding a time delay to the measured pressure signal. Figure 5.42 shows the response of the adaptive controller to two phase shifts. The first shift occurred at t = 0.95 sec and shifted the optimum control phase from –300 degrees to –170 degrees. The controller responded by increasing the mean control phase until the oscillations were damped. At t = 2.3 sec, the phase shifter knob was rotated back to its original position, resetting the optimum control phase is to –300 degrees. The middle plot in this figure shows the dynamic pressure as a function of time. It shows the growth of the initial disturbance, followed by the damping effect of the adaptive controller. The bottom plot shows the observed amplitude calculated by the real-time observer.

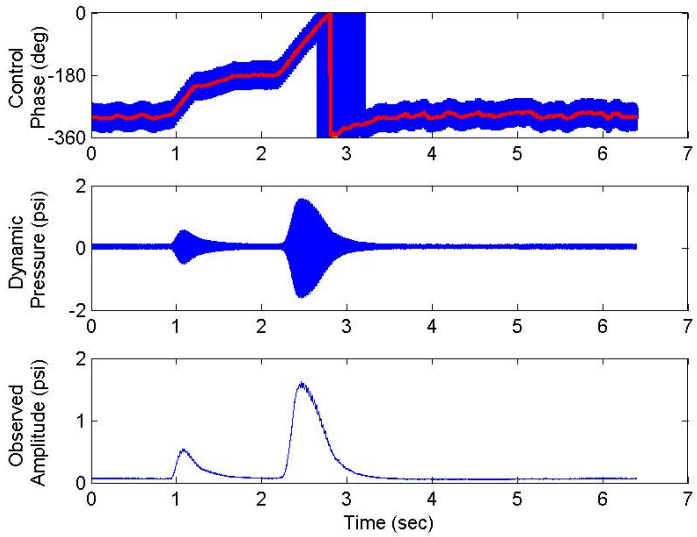

Figure 5.42: Typical "phase-shifter" experiment

One question that comes to mind when examining these plots is why the adaptive controller always seems to prefer to adapt with a positive phase adjustment to achieve the optimum control phase. In the above case, the most expedient path at t = 2.3 seconds would have been to lower the control phase steadily from –170 degrees until the new optimum phase of –300 degrees was reached. Instead, the controller chose the "longer" path, increasing the control phase by a total of 230 degrees instead of reducing the phase by 130 degrees. The answer lies in the nonlinearity of the system. Referring to Fig. 5.43, it can be seen that the van der Pol model predicts that a lightly damped system is driven to its maximum amplitude when $\phi_{rel,mean} = -90$. Therefore, if $0 < \phi_{rel} < 90$deg, the controller makes a negative adjustment; if $-90\text{deg} < \phi_{rel} < 0$, the controller makes a positive phase adjustment. However, if a large phase correction is required to "return" to the optimum control phase, the controller will always adjust in the same direction (in this example, a negative phase correction was applied). The net effect of this unidirectional phase adjustment is that the controller requires more time to make a large correction in one direction than in the other direction. In addition to the additional time required to converge to the optimum control phase, there is another effect – the controller briefly increases the instability amplitude by passing through the phase of maximum driving on its approach to the optimum control phase through the "longer" path. Consequently, there is a brief period during which the controller is driving the amplitude of the unstable system higher en route to finally damping the oscillations, as observed in Fig. 5.42. In these experiments, this behavior was exaggerated due to the large abrupt phase changes imposed upon the system. It is expected, however, that in practice (e.g., engine control) that the operating conditions would vary less rapidly, resulting in small control phase adjustments of less than 90 deg.

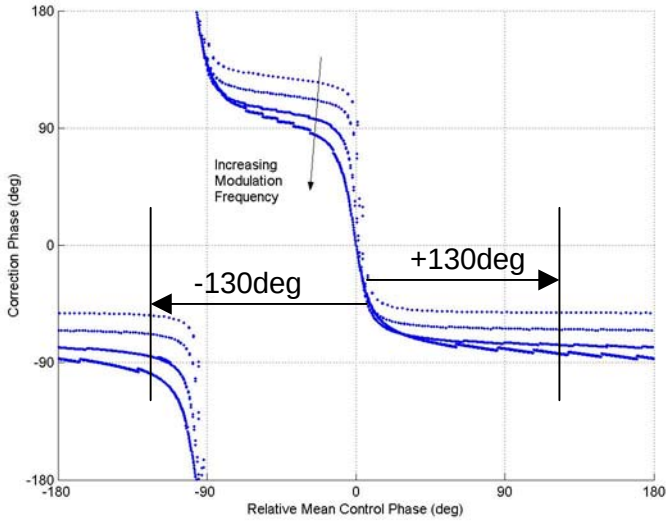

Figure 5.43: Nonlinear response of a lightly damped system causes asymmetry in the phase correction factor

The above explanation assumes that there is sufficient nonlinearity in the system to cause an asymmetry in the phase correction factor. However, the adaptive controller characterization experiments showed that the phase correction plots (see Figs. 5.40 and 5.41), did not exhibit the kind of asymmetry shown in Fig. 5.43. In both figures, increasing the control phase by nearly 180 degrees resulted in a negative phase correction, and increasing decreasing the control phase by nearly 180 degrees resulted in a consistent positive phase correction. There are two other sources of nonlinearity that were not investigated in the phase sweep characterization experiments. First, the mean phase sweep rate in those experiments was sufficiently slow as to provide a "quasi-steady" mean phase for observing the system response to control phase modulations. In the case of the adaptive controller, the mean phase was held steady during the course of an adaptation cycle. However, after this cycle was complete, a phase correction step was made in an attempt to damp the pressure oscillations. A typical value for the maximum step size was 10 degrees/step. If the modulation frequency was 40Hz, this step resulted in a mean phase change of 400deg/sec, which was 10 times faster than the sweep

frequency that was used in the characterization experiments. Although the mean phase is held constant through the adaptation cycle, delays in system response would have generally caused the amplitude response to be slightly skewed from what is expected.

The second source of nonlinearity is the gain that was applied to the control signal when the adaptive controller was on. A very important difference between these adaptive control experiments and the phase sweep characterization experiments discussed earlier was that the adaptation experiments did not use a constant amplitude control signal. During these experiments, the control signal amplitude was proportional to the amplitude of the pressure oscillations by a gain factor γ. The purpose of this gain factor was to provide the maximum response to large amplitude pressure oscillations for rapid damping and to provide minimal excitation when the pressure amplitude was low, thus preventing system destabilization. Using this gain factor instead of the constant amplitude signal in the previous experiments introduced additional nonlinearity into the system response. While this nonlinearity has not been modeled explicitly, it may tend to skew the phase correction factor in one direction or the other, thus resulting in the observed behavior.

Recovery Time

The goal of this first set of experiments was to determine how changes in key control parameters affect the rate of the adaptive controller's response to abrupt changes in the operating conditions, simulated by the phase shifter. In controls applications, a standard method for measuring system response to disturbances is the settling time, which is typically measured after a step change in the input function. In order not to confuse the measurement of interest in this case with the classical definition of settling time, the characteristic measure of the adaptation speed will be referred to here as the "recovery time", which is the time it takes for the controller to return to a pressure amplitude near its pre-disturbance level. Figure 5.44 illustrates how the recovery time

was measured. First, a moving average smoothing function was applied to the measured amplitude, and the derivative of the pressure amplitude was calculated. Then, the derivative of the amplitude function was used to find the maximum slope of the amplitude. The amplitude function at this maximum derivative point was measured and called the "reference point." The "starting point" of the calculation was taken as the point where the amplitude increased above 25 percent of the amplitude at the "reference point" (this point is slightly before the maximum derivative value is measured). Next, the amplitude was measured at the starting point. Finally, the recovery time was measured as the time required for the adaptive controller to return the pressure amplitude to a value below the amplitude at the starting point.

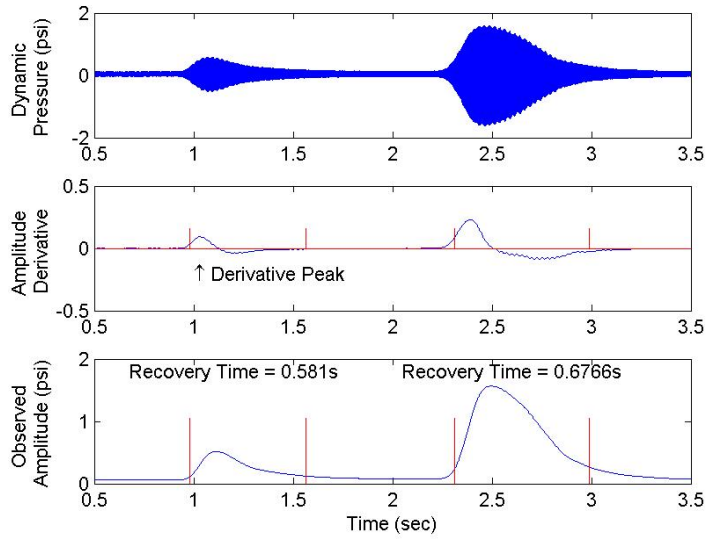

Figure 5.44: Method for measuring the "recovery" time of the controller

Over the course of several experiments, the following parameters of the adaptive controller were varied: a) phase modulation frequency (f_{mod}), b) phase modulation amplitude (θ), and c) the maximum adaptive step size ($\Delta\phi_{max}$). The adaptive step size determines the maximum possible correction to the control phase. A small adaptive step

size is slower to respond to abrupt changes in the optimum control phase, but is less susceptible to "wandering" in search of a better control phase after the optimum phase has been found. Note that the step size is scaled by the correlation coefficient, which is always less than 1.0. As the controller nears the optimum control phase, the correlation coefficient is reduced and the step size is scaled downward. The effect of this modification is to slow the response of the controller as it approaches the optimum control phase. For example, in the top plot of Fig. 5.42, there is a change in the rate of adaptation at t = 1.2 sec and also at t = 2.8 sec. This change in adaptation rate is due to the reduction of the correlation coefficient as the adaptive controller gets close to the optimum control phase.

Figure 5.45 describes the effect of the phase modulation amplitude θ on the recovery from an abrupt phase change. For the three test cases shown, the modulation frequency, f_{mod} was 40Hz and the maximum adaptation step size was 8 degrees. There are four significant attributes to note in this figure:

1) The recovery time is approximately the same for the two cases with the higher modulation amplitude. All three cases should have the same recovery time due to their common maximum adaptation rate. However, in the case of the 20 degree modulation amplitude, the correlation coefficient is smaller due to the small amplitude of the modulation (see Fig. 5.39). The reduction in correlation coefficient reduces the actual adaptation rate, thus slowing the adaptation process. Note that at its steepest point, the rate of adaptation for 20 degree modulation is approximately the same as the maximum rate for the 40 degree modulation.

2) The increased phase modulation amplitude is visible by the larger amplitude oscillations in the observed pressure amplitude between 40 degrees and 80 degrees. It is difficult to see the amplitude oscillations for

the 20 degree modulation because of significant noise on the signal for this test case.

3) The "baseline" amplitude (e.g., at t = 1.5 sec) increases as the phase modulation amplitude increases. This amplitude, representing the controlled amplitude when the optimum phase is achieved during active modulation, is elevated due to a higher mean deviation from the optimum control phase, which will be discussed later in this chapter.

4) Even though the "baseline" amplitude is maximum at the largest phase modulation amplitude, the peak amplitude after the abrupt phase shift was minimum because of the short recovery time.

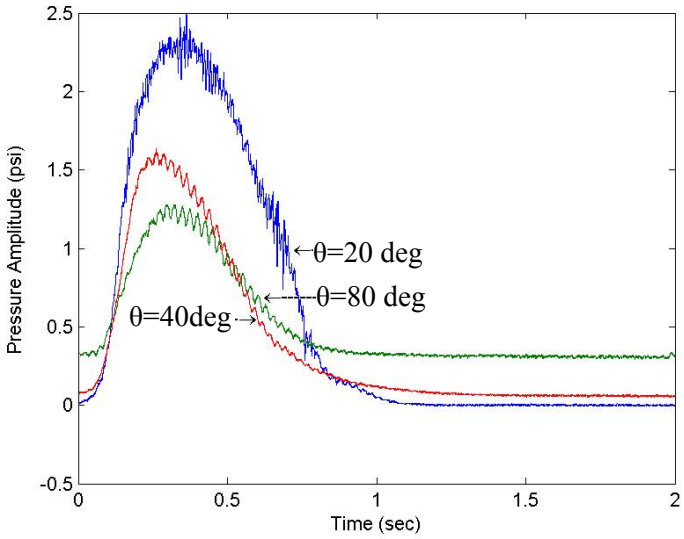

Figure 5.45: Dependence of the pressure amplitude recovery time and baseline amplitude on the phase modulation amplitude, θ.

Figure 5.46 describes the impact of the maximum phase adaptation step size on the recovery time, for both positive and negative phase adjustments. In each case, the first pulse requires a positive phase adjustment (+130 degrees) to bring the oscillations under control, and the second pulse requires a negative phase adjustment (-130 degrees).

However, as discussed above, the controller always makes a positive adjustment for large phase changes due to the nonlinear response of the system, requiring the controller to increase the control phase by a total of 230 degrees during the second pulse recovery, leading to longer recovery times. As the maximum adaptation step size ($\Delta\phi_{max}$) is increased, the recovery time is shortened and the peak amplitude is reduced.

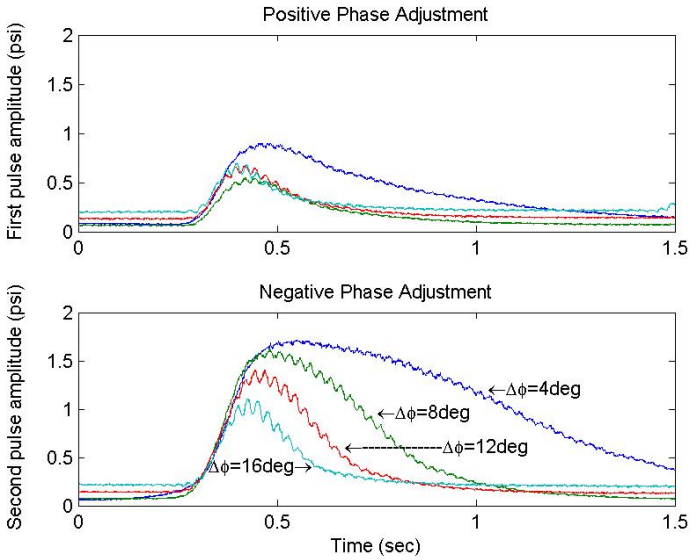

Figure 5.46: Dependence of the pressure amplitude recovery time and baseline amplitude on the maximum phase adaptation step size, $\Delta\phi_{max}$.

Figure 5.47 shows the recovery time dependence upon the maximum allowable step size, $\Delta\phi_{max}$, and the modulation frequency, f_mod for several test cases. The plots on the left describe the recovery time for the first pulse, and those on the right describe the recovery time for the second pulse. The recovery times for the second pulse (right) are always longer than the recovery times for the first pulse (left) because of the unidirectional phase adaptation. However, as the modulation frequency increases, the difference of the recovery time for the first and second pulses decreases. As the maximum phase change per step ($\Delta\phi_{max}$) is increased, the required number of adaptation cycles to reach the optimum phase decreases, as does the recovery time. The 20Hz

modulation rate clearly does not provide optimum performance. Both the 40Hz and 60Hz modulation rates appear to provide adequate recovery times.

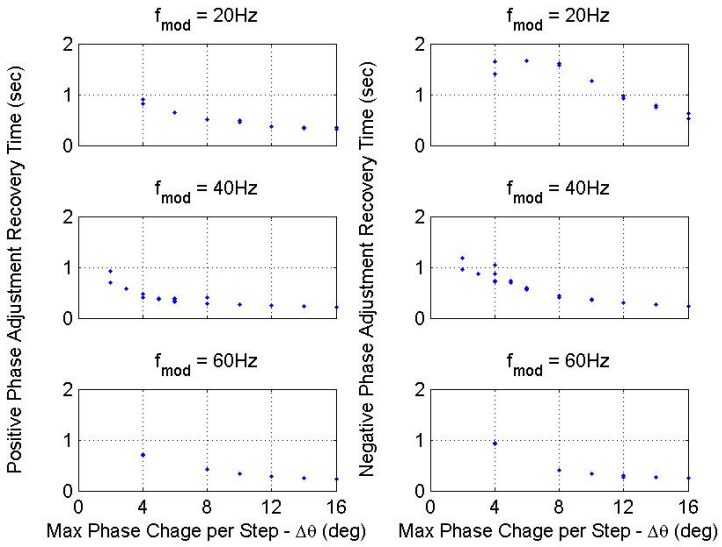

Figure 5.47: Recovery time as a function of the modulation frequency and the maximum control phase correction step size.

Figure 5.48 presents the same data plotted as a function of maximum adaptation rate, i.e., the maximum rate at which the controller converges to the proper control phase. This number is simply the maximum step size multiplied by the adaptation rate ($f_{mod}*\Delta\phi_{max}$). The data in Fig. 5.48 indicates that the three modulation frequencies provide roughly equivalent performance if the maximum adaptation rate is higher than 200deg/sec. When the maximum adaptation rate is lower than 200 degrees/sec, the recovery time can increase dramatically, especially if the calculated correlation coefficient is low due to low modulation amplitude.

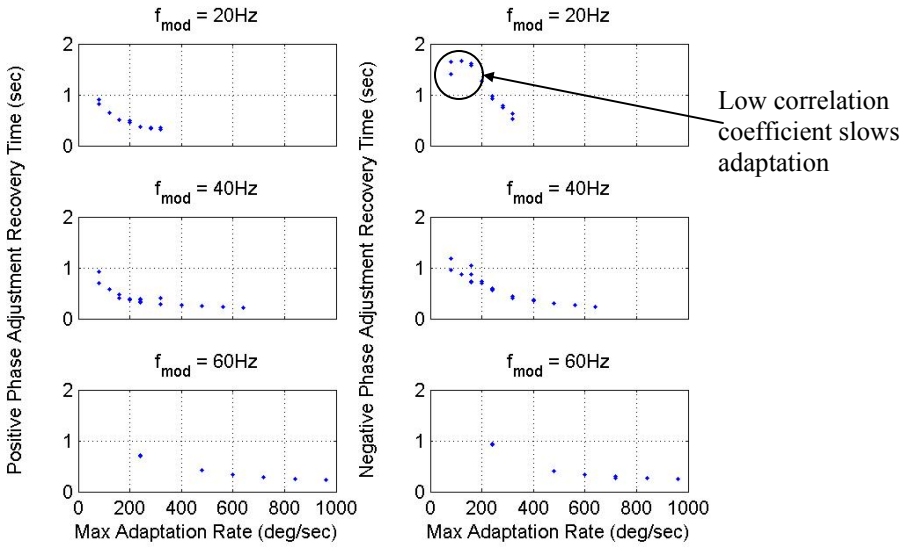

Figure 5.48: Recovery time as a function of the modulation frequency and the maximum adaptation rate

Adaptive vs. Fixed-Phase Performance

It is also of interest to compare the adaptive controller performance in damping an instability with that of a fixed-phase controller once the optimum control phase has been identified. As illustrated in Figs. 5.45 and 5.46, increasing the phase modulation amplitude lowers the damping effectiveness of the controller when the optimum control phase has been identified. Figure 5.49 shows the dependence of the ratio of the controlled pressure amplitudes for the adaptive controller and the fixed-phase controller measured in dozens of experiments in the acoustic feedback facility. As the modulation phase magnitude increases, this ratio increases, indicating that the adaptive controller's effectiveness at damping pressure oscillations is somewhat limited with higher phase modulation amplitude.

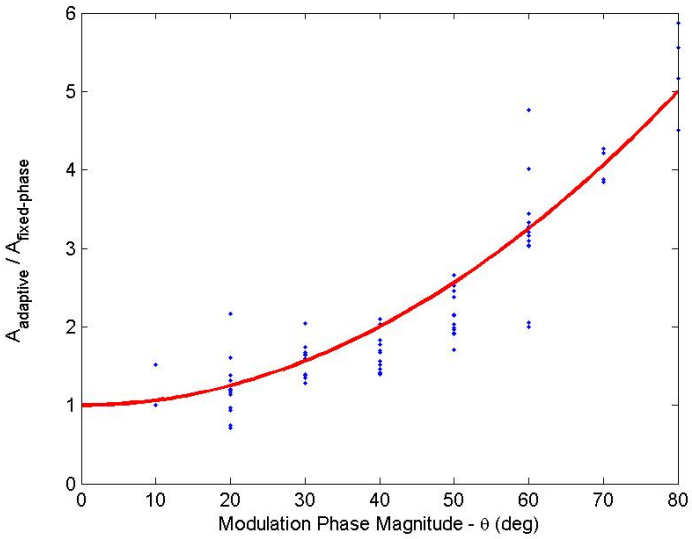

Figure 5.49: Comparison of the controlled amplitudes with the adaptive controller compared to the fixed-phase controller

The reason for the lower damping is that as the adaptive controller modulates the control phase, it produces a mean effective phase error that is equal to $2\theta/\pi$ (mean distance under the sine curve). For example, if the phase modulation amplitude is 50 degrees, there is a mean phase error of approximately 32 degrees due to the adaptation process. The effect of this mean phase error varies from system to system. In the case of the acoustic feedback facility, where the background noise is low, the amplitude of the controlled system can be very small. A mean phase error of 32 degrees may or may not have a significant impact on the overall amplitude levels, depending upon factors such as background noise and control authority. This effect must be weighed against the error induced by using the wrong control phase for a fixed-phase controller. Figure 5.50 demonstrates the effect of having the wrong control phase when using a fixed-phase controller. For this experiment, the adaptive control was turned off and fixed-phase control was used instead. The control phase was varied in 10 degree increments above and below the optimum control phase. In this case, using the optimum control phase damps the pressure oscillations to an amplitude of 0.10psi. An error of +/-30 degrees

from the optimum control phase results in an increase in controlled amplitude from .10 to approximately 0.22psi, an increase of 120 percent. According to the correlation described above, the same increase should be observed when the adaptive controller modulates the phase at $30*\pi/2 = 47$deg According to curve fit shown in Fig. 5.49, using a phase modulation amplitude of 47 degrees results in an increase of the controlled amplitude by approximately 120 percent (on average). This brief analysis indicates that the mean phase error reduces damping by an amount approximately equal to having an error in the control phase of $2\theta/\pi$. Note that these results depend upon several factors: the level of background noise, the controller gain, and the amount of damping in the unstable system. However, this illustration shows one of the key tradeoffs when the adaptive controller is used: as the modulation phase magnitude is increased to provide quicker response, the damping effectiveness is reduced.

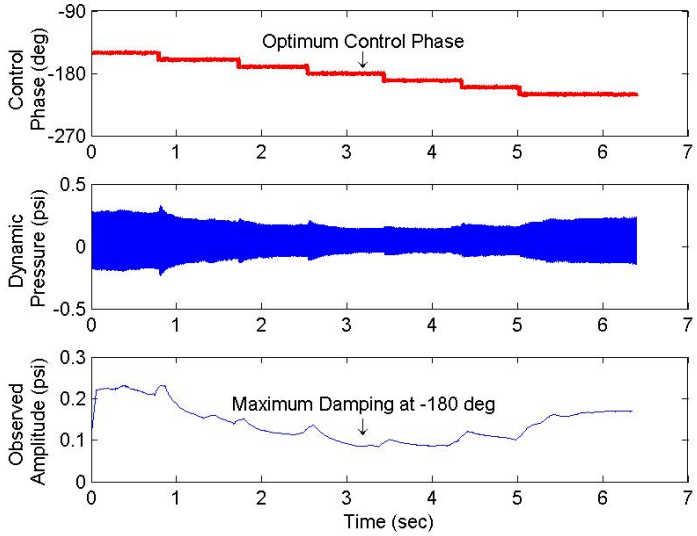

Figure 5.50: Effect of a phase error when using the fixed-phase controller

The question of damping effectiveness ultimately is a question of what is an acceptable level of pressure oscillations. Figure 5.51 shows results from a typical

experiment in which the adaptive controller was switched on and off. When the controller was switched off, the dynamic pressure rapidly increased to its limit cycle amplitude of 0.95psi. When the adaptive controller was switched back on, the oscillations were quickly damped to an amplitude level of approximately 0.1psi, a 20dB reduction, which by most standards is an acceptable level of damping. However, this damping performance strongly depends upon several factors, including the feedback mechanism of the instability, external excitation sources, and the control (actuation) authority. For example, a system that is mostly driven by random noise is generally less controllable than a system whose driving is solely provided by a feedback mechanism.

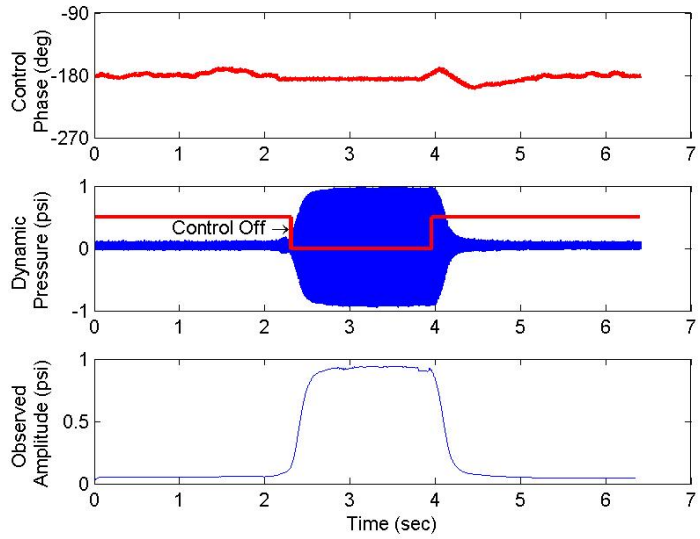

Figure 5.51: Dependence of the pressure amplitude response to adaptive control

5.5 Summary

This chapter presents the development and characterization of the adaptive control algorithm and compares its formulation and application with the online identification algorithm introduced in Chapter 4. The controller continually adapts to find the control phase where damping is optimized. Because of its performance characteristics, the developed adaptive controller is well-suited for control of Dry Low NOx gas turbine combustors and for control of a variety of other combustors as well.

5.5.1 Controller development and model predictions

The advantages of the adaptive controller over the fixed phase controller were examined. In particular, it was shown that the adaptive controller is more robust than the online identification algorithm for the following reasons:

- The adaptive controller continually seeks the optimum control phase, which is especially important when encountering changes in operating parameters or rapid transient events.
- It does not require exact knowledge of the phase lag parameter.
- It experiences only cause a small delay in converging to the optimum control phase due to a sudden disturbance rather than causing incorrect identification of the optimum control phase.

The phase correction factor was introduced and studied using both linear and nonlinear models.

- It was shown that the phase correction factor approaches +/-90 degrees when the relative control phase (distance from the optimum control phase) is sufficiently removed from zero.

- For low phase modulation frequencies, f_{mod}, this phase correction factor curve is relatively flat and is displaced from the "ideal" +/-90 degree position because of the presence of a phase lag. If the phase modulation frequency is too low, the phase lag error can cause the adaptive controller to move in the wrong direction.
- As the phase modulation frequency is increased, the phase correction factor approaches the +/-90 degree asymptotes, but the slope of the curve increases.
- The phase correction factor curve crosses zero at the optimum control phase, regardless of the phase modulation frequency.
- The phase correction factor curve does not depend upon the phase modulation amplitude, θ.
- For lightly damped systems, the phase of maximum driving is not equal to –180 degrees, which causes the phase correction factor curve to be asymmetric. This asymmetry is the most likely cause of the observed tendency of the controller to make phase corrections in one direction (positive or negative).

The control algorithm is based upon some assumptions of linearity in the system response to control phase modulations. It is assumed that the control phase modulations are small, and that the resulting oscillations in the pressure amplitude are quasi-sinusoidal and linear. This assumption holds in the "neutral response" region of the phase map. However, as the optimum control phase is approached, this assumption is no longer valid.

The limitations of this assumption were explored and it was shown that as the adaptive controller approaches the optimum control phase, a first harmonic of the phase modulation frequency appears in the amplitude response. It was shown in later experiments that this first harmonic is very weak for low phase modulation amplitudes, as predicted by the model. As the phase modulation amplitude increases, so does the

response of the first harmonic function. Very close to the optimum control phase, the first harmonic may become larger than the fundamental response.

5.5.2 Experimental results

Several experiments were performed using an acoustic test facility and a liquid fuel ramjet combustor simulator. The liquid fuel experiments demonstrated the following performance characteristics of the adaptive controller on a realistic combustion system:

- Ability to correctly identify the optimum control phase
- Ability to rapidly adjust to abrupt changes in the optimum control phase
- Ability to maintain control of a combustor through transient conditions

A detailed study of the influence of the adaptive control parameters was conducted in the acoustic feedback facility. This study consisted mainly of two types of experiments:

- Characterization experiments to determine the response of the system to control phase modulations over the entire range of possible control phases
- Performance experiments to test and optimize the adaptive controller parameters

Table 5.3 describes the various control parameters that were investigated, and the findings concerning each of them:

Table 5.3: Key Control Parameters

Parameter	Symbol	Unit	Description	Effects of increasing parameter
Phase Modulation Frequency	f_{mod}	Hz	Frequency at which the control phase is modulated	• Phase lag approaches –180 deg; improves phase lag assumption • Added slope to phase correction factor curve • Lower amplitude response; lower correlation coefficient • Lower recovery time for fixed step size
Phase Modulation Amplitude	θ	deg	Amplitude of the control phase modulation	• Increased amplitude response; increased correlation coefficient • Increased mean control phase error; reduces damping effect of control • Increased response of first harmonic near the optimum control phase
Maximum step size	$\Delta\phi_{max}$	deg	Maximum size of the control step that can be made per adaptation cycle	• Lower recovery time for fixed modulation frequency • Increased "wandering" about the optimum control phase after convergence

5.5.3 Parameter Selection Strategy

The analysis provided in this chapter presents some of the tradeoffs between the different control parameters; however, little guidance has been provided concerning the initial choice of these parameters for the adaptive controller. While the there are no specific rules for choosing the adaptive control parameters, the following guidelines emerge from this study:

- The minimum modulation frequency should be at least 0.1 times the unstable natural frequency of the combustor, thus improving the phase lag approximation of –180 degrees. Typically, modulation frequencies in the range 0.15 – 0.25 * f_0 work well. As the modulation frequency is further

increased, the amplitude response is diminished, as is the correlation coefficient.

- The phase modulation amplitude should be at least 40 degrees, thus improving the amplitude response to the control phase modulations, and the correlation coefficient. As the modulation amplitude is further increased, the mean phase error is increased, which reduces the damping effectiveness of the adaptive controller.
- The maximum step size should be approximately 10 degrees. This step size strikes a balance between fast adaptation (high values) and the tendency of the adaptive controller to "wander" in search of a better control phase, even after the optimum phase has been found.

A note about phase lag: it has been assumed throughout these analyses and experiments that the system to be controlled has a second-order response, thus resulting in a phase lag of 180 degrees. Actually, this phase lag value represents the *minimum* lag that can be achieved for a given modulation frequency. This phase lag does not take into account time delays due to, e.g., actuator response, fuel evaporation, mixing and reaction processes. These time delays must be accounted for in addition to the second order phase lag of 180 degrees. However, as discussed earlier in this chapter, these values need not be precisely known for effective performance of the adaptive controller. While it would be beneficial to have as good an estimate of these delays as possible, as long as the total phase lag can be determined to within +/-90 degrees, the developed adaptive controller should perform well.

CHAPTER 6

CONTROLLABILITY LIMITATIONS

This chapter describes an experimental and theoretical investigation of the limitations of systems that actively control combustion instabilities. Results of active control tests on a variety of combustors indicate that the characteristics of the unstable combustor inherently limit the controller's effectiveness, regardless of the magnitude of its control authority and ability to finely tune the gain and phase of the control signal. An examination of time domain pressure signals in actively controlled combustors revealed that one source of control system limitation is related to a "beating" phenomenon that is characterized by frequent and irregular "necking" of the amplitude of the pressure oscillations [61,62]. This chapter describes an investigation into possible causes of this "beating" in controlled combustors. The theoretical phase of this study simulated the behavior of controlled and uncontrolled combustors, accounting for the presence of a time delay in the control loop, random noise forcing and a positive feedback loop that drove the instability. The predictions of the simulations were compared with measured data obtained in studies of the liquid fuel ramjet combustor simulator. Open loop experiments were performed to determine the time delay of the control loop that was subsequently incorporated into the model. Simulations of the performance of a combustor controlled in a closed loop indicate that the "beating" phenomenon depends in a complex manner upon the relationship between the random noise and the feedback process that drive the instability. Furthermore, the results suggest that instead of attributing the "beating" phenomenon to a poorly performing controller, its cause is likely the combined effects of random excitation and the inherent time delay in the control loop.

6.1 Background

While there has been significant progress in the development of Active Control Systems (ACS), future progress in this area will require better understanding of the fundamental processes that control the operation and performance of these ACS. Development of such an understanding will require that we determine, e.g., why are some control systems more effective than others? or why can a specific ACS satisfactorily damp combustion instabilities in one combustor over a certain range of operating conditions and fail to attain the same success in other combustors? To answer these questions, it is necessary to understand the physical processes that limit the controller's effectiveness at different combustors and operating conditions.

In an effort to answer the above questions, the study presented in this chapter investigated the effects of the control loop's time delay and combustor noise upon the controllability limits of an ACS in an unstable liquid fuel combustor. Hibshman et al [61] and Banaszuk et al [62,63] have previously studied the role of time delays on the controllability of a liquid fueled gas turbine combustor at UTRC. They presented a detailed analysis of the "peak-splitting" phenomenon that occurs when large control actuation is used to control an unstable system with a large time delay, and showed the resulting limits on the controllability of the system. They used a linear model driven by broadband noise to generate pressure oscillations in the model. They included analysis of the FFTs of the pressure signal and performed a Nyquist analysis to predict the "beating" exhibited by the combustor pressure oscillations. This study extends the UTRC analysis by examining the time dependence of the pressure oscillations in actively controlled and uncontrolled combustors under various operating conditions in an effort to elucidate the causes of the "beating" phenomenon. The results of these simulations are correlated with those of a parallel experimental study to better understand the control system's limitations.

Experiments described in this chapter were performed on the Liquid Fuel Ramjet Combustor Simulator described in Section 2.3. The unstable system was simulated using the model shown in Fig. 6.1. The top block represents the plant (in this case a combustor) with an open loop transfer function ($\kappa_1 s$ / …) and internal feedback mechanism represented by κ_{plant} and τ_{plant}. An external noise source drives the plant, and the resulting response of the plant is determined. The active control system is shown as a separate external feedback loop. The active control is represented by the blocks $\kappa_{control}$ and $\tau_{control}$. Note that the unstable plant can be forced with an external noise source and/or or a positive feedback loop that simulates the process that drives combustion instability.

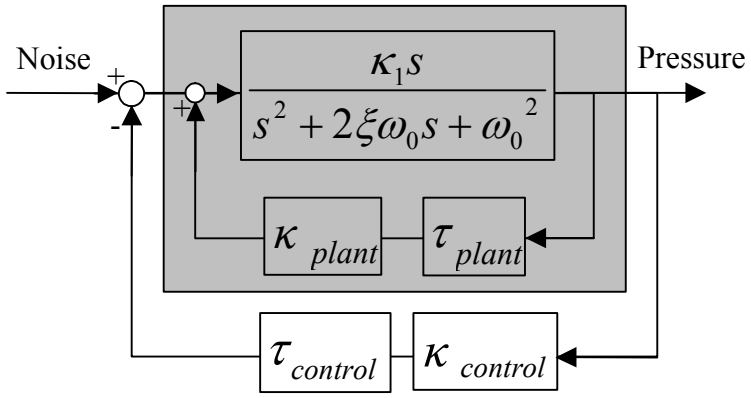

Figure 6.1. A block diagram of the investigated actively controlled, unstable combustor model.

6.2 Open Loop Response

This section describes results of theoretical and experimental studies of the open loop response of the investigated combustor to various excitations. The objective of these studies was to gain insight into the dependence of the of the ACS performance upon the time delay in the control loop, system noise and the characteristics of the destabilizing mechanism.

To elucidate the processes that drive the pressure oscillations in unstable combustors, we first examined the characteristics of the unstable pressure oscillations in the investigated combustor. Figure 6.2 shows a typical time trace of the pressure in the uncontrolled combustor operating at an equivalence ratio Φ=0.8. The pressure trace exhibits irregular "beating" of the pressure amplitude. To gain insight into the causes of the "beating" phenomenon, we first investigate the variation of the phase and frequency of the unstable oscillations with time by correlating the unstable oscillations with a reference sinusoidal signal, which has a fixed frequency that equaled that of the unstable oscillations. Figure 6.3 shows such a correlation, for the time interval between t=0.9 and t=0.96 seconds where one of the "necks" occurred. In this correlation, the frequency and phase of the reference signal were chosen to equal those of the combustor pressure oscillations during the initial time interval of the comparison, i.e., in the time interval immediately after t=0.9 seconds. An examination of Fig. 6.3 shows that the frequency of the unstable oscillations remains unchanged while the phase between the pressure and reference signal oscillations changed by a finite amount at the "necks" and remained practically constant during the time intervals between the "necks". Specifically, Fig. 6.3 shows that the phase of the pressure oscillations changed by approximately 45 and 135 degrees at the "necks" at t=0.915 and t=0.955 seconds, respectively. The pressure oscillations are shown with a reference signal whose frequency and phase matched those of the pressure signal during the initial period of the oscillations (i.e., when t=0.90 seconds and shortly thereafter).

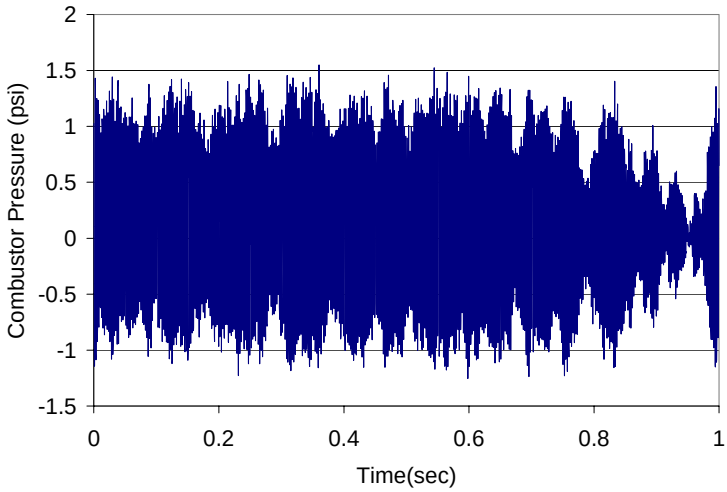

Figure 6.2. A time trace of measured, uncontrolled, combustor pressure.

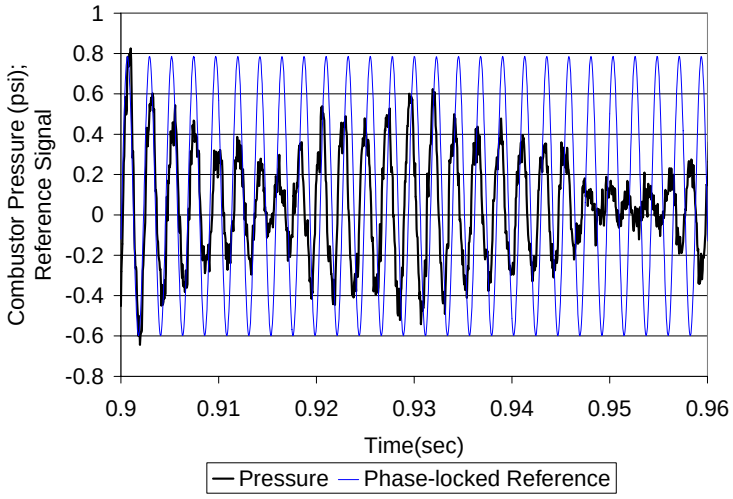

Figure 6.3. A correlation of the time trace of the pressure shown in Fig. 6.2 during the time interval between t = 0.9 and t=0.96 seconds with a reference signal.

To determine whether the above described phase behavior was caused by combustor noise, we simulated the response of the combustor to white noise excitation. This problem was also studied by Banaszuk et al. [62] who theoretically investigated the response of a stable linear resonator to white noise excitation. This simulation was performed by setting the gains on both feedback loops in the model, see Fig. 6.1, to zero to eliminate the effects of driving and active control and then forcing the resonator with

random noise. Figure 6.4 shows a typical simulation of the system's response during a period of one second. As in Fig. 6.2, it also shows evidence of "beating", indicating that random noise can produce such behavior in an unstable combustor. The simulated combustor response was then correlated with a reference signal in a manner similar to that in which the combustor pressure was correlated with a reference signal in Fig. 6.3. It is noteworthy that in both cases the phase changes by a fixed amount when it passes through the "neck". This finding is somewhat surprising given the fact that it was caused by white noise excitation. Nevertheless, the correlations of the measured data and the results of the simulation in Figs. 6.4 and 6.5, respectively, suggest that the characteristics of unstable combustor oscillations are affected by the presence of white noise.

As in Fig. 6.3, the pressure signal is displayed with a reference signal whose frequency and phase matched those of the simulated pressure oscillations during the initial period of the oscillations (i.e., when t=0.25 seconds and shortly thereafter). On the other hand, a comparison of the measured and simulated pressure oscillations over a longer time interval, as shown in Figs 6.2 and 6.4, respectively, shows considerable differences between the two plots. Specifically, the cycle-to-cycle variations generated by the white noise forcing in the simulation are much more pronounced than those exhibited by the measured data. These comparisons suggest that while white noise probably affects the characteristics of the oscillations in unstable combustors, other processes should be considered when trying to understand the observed phenomena.

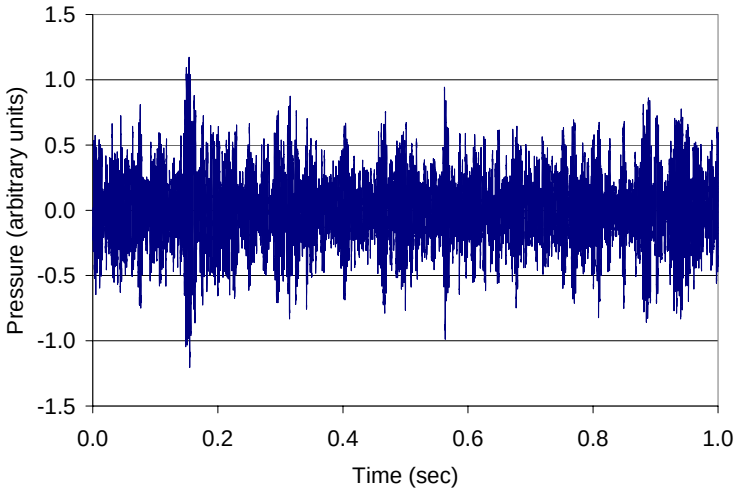

Figure 6.4. A time trace of the simulated combustor pressure oscillations forced by white noise excitation in an uncontrolled combustor.

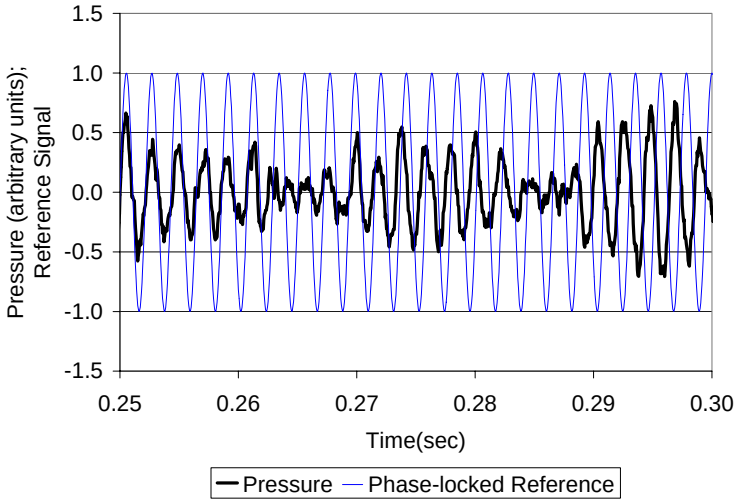

Figure 6.5. A correlation of a time trace of the pressure shown in Fig. 6.4 during the time interval between t = 0.25 and t=0.30 seconds

Next, we studied the effect of the time delay between the response of the heat release in the combustor and the actuator command. This time delay is determined by measuring the pressure response to periodic pulsing of the fuel flow rate. Experiments were carried out at two operating conditions with same airflow rate but different equivalence ratios of 0.8 and 1.0. Figures 6.6 and 6.7 show the actuator command consisting of a constant value with periodic negative pulses, which causes the valve to

open, and the measured pressure signal during long and short time intervals respectively. In addition, Fig. 6.7 shows the measured fuel flow rate and a reference signal similar to the one shown in Figs. 6.3 and 6.5. The frequency and duration of the pulses in the command signal were 20 Hz and one millisecond, respectively. Figure 6.6 shows that a sharp pressure spike follows each pulse in the actuator command. Note that a negative pulse of the control signal command results in an increase in the fuel flow rate. It is noteworthy that in addition to exhibiting synchronized spikes, the pressure in Fig. 6.6 exhibits quasi-random amplitude variations that are not synchronized with the command signal. The plots in Fig 6.7 indicate that while the fuel flow rate responds instantaneously to the command, more than two cycles elapse before the combustor pressure responds to a command signal pulse. The response of the pressure oscillations to a command signal pulse starts when it exhibits an abrupt change in amplitude and phase with respect to the reference signal. Note that the pressure is correlated with a reference signal whose frequency and phase equal those of the pressure signal when t = 0.39 seconds and shortly thereafter. The time dependence of the fuel flow rate into the combustor is shown at the bottom of the figure. The time delay between the control signal pulse and resulting response of the combustor pressure oscillations is marked by an arrow. Note that the fuel flow rate responds instantaneously to the pulse in the command signal and that the increase in fuel flow rate increases the amplitude of the pressure oscillations.

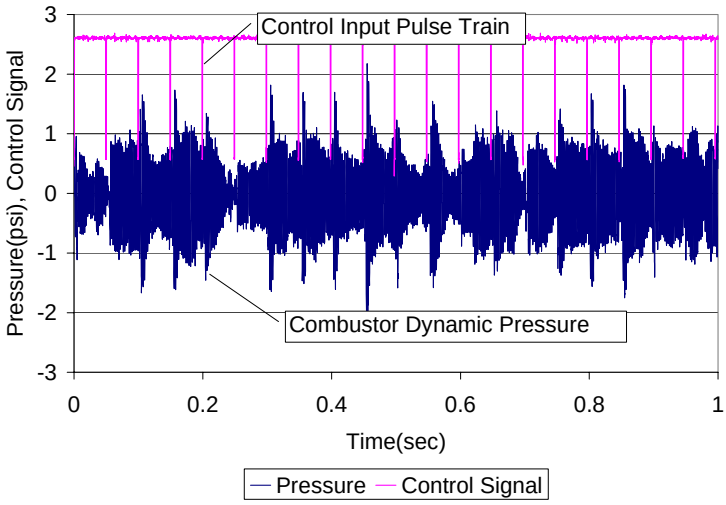

Figure 6.6. Time dependence of the actuator control signal and combustor pressure measured in open loop response tests at equivalence ratio Φ=0.8.

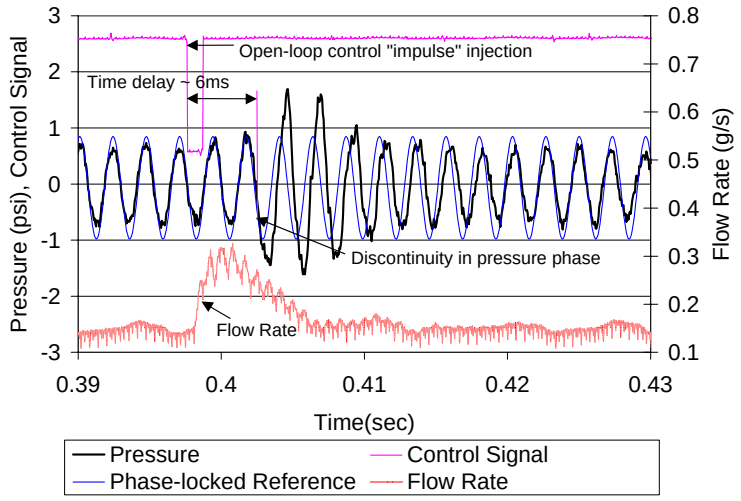

Figure 6.7. Time dependence of the control signal and combustor pressure shown in Fig. 6-a during the time period between t=0.39 and t=0.43 seconds.

The response of the combustor when operated at an equivalence ratio of 1.0 to similar open loop forcing is described in Figs. 6.8 and 6.9. However, the flow rate response is omitted in Fig. 6.9 to simplify the figure. Figure 6.8 shows that in contrast to the pressure spikes that were excited when the equivalence ratio equaled 0.8, the presence of pulses in the command signal produced a significant reduction in the pressure amplitude when the equivalence ratio equals 1.0. Figure 6.9 shows that the response to

the pulse is delayed by 5 to 6 milliseconds (note the period of the oscillations equals 2.25 milliseconds). Note that the pressure is correlated with a reference signal whose frequency and phase equal those of the pressure signal when t=0.21 seconds and shortly thereafter. The time delay between the control signal pulse and resulting response of the combustor pressure oscillations is marked by an arrow. In contrast to the results shown in Fig 6.7 , in this case the "pulsed" increase in fuel flow rate decreased the amplitude of the pressure oscillations.

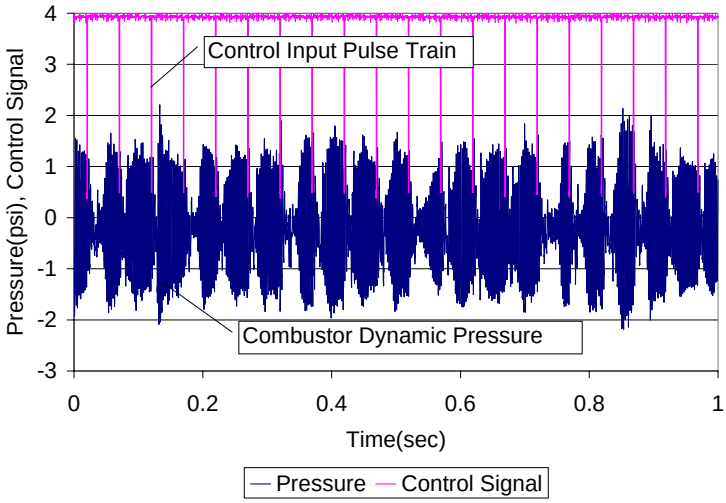

Figure 6.8. Time dependence of the actuator control signal and combustor pressure measured in open loop response tests at equivalence ratio Φ=1.0.

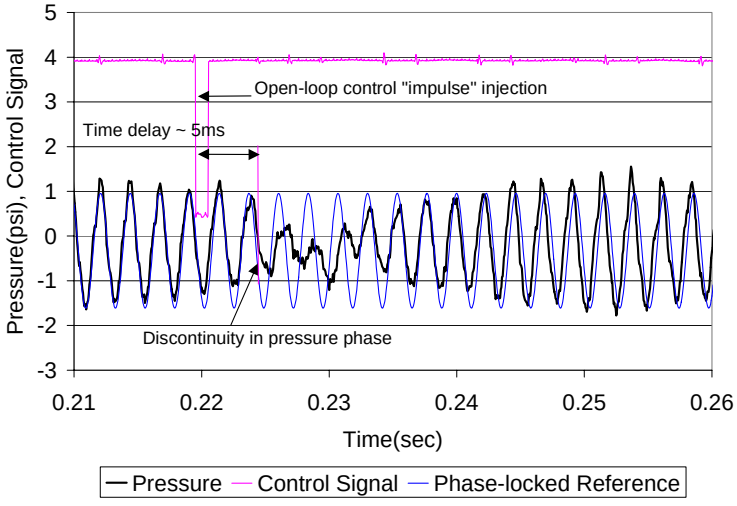

Figure 6.9. Time dependence of the control signal and combustor pressure shown in Fig. 7-a during the time period between t = 0.21 and t = 0.26 seconds.

The different response of the pressure oscillation to a pulse in the fuel flow rate in the two operating conditions may be explained as follows. At the leaner operating condition, the additional fuel flow rate introduced by the pulse can readily react with available air and, thus, produce an additional heat release that increases the amplitude of the pressure oscillations. In contrast, at an equivalence ratio of 1.0 the increase of fuel flow rate by the pulse likely creates local fuel rich regions that may cause temporary extinction of the flame. This, in turn, reduces the magnitude of the heat release oscillations and, thus, the magnitude of the pressure oscillations.

6.3 Closed Loop Response

The results of the above described studies suggest that the open loop response of the oscillations in the investigated liquid fuel combustor are affected by persistent random noise excitation and a significant pure time delay in the control loop. Since it was anticipated that these phenomena would significantly impact the performance of the ACS, the effect of these phenomena was studied theoretically using the simulation. First, the delay in the controller loop was set to zero and the relationship between gain of the controller and pressure attenuation was studied. As expected, it was found that unlimited attenuation could be obtained as the gain of the controller was increased. Next, a time delay of two cycles was introduced into the control loop. With this time delay, the maximum attenuation that could be attained was about 50 percent of the magnitude of the spike in the frequency spectrum with only negligible attenuation of the RMS pressure. When the controller's gain was increased, the controller became less effective as its attenuation was further diminished. Similar results were obtained in the UTRC rig [62].

Next, the closed loop performance of the developed ACS was investigated in the developed liquid fuel combustor at equivalence ratios of 0.8 and 1.0. The FFT and time dependence of the pressure oscillations under these operating conditions are shown in Figs. 6.10 and 6.11 for an equivalence ratio of 0.8, and 6.12 and 6.13 for an equivalence ratio of 1.0. Figures 6.10 and 6.11 indicate that the spikes in the frequency spectrum and the RMS pressure were attenuated by more than 20 and 10 dB, respectively, at an equivalence ratio 0.8 when active control was applied. Interestingly, this performance is significantly better than that predicted by the simulation. A close examination of the time dependence trace of the pressure prior to and during active control, shown in Fig 6.11, may provide an explanation of the cause of this difference. As discussed above, the pressure oscillations in the uncontrolled combustor appear to be more "coherent" than the oscillations excited by white noise in the simulation. Specifically, while the measured oscillations in the uncontrolled combustor display significant cycle-to-cycle amplitude variations, they don't exhibit the occasional "necking" that characterizes the simulated resonator's response to white noise forcing. When ACS is on, the pressure oscillations in the combustor bear striking similarity to the simulated response of the combustor to white noise forcing shown in Fig. 6.5. This similarity suggests that the ACS attenuates the "coherent" portion of the instability but has only limited effect on that part of the instability that is caused by random noise forcing.

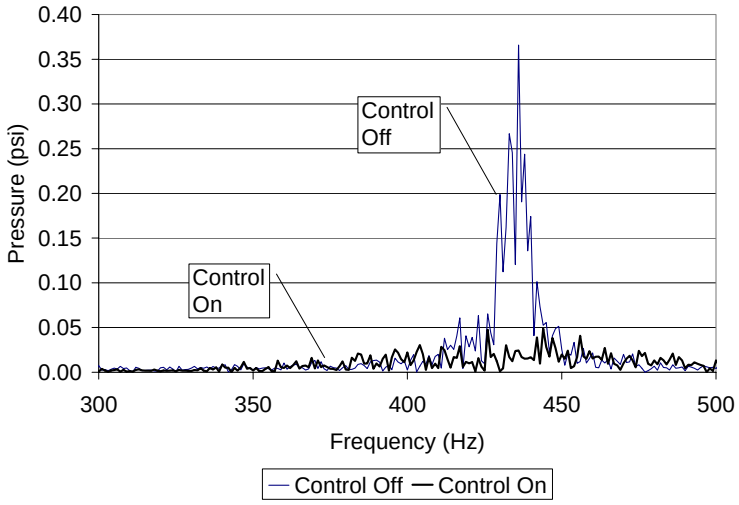

Figure 6.10. A comparison of the spectra of the pressure oscillations measured in the presence and absence of closed loop active control when the equivalence ratio Φ=0.8.

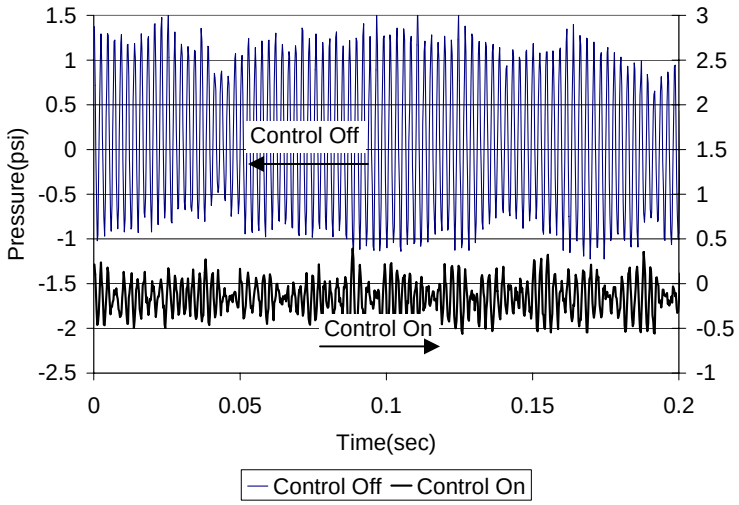

Figure 6.11. Time dependence of the measured combustor pressure in the presence and absence of closed loop active control when the equivalence ratio Φ=0.8.

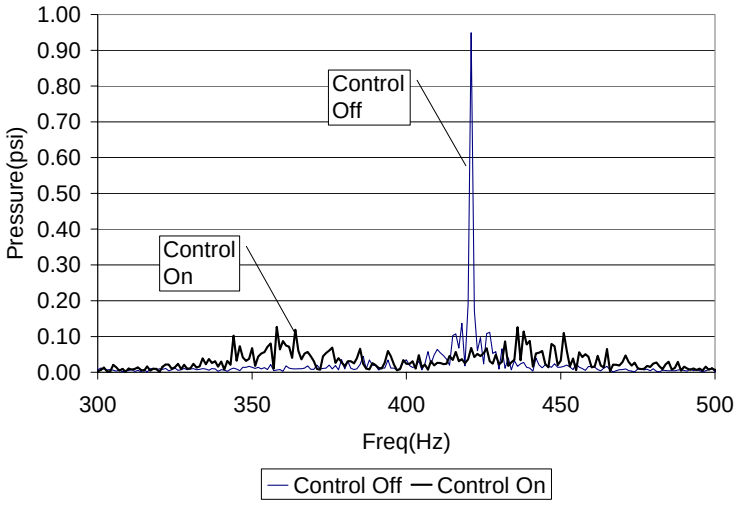

Figure 6.12: A comparison of the spectra of the pressure oscillations measured in the presence and absence of closed loop active control when the equivalence ratio Φ=1.0.

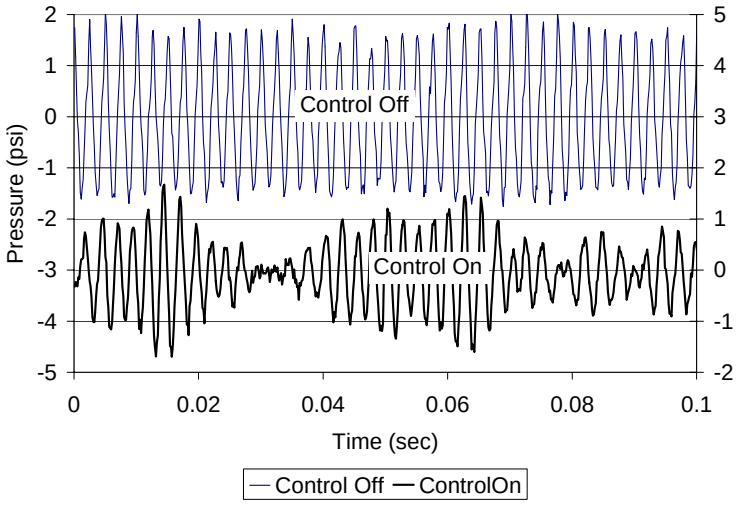

Figure 6.13. Time dependence of the measured combustor pressure in the presence and absence of closed loop active control when the equivalence ratio Φ=1.0.

Figures 6.12 and 6.13 describe the performance of the controller when the combustor operates at an equivalence ratio of 1.0. Figure 6.12 indicates significant peak attenuation of approximately 20 dB of the spike in the FFT. However, Fig. 6.13 shows that the time trace of the attenuated signal displays "beating" with relatively large amplitude. The measured RMS attenuation in this case is about 50 percent. It is

noteworthy that the FFT of the attenuated pressure shows small peaks around 360 and 440 Hz, suggesting that at least part of the "beating" is due to excess gain in the controller, a well-known phenomenon that is discussed in [62]. Again, as when the equivalence ratio equaled 0.8, the actual performance of the ACS is significantly better than that predicted by the simulation. The discrepancy between the measured and predicted results suggests that random noise is not the sole cause of instabilities and that models of unstable combustors should include the effects of both white noise and a deterministic positive feedback model of the mechanism that drives the instability.

To examine the above suggestion, the gain on the positive feedback in the simulation was adjusted in a way that produces a simulated instability with "beating" behavior, which closely approximates that exhibited by the experimental data. Next, the optimal gain that yielded maximum attenuation was determined by adjusting the gain until the peak in the predicted FFT spectrum was minimized. Simulations of the FFT and time dependence of the uncontrolled and controlled combustor are shown in Figs. 6.14 and 6.15. They show that the spike in the pressure spectrum and the RMS pressure are attenuated by 20 and 10 dB, respectively, in very good agreement the data measured in the tests with an equivalence ratio of 0.8. These predictions were obtained with a combustor model that included white noise forcing and positive feedback driving that simulated the measured data. An active controller that included the measured time delay was used to damp the pressure oscillations.

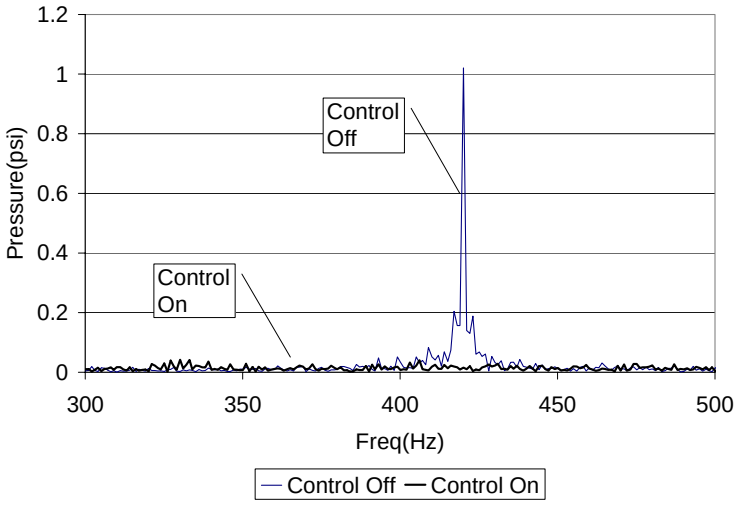

Figure 6.14. A comparison of the predicted combustor pressure spectra in the presence and absence of close loop active control.

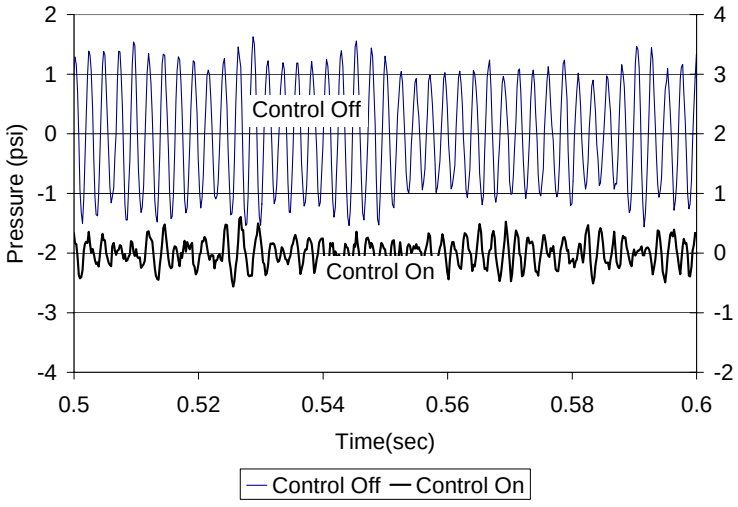

Figure 6.15. A comparison of the predicted time dependence of the combustor pressure oscillations in the presence and absence of closed loop active control. The spectra of these time series data are presented in Fig. 6.14.

6.4 Summary

The dependence of the performance of an ACS on the time delay in the control loop, noise and the complex nature of the instability was investigated in a liquid fuel combustor. The "beating" phenomenon exhibited by the pressure oscillations under controlled and uncontrolled operating conditions can be related to the presence of persistent driving by white noise. The open loop response tests show that the combustor responds with a significant time delay to a command signal. When the measured time delay is incorporated into a simulation of an actively controlled combustor that is forced by white noise, the controller attains very limited attenuation. On the other hand, actual active control tests shows that the ACS performs much better than the simulation predictions suggest. Nevertheless, the "beating" phenomenon persists in the pressure oscillations of the controlled combustor, suggesting that the presence of random noise and time delay limit the controller's effectiveness. This hypothesis is supported by the prediction of a simulation that accounts for the effects of both white noise excitation, time delay in the control loop and a positive feedback that simulated the uncontrolled combustor behavior.

CHAPTER 7

CONCLUSIONS, APPLICATION AND RECOMMENDATIONS FOR FUTURE RESEARCH

This chapter describes the main findings of this thesis, the author's perspective on application of these findings, and recommendations for future work in the areas that were investigated:

- Experimental determination of combustor stability margin
- Development and characterization of an adaptive controller for combustion instabilities
- Controllability limitations due to system noise and time delay

7.1 Combustor Stability Margin

Chapter 3 presented a novel experimental technique that was developed for determining the stability margin of a combustor. This method determined the gain and phase of the transfer function between the heat release and combustor pressure by measuring these two parameters under stable and unstable operating conditions. By driving pressure oscillations using a siren, it was possible to determine the transfer function from pressure oscillations to heat release oscillations. By driving heat release oscillations using the developed fuel injector actuator, it was possible to determine the transfer function from the heat release to the pressure. Multiplying these two functions by one another provided an overall picture of the stability margin of the combustor for the frequency range studied.

A similar approach could be used on full-scale industrial gas turbine combustors for early detection of operating regimes where the combustor is likely to become unstable. Such a predictive capability would allow the combustor to be redesigned in the early development stages to limit the susceptibility to observed pressure oscillations. Modifying a test rig to accommodate this experimental technique would require the following capabilities and present associated technical challenges:

- Reliable acoustic pressure and heat release measurements - Acoustic pressure measurements are routinely made by all gas turbine manufacturers and do not present a technical challenge. On the other hand, making accurate heat release measurements in a full-scale high pressure industrial combustor is more challenging, due primarily to limited optical access and complex geometries of industrial combustors.
- Capability to independently modulate the heat release and acoustic pressure – An actuator that was developed for generating heat release measurements over wide frequency and amplitude ranges was discussed in Chapter 2. This actuator design can be scaled to modulate the fuel flow for generating the required heat release oscillations. On the other hand, driving large amplitude acoustic pressure oscillations in a controlled manner is more challenging. A scaled-up version of the siren that was used in these tests could be designed, but the high heat load of the exhaust gases would present a design challenge. Another option would be to drive pressure oscillations in the combustor section directly by using an acoustic driver coupled with a horn or acoustic waveguide; however, this approach also presents technical challenges, including the design of such a device that can be driven over a wide range of frequencies for this harsh environment. If such a device is developed, it must be implemented without substantially altering the boundary conditions that control the natural behavior of the combustor.

Further development of this experimental technique could be performed by adding the capability to drive pressure oscillations over a range of pressure amplitudes. This enhancement requires an actuator (or siren) that independently controls the frequency and amplitude of the driven pressure oscillations, subject to the technical challenges described above. Such an actuator would provide the ability to drive pressure oscillations in both the linear and nonlinear regimes for better overall characterization of the flame response. There are also promising techniques for determining stability margin using passive measurements, without external forcing, e.g., [57]. The benefit of this approach is that no special actuators are required, thus making the hardware design challenges much more tenable.

7.2 Adaptive Controller Development and Characterization

The second area investigated in this thesis was the development and characterization of a practical adaptive controller that utilizes a real-time observer. The controller continually modulates the phase of a control signal that is used to damp the pressure oscillations in the combustor. By measuring the system response to the control phase modulations, the controller continually calculates the *direction* in which the control phase needs to be adjusted to minimize the pressure oscillation amplitude in the combustor. This method is more robust than the investigated online identification method which calculates the optimum control phase directly.

The controller algorithm was analyzed using a van der Pol model and its performance was investigated in a number of different experiments. The controller parameters can be modified to maximize adaptation speed or to maximize damping with slower adaptation. The controller can be configured to provide very rapid adaptation, with the following tradeoffs:

- Increasing the modulation frequency results in a lower correlation coefficient
- Increasing the modulation amplitude results in damping penalty ~ $2\theta/\pi$
- Increasing the adaptation step size results in damping penalty from overshoot

The developed adaptive controller has potential as a very useful feature on gas turbine engines. It continually adapts to changes in operating conditions and handles rapid transient events (e.g., from a change in fuel composition) well. The main challenge is to couple the controller with a capable and reliable actuator. Two actuator designs have been demonstrated in the literature to provide sufficient actuation authority for use with industrial full-scale high pressure combustors, see [21, 59]. With the control authority thus demonstrated, the primary concern then becomes reliability. An actuator that operates at 100-200Hz (typical frequency range for combustion instabilities in DLN combustors) will accumulate over 3 billion cycles in one year. If the actuator fails at a critical time, the engine may trip or be forced to shutdown for actuator replacement. Concerns over reliability are the main reason that gas turbine manufacturers are reluctant to rely exclusively on active control systems for damping combustion instabilities. Instead, the preferred route is to pursue passive control design options that eliminate the need for active control.

However, active control would be highly beneficial in the development process. Delays in development due to unexpected combustion instabilities can be very costly, especially in the final stages of prototype development and testing. Having an active control system available as a measure for risk mitigation could be a valuable investment for gas turbine manufacturers. The developed adaptive controller may provide the necessary margin against combustion instabilities to allow the engine to meet its performance requirements while passive control options are developed.

Returning for a moment to actuator authority, there is another consideration as to how an actuator is connected to a combustion system. The developed adaptive controller

would work well with either a “bolt-on” or “integrated” actuator. The distinction between these two approaches is that in the “integrated” approach the combustor designers are planning on having an active controller with its actuator available at all times. In the “bolt-on” approach, the active control system may be an afterthought or at least is not considered in the design of the combustor. This distinction is important in how the fuel delivery system is designed. In many gas turbine designs, the fuel nozzles are designed for a high pressure drop so that there is minimal feedback of the pressure oscillations into the fuel system. Furthermore, the auxiliary systems (fuel control valves, piping, etc.) may be designed to operate near the maximum available fuel pressure from the supply line. Inserting an actuator for active control into this fuel delivery system may not be very effective, depending upon the actuator design and the fuel system design. For example, an actuator that is optimized for a large pressure drop may alter the performance of the fuel nozzle or limit the maximum fuel flow rate into the combustor. On the other hand, if the same actuator is integrated into the combustor design, it may be possible to design a less restrictive fuel nozzle that is optimized to include the actuator in its fuel delivery system. In short, the fuel system design (and particularly the geometry between the actuator and the fuel nozzle) plays a critical role in the ability of the active control system to be effective at damping combustion instabilities.

Further development and optimization of the adaptive controller could be achieved in a few areas. The controller presented in Chapter 5 uses phase modulation to determine the optimum control phase. However, determining the optimum control gain should also be investigated. One method for determining the optimum control gain is to set a target level for the pressure amplitude. The control gain is then adjusted to meet the target value. However, if this target pressure amplitude is beyond the controllability limitations of the system, then the gain should be optimized to provide the maximum controllability for the minimum control effort. Since too much gain may destabilize the

system, it is important to consider this limitation also. Some efforts in this areas have been pursued by Coker, *et al.* in [64].

A second area for optimizing the adaptive controller is to use intelligent online adaptation of the control parameters. For example, the adaptation step size or modulation amplitude could be modified as the controller approaches the optimum control phase or after the combustor has maintained a stable operating condition for some duration. The intelligent online adaptation would enable maximum benefits of rapid adaptation and maximum damping while minimizing the tradeoffs between these competing requirements.

Finally, this adaptive controller is set to damp a single unstable mode of the combustor. The developed observer is capable of detecting and controlling multiple modes simultaneously, but the adaptive control algorithm is presently designed to control only one mode at a time. A useful extension of the current research would be to modify the adaptive controller to find the optimum gain and phase for simultaneous control of multiple unstable modes.

7.3 Controllability Limitations

The sixth chapter presented a study of the limitations on controllability of an unstable system, regardless of whether adaptive or fixed-phase control is applied. The predictions of a simple linear model were correlated with experimental results, indicating that the limit of controllability is affected by the amplitude of the noise in the unstable system. It was shown that the characteristic "beating" or "peak-splitting" that is sometimes observed when active control is applied can also be attributed to noise and time delays *within the unstable system*. The conclusion of this chapter was that there are

inherent limitations in controlling some unstable combustors, even when an "ideal" closed-loop controller is used.

The research performed in this brief study of controllability limitations provided some insight into two important factors limiting the controllability of a system. It would be interesting to further examine the relationship between pure feedback instability and noise-driven systems. The model used in this study could be expanded to account for combinations of driving mechanisms that might be present in an industrial combustor.

This area of study could also be expanded to include the actuator response characteristics, and the combustor response to different methods of fuel modulation. Presently, the preferred approach is to use sinusoidal modulation of the fuel flow at the same frequency as the combustion instability. However, depending upon actuator design and capabilities, it may be more effective to use a duty cycle injection approach, similar to the method used in automotive injectors. Some of the other cited authors have used automotive-style injectors in their research, and it would be beneficial to understand the impact of the actuation methodology on the controllability.

APPENDICES

APPENDIX A

REAL-TIME OBSERVER OVERVIEW

The following overview of the developed real-time observer was provided by Dr. Yedidia Neumeier. A detailed analysis of the observer algorithm is given in [25].

Theory

The objective of the developed observer is to determine the **real time** dependence of the characteristics of the oscillations in the combustor. The notion **real time** means that the evaluation is carried over time interval comparable to that of the period of oscillations. This demand excludes the use of windowed FFT because it required a time window much larger than a single period. Time localization can be achieved by Wavelet analysis. However, since we do not know in advance the frequencies of the oscillations we would have to use a large bank of wavelet functions. To overcome these difficulties, the observer uses a pair of wavelet like, orthogonal functions whose time stretch scale is constantly and rapidly adapted in a feedback process.

The developed observer assumes that the combustor oscillations are quasi-periodic, consisting of several modes **whose frequencies are not necessarily harmonically arranged**. Accordingly, the measured unstable combustor pressure is expressed in the following series solution form:

$$p(t) = \sum_{i=1}^{i=K} p_i(t) \tag{A.1}$$

Where

$$p_i(t) = A_i(t)\sin\left(\omega_i t + \phi_i(t)\right) \tag{A.2}$$

The quantity $p_i(t)$ is one of the K modes present in the combustor whose frequencies, ω_i, amplitudes A_i, and phases, ϕ_i, vary with the time.

Given that;

$$\hat{A}_i(t) = \sqrt{\left(S_i(t)^2 + C_i(t)^2\right)} \tag{A.3}$$

$$\hat{\phi}_i(t) = \tan^{-1}\left(C_i(t)/S_i(t)\right)$$

The observer approximates the modes' amplitude and phase by use of the following expressions that are similar to those used in Fourier series analysis:

$$S_i(t) = \frac{2}{T_i}\int_{t-T_i}^{t} p(\tau)\sin(\omega_i\tau)d\tau \quad C_i(t) = \frac{2}{T_i}\int_{t-T_i}^{t} p(\tau)\cos(\omega_i\tau)d\tau \tag{A.4}$$

where

$$T_i = \frac{2\pi}{\omega_i}$$

The integrals in Eq.(A.4) are not “conventional” Fourier series integrals because their limits of integration, require the yet unknown, time dependent, period T_i, of the analyzed mode which in turn is one of the quantities to be determined by this analysis. To deal with these issues, the developed observer employs a fast iterative (feedback) procedure that determine the unknown, time dependent, periods, of the unstable modes.

To gain insight into the developed iterative solution procedure for the unknown frequency, assume that the pressure in Eq.**(A.1)** consists of single frequency, ω_1. To determine the characteristics of this mode, we solve Eq.**(A.4)** assuming initially that the

unknown frequency equals an arbitrary frequency ω_2 different than the correct frequency ω_1. It can be shown (a proof will not be given here because of paper length limitation) that when the assumed frequency ω_2 is substituted into Eq.**(A.4)** and the calculated coefficients S and C (the subscripts of these coefficients are omitted in this discussion for convenience) are substituted into Eq.**(A.3)** and **(A.2)**, the "reconstructed" time dependent solution obtained from Eq.**(A.2)** oscillates with the correct frequency ω_1, even though an "arbitrary" frequency, ω_2, was used in Eq.**(A.4)**. It can be further shown [25] that the calculated coefficients S and C vary periodically with time and that their time derivatives are given by:

$$\frac{dS}{dt} = \mathrm{K}(-\sin\alpha + \sin\beta) \qquad \frac{dC}{dt} = \mathrm{K}(\cos\alpha + \cos\beta) \tag{A.5}$$

$$\alpha = (\omega_1 - \omega_2)t - \pi\frac{\omega_1}{\omega_2} \qquad \beta = (\omega_1 + \omega_2)t - \pi\frac{\omega_1}{\omega_2}$$

$$\mathrm{K} = \frac{\omega_2}{\pi}\sin\left(\pi\frac{\omega_1}{\omega_2}\right)$$

Equations (A.5) can be used to obtain the correct frequency ω_1 from the calculated coefficients and their time derivative:

$$\omega_1{}^2 = \omega_2{}^2 + \frac{\omega_2\left(\frac{dS}{dt}\sin\omega_2 t + \frac{dC}{dt}\cos\omega_2 t\right)}{S\cdot\cos\omega_2 t - C\cdot\sin\omega_2 t} \tag{A.6}$$

The RHS of Eq. (A.6) consists of two terms. The first term is the current estimate of the frequency and the second one is a correction term. In the case of pure tone oscillations,

full implementation of the correction term bring the estimated frequency to the correct value after one step. However, with the presence of other modes and/or noise in the observed signal such correction to the frequency is not feasible. Instead, we "filter" the correcting term so that each update is only partial. Thus, the estimate frequency $\hat{\omega}$ at each time step is given by:

$$\hat{\omega}^2\Big|_{t+\Delta t} = \hat{\omega}^2 + \frac{\hat{\omega}\left(\frac{dS}{dt}\sin\hat{\omega}t + \frac{dC}{dt}\cos\hat{\omega}t\right)}{S\cdot\cos\hat{\omega}t - C\cdot\sin\hat{\omega}t}\cdot\frac{\Delta t}{\tau} \tag{A.7}$$

$$\tau = \frac{1}{n\hat{T}} \tag{A.8}$$

Where $\hat{T} = \frac{2\pi}{\hat{\omega}}$. The choice of the filter time-constant τ is such that the estimated frequency converges in *n* oscillation periods.

The successive estimations of the frequency are used in the integrals (A.4) by substituting the estimated frequency $\hat{\omega}_i$ instead of the unknown frequency ω_i. This procedure constitutes the feedback process of the observer;

1. Estimate mode frequency
2. Calculate the mode coefficients using the integrals (A.4)
3. Update frequency using Eq.(A.7)
4. Go back to step 1

Assuming that the above described feedback process is stable, the converging time of the algorithm, is of the order of a single period of the oscillations.

With the above described feedback process we could in principle implement the observer. However, the numerical effort that would be required to perform the integrals (A.4) at

each time step may be too large for real time processing. Analysis by Markopoulos [25] showed however, that the integral equations (A.4) and the frequency Eq. (A.7) can be transformed into the following set of ODEs;

$$\frac{dS_i}{dt} = \frac{2}{T_i}\left[p(t) - p(t-\hat{T}_i)\right]\sin(\hat{\omega}_i t) \qquad \text{(a)} \qquad \text{(A.9)}$$

$$\frac{dC_i}{dt} = \frac{2}{\hat{T}_i}\left[p(t) - p(t-\hat{T}_i)\right]\cos(\hat{\omega}_i t) \qquad \text{(b)}$$

$$\frac{d\hat{\omega}_i^{\,2}}{dt} = \frac{1}{n\hat{T}_i}\cdot\frac{\left(\frac{dS_i}{dt}\sin\hat{\omega}_i t + \frac{dC_i}{dt}\cos\hat{\omega}_i t\right)}{S_i\cdot\cos\hat{\omega}_i t - C\cdot\sin\hat{\omega}_i t} \qquad \text{(c)}$$

$$\hat{T}_i = \frac{2\pi}{\hat{\omega}_i}$$

The integration of the set (A.9) requires only little effort compare to the solution of the integral Eqs.(A.4). However, there are "strings attached to this deal". Although the solution of the ODEs(A.9) provide the correct mode's frequency, it does not converge to the correct amplitude. This happens because the amplitude calculation is sensitive to error in initial conditions. To see that, consider a pure sinusoidal signal with frequency ω and assume that we start our calculation with $S_i = 0$ and $C_i = 0$ $\hat{\omega}_i = \omega$. Because the assumed frequency perfectly match the true frequency $p(t) - p(t-\hat{T}_{i)} = 0$. Therefore, Eq.(A.9) yields $\frac{dS_i}{dt} = \frac{dC_i}{dt} = 0$ which causes the solution to "stuck" at zero. To mitigate this problem without too big a penalty in computation efforts we use a "frozen" solution to update the solution of the ODEs (A.9). The solution is called "frozen" because it is

based upon the solutions of the integrals (A.4) with the lower limit of the integration constant (frozen) during a period of integration. The procedure is done as follows. First, we introduce two frozen variables $\langle s_i \rangle$ and $\langle c_i \rangle$. The two states are obtained solving the following equations, which are the time derivative of Eq.(A.4) when the lower integration limit is set to constant and the integration is initialized at t_{LR}.

$$\frac{d\langle s_i \rangle}{dt} = \frac{2}{\hat{T}_i} p(t) \sin \hat{\omega}_i (t - t_{LR}) \tag{A.10}$$

$$\frac{d\langle c_i \rangle}{dt} = \frac{2}{\hat{T}_i} p(t) \cos \hat{\omega}_i (t - t_{LR})$$

Next we amend the mode's coefficient equations (A.9) a,b as follows:

$$\frac{dS_i}{dt} = \frac{2}{\hat{T}_i} \left[p(t) - p(t - \hat{T}_i) \right] \sin \hat{\omega}_i (t - t_{LR}) \tag{A.11}$$

$$\frac{dC_i}{dt} = \frac{2}{\hat{T}_i} \left[p(t) - p(t - \hat{T}_i) \right] \cos \hat{\omega}_i (t - t_{LR})$$

The term t_{LR} in Eqs. (A.10) and (A.11) is the time of Last Reset (LR) and its use is as follows. Starting with $t_{LR} = 0$ we integrate (A.10), (A.11) and the frequency equation (A.9)-c until $t - t_{LR} \geq \hat{T}_i$ at that point in time we perform the following reset

$$t_{LR} = t\,; \qquad S_i = \langle s_i \rangle\,; \qquad C_i = \langle c_i \rangle\,; \qquad \langle s_i \rangle = 0\,; \qquad \langle c_i \rangle = 0$$

After the reset is performed we resume the integration of the above equations until the next reset time. The coefficients $\langle s_i \rangle$ and $\langle c_i \rangle$ that start at zero after the reset arrived at the true value once the cycle is completed and therefore they are used to update the value

of the coefficients S_i and C_i which are continuously updated between resets. This way we enjoy the instantaneous update and are protected from the error described above. In this form the computation effort of the mode observation is equal to that required for integration of a fourth order system and thus is easily handled in real time.

The discussion so far focused on observation of a single mode. As mentioned in the beginning of this section, the signal is assumed to consist of plurality of modes that are not necessarily harmonic. Analytical solution that can predict the response of the developed observer to such a signal does not exist yet. However, as will be demonstrated in the next section, when operating on multi mode signal the observer tends to "lock" itself on the dominant mode. If this mode is then reconstructed in time and subtracted from the original signal the resulted net signal that is now dominated by the next larger mode can be fed to an identical observer. Thus, by successive feed forwarding process a set of observers can hierarchically identify the various modes in the signal. Moreover, the feed forward process can be extended to include a feed back process in which the signal of the secondary modes are fully or partially subtracted from the input signal of the previous observer stages in order to "clean" it and allow a better primary mode observation. Thus, the multi stage observer can work either in a feed forward mode in which only the more dominant modes are subtracted from the pressure signal to obtain the less dominant mode or in a feedback mode in which a fraction of the reconstructed secondary modes are used as well to "clean" the input signal to the more dominant mode observes. All the technical details required for practical implementation of the above described observer can be found in the patent [65].

The discussion so far did not address the observer stability. Efforts so far [25] proved analytically the asymptotic stability in a case of a single mode input and single stage observer. Indeed, an analytic stability proof for multi mode signal observation with random noise seems at that point beyond achievement. However, extensive numerical investigation, whose results are discussed in the following section, showed fast convergence and good stability even in "hard cases" where two or more equally strong modes with close frequencies dominate the signal.

Observer Performance

First, we tested the observer on a synthetic signal. The signal was a combination of two equally strong inharmonic modes with frequencies 230 and 370 Hz and 50% random noise. It was constructed with the following formula;

$$\begin{aligned} &observer\ input = \sin(2\pi \cdot 230 \cdot t) + \cos(2\pi \cdot 370 \cdot t) \\ &+ random\ noise\ between \pm 0.5 \end{aligned} \qquad \text{(A.12)}$$

The observer consisted of three stages with 50% feedback. This mean that the input to stage 1 was the raw signal (A.12) minus 50% of the reconstructed signal of the 2th and 3th stages, the input to the second stage was the raw signal minus 100% of the reconstructed signal of stage 1 minus 50% of the reconstructed signal of stage 3 and the input to stage 3 was the raw signal minus the sum of 100% of the reconstructed signals of stage 1 and 2. The partial, rather than full, feedback is used to ensure hierarchy in the observation process in which the first stage always converges the mode with the largest amplitude and the second and third stages converge to the two consecutive modes in decreasing order, respectively. The factor *n* in formula (A.9)-c was set to 3 in all stages.

This mean a convergence time constant of about 3 periods of the observed frequency (meaning the frequency to which the observer converged). The algorithm was performed with time step of 1/5000 sec.

Figure A.1 shows the time dependence of the two observed frequencies both starting from an initial guess of 1000Hz, it clearly shows that the observed frequencies converged to the correct values. Figure A.1 further shows that the two observed frequencies drop initially almost together reaching the vicinity of 370 Hz in about 20 milliseconds. This converging rate is in agreement with the expected three periods time constant imposed by the setting of n=3 in Eq.(A.9)-c. When the estimated frequencies reached 370 Hz the observer reach a singular point because the modes are of equal strength and either stage may converge to any of the two frequency. Figure A.1 shows that the two stages started to converge to the first encountered mode at 370 Hz, however, after 5 msec one of the stages, (in this case it happened to be the second stage), continue in the convergence process toward the lower frequency mode. The convergence from an initial estimate of 1000 Hz shows that the observer has very large domain of attraction and the rejection of the singular point suggests that the observer only stable points are at the correct frequencies.

Figure A.1 indicates that the second stage trace of the frequency of the 230 Hz mode is smoother than the 370 Hz mode observed by the first stage. This is so because the output of the first stage is fully subtracted from the input to the second stage thus cleaning the input from traces of the 370 Hz mode while only 50% the output of the output of the second stage is subtracted from the input of the first stage thus leaving significant portion of the 230 Hz mode. Finally, the signal reconstructed from the observed parameters of

the modes subsequent to convergence is shown in Figure A.2 together with the original signal. The trace clearly shows that the observer rejected the noise and accurately reconstructed the "uncontaminated" input signal.

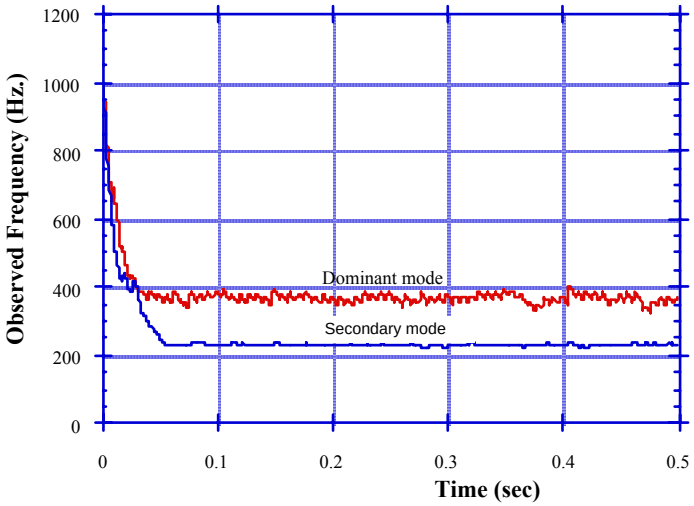

Figure A.1 Observed frequency of the two modes

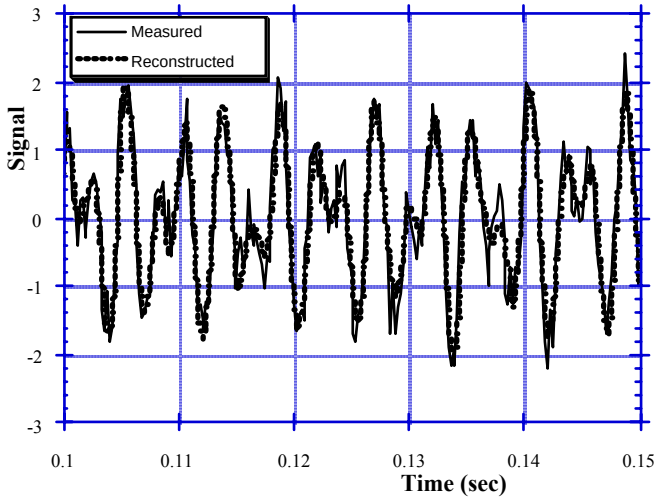

Figure A.2 Comparison between the noisy and two-modes reconstructed signals

Next, the ability of the observer to follow mode transition that was measured in an unstable gas rocket motor simulator is demonstrated [66]. The measured pressure signal, shown in Figure A.3, exhibited a transition from low to high frequency oscillations between .05 and .064 seconds. This signal was analyzed with two feed forward stages observer without feedback, i.e., the input to the first stage consisted of the raw signal alone and did not include a feedback from the second stage while the output of the first stage was fully subtracted from the input to the second stage. Figure A.4 shows the time dependence of the primary and secondary modes that were computed from the observed frequencies and coefficients. Figure A.4 shows that the time dependence of the dominant mode, in the left frame, appears to be a nearly sinusoidal, and its period abruptly changes around .065 seconds. Examination of the secondary mode, shown in the right frame of Figure A.4, indicates that even during the initial dominance of the lower frequency mode the observer was able to trace the higher frequency mode. Figure A.4 further indicates that the initially secondary high frequency mode becomes dominant at .067 seconds, at which point the low frequency mode reduced to secondary, low amplitude, low frequency residue. The time variations of the calculated frequencies of the two observed modes are shown in the left picture of Figure A.5. The frequency trace indicates that the observed frequency of the dominant mode changed from 650 to 1250 Hz. within only three milliseconds. The transition time of three milliseconds agrees with the three periods time constant discussed above. It is important to note that during the transition of the primary mode from low to high frequency, the secondary mode remained more or less unchanged and it dropped only after the transition of the primary mode was completed. Finally, the right frame in Figure A.5 presents a comparison of the measured pressure oscillations and

those obtained by synthesis of the two observed modes. It yet again confirms that the observer can "reproduce" the input pressure with high fidelity.

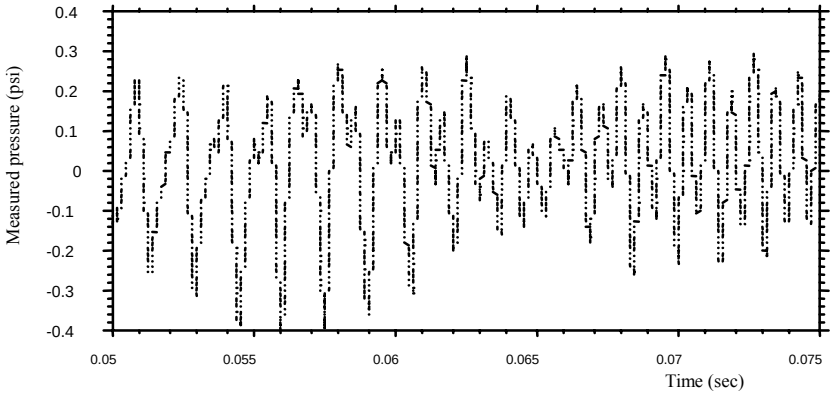

Figure A.3 Signal of unstable pressure oscillations measured in GT. gas rocket

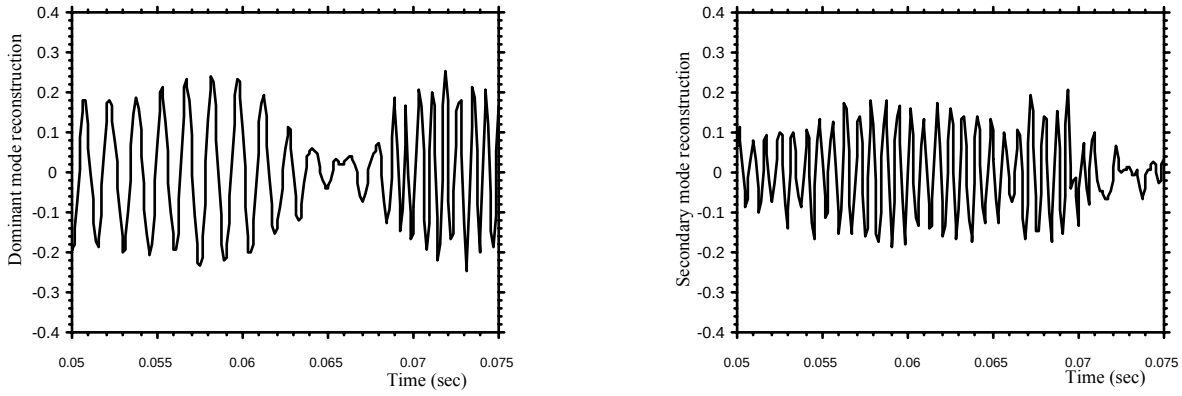

Figure A.4 Time reconstruction of the dominant left, and secondary right modes

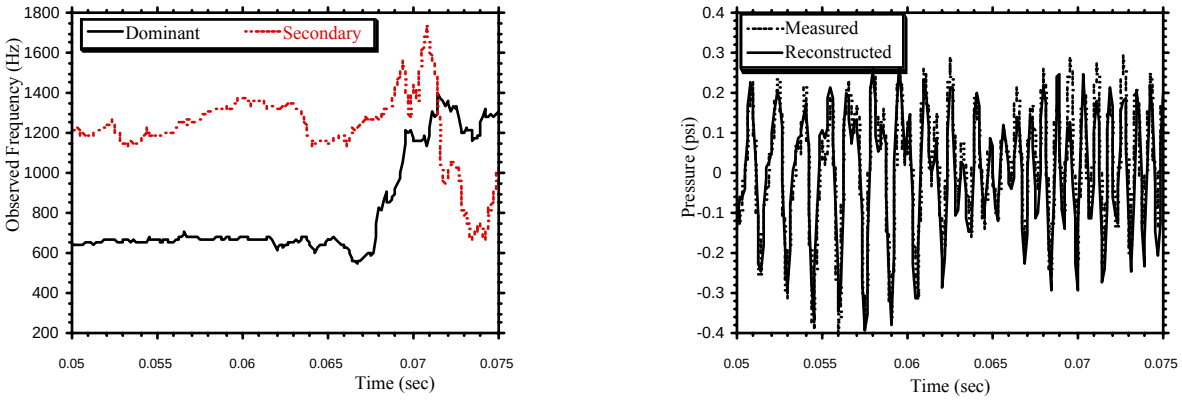

Figure A.5 Observed frequencies of the two modes left and comparison between the measured and two-modes reconstructed signal, right.

APPENDIX B

ACTUATOR PERFORMANCE FOR FUEL FLOW MODULATION

As described in Chapter 2, the actuator used for supplying fuel flow modulations to the combustor utilizes an Etrema magnetostrictive actuator. The actuator gain and phase characteristics (supplied by the manufacturer) are shown in Fig. B.1. These curves show the magnitude and phase of the impedance as a function of frequency. With a resonance frequency of approximately 2600Hz, the electro-mechanical gain of the actuator is relatively constant over the range: 0 – 1000Hz, increasing dramatically between 1000-2500Hz. These curves indicate that the actuator can provide reasonably constant modulations of the reed valve position over a frequency band that is much greater than the unstable frequencies of interest, i.e., the unstable modes in the combustor which are typically 100-500Hz. One important aspect of the magnetostrictive actuator characteristics is that the phase of the response function is relatively constant (+/- 10deg) over the range 200-2000Hz. However, below 200 Hz there is a rapid phase change in actuator response. This rapid phase change can have a significant impact on the ability to control multiple unstable modes, depending upon the control application.

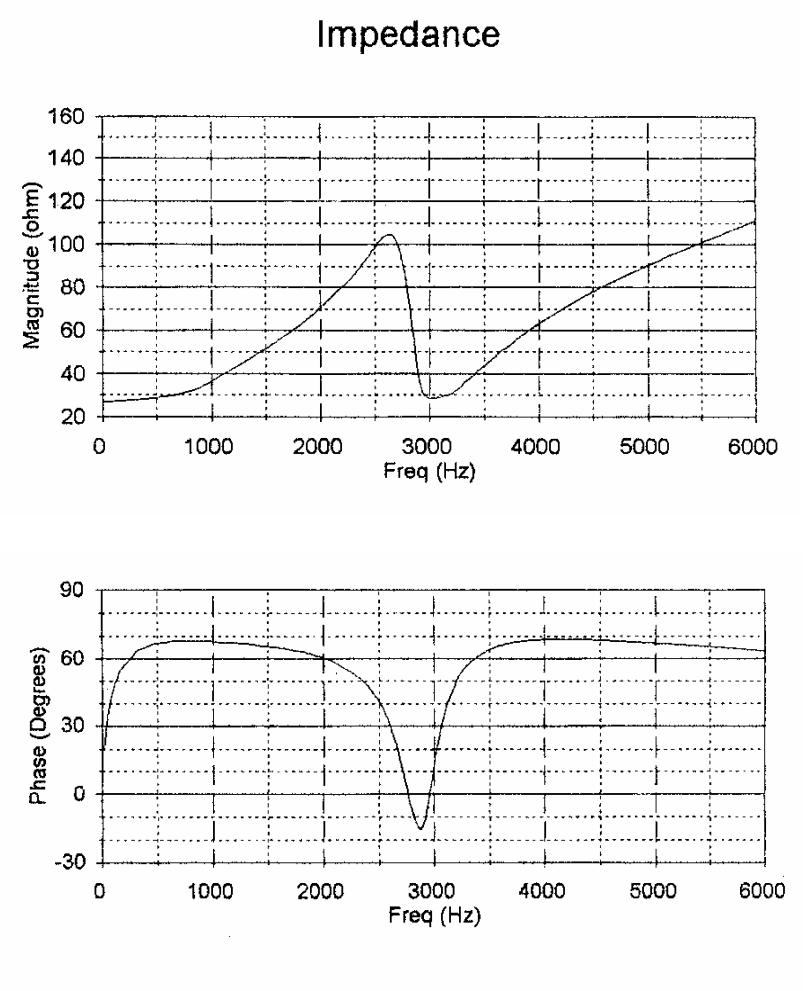

Figure B.1: Impedance characteristics of the Etrema AA140J025-ES1 actuator

Although the actuator has a high resonance frequency, and the response is relatively constant over the range of interest, the design of the reed valve for fuel actuation can also have a substantial impact on the actuation performance. The true performance of the fuel injector actuator depends upon the attributes of the magnetostrictive actuator coupled with the injector. After the fuel injector was designed, several tests were performed to determine how well it could modulate the heat release response, especially at higher frequencies (>500Hz).

The tests were performed in a gas rocket setup designed for active combustion instability control experiments, as shown in Fig. B.2. A water cooled pressure transducer was used to monitor the pressure response in the combustion chamber, and a photomultiplier (PMT) was used to measure the heat release response. Computers for data acquisition and control are also shown in the setup.

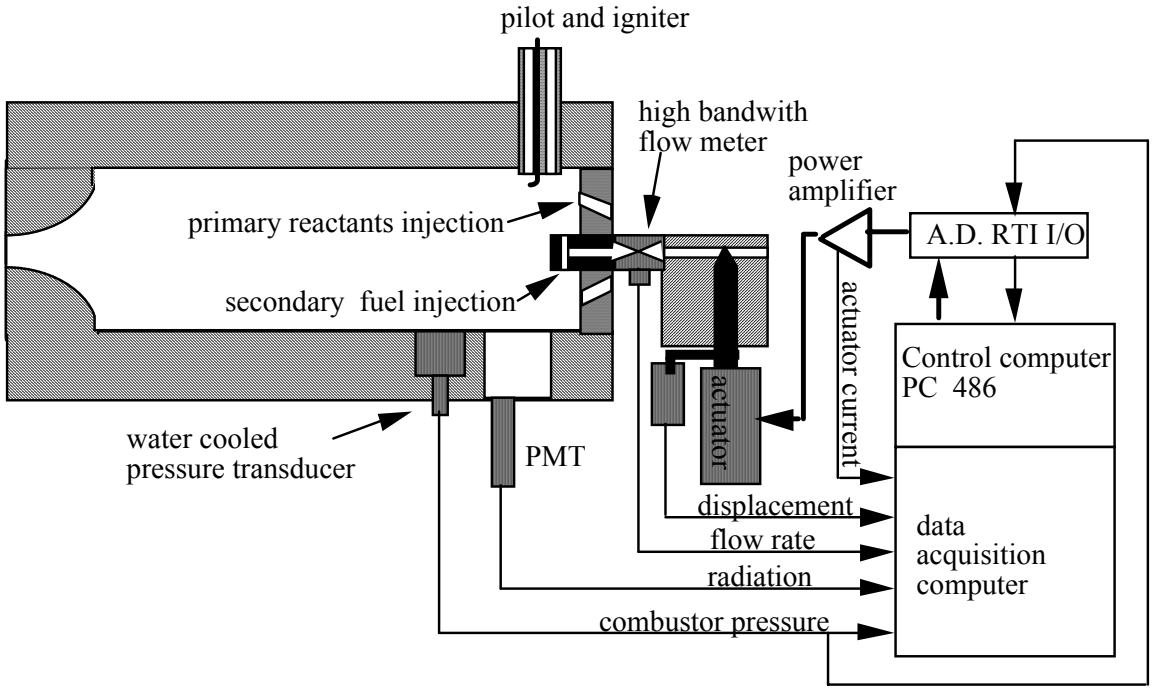

Figure B.2: Schematic of actively controlled gas rocket setup

First, open-loop tests were performed to determine the frequency response of the combustion process to fuel flow modulations. Of particular interest was whether heat release modulations could be observed at frequencies above 500Hz. During these tests, fuel flow through the secondary fuel injector was modulated at specific frequencies up to 800Hz. Results from a typical experiment are shown in Fig. B.3. The left frame shows the frequency spectrum of the measured heat release and the right frame shows the spectrum of the pressure. It is clear from the heat release response (left) that large

amplitude heat release oscillations of 600Hz were easily driven by the actuator. Notice that the driven oscillations were an order of magnitude higher than the heat release oscillations at the natural unstable frequency of 360Hz.

Acoustic pressure oscillations at 600Hz were also detectable (right), although their magnitude was much smaller in relation to the unstable natural modes (360Hz and harmonics). The difference between the response of the pressure and heat release can be explained as follows. At the natural acoustic modes of the combustor, there is a large acoustic gain for small amounts of heat release. A close look at the heat release (left) shows that there are small heat release peaks at the same frequencies as the natural acoustic modes. At 600Hz, there is relatively little acoustic gain to amplify the effect of the heat release oscillations on the acoustic pressure. Thus, the acoustic pressure is four time smaller at 600Hz, whereas the heat release input is ten times larger. It follows that if the actuator modulated heat release oscillations at the natural unstable frequency of 360Hz, it would be able to control the natural pressure oscillations (as long as the correct phase were applied).

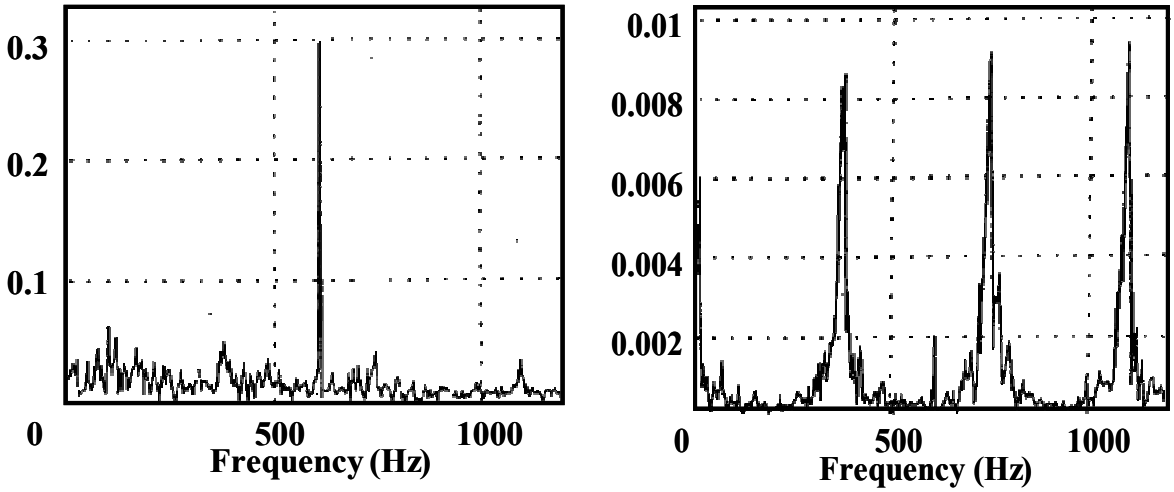

Figure B.3: Spectra of heat release rate measured by PMT (left) and acoustic pressure (right) in the combustor with 600 Hz fuel actuation.

In another set of open-loop tests, two different experiments were employed to determine the transfer function between the actuator command and the combustor response. In the first experiment, a "long" combustor setup identical to the one shown in Fig. B.2 was used. In the second experiment, a "short" combustor setup was used. This experimental setup drove the natural frequency from 360Hz to over 1000Hz. Thus, the experiments could be operated in a "sub-resonant" frequency range. One limitation of the "short" combustor experiments was that the PMT had to be removed; in this case, only the pressure transducer was available for correlation analysis. Fig. B.4 shows the transfer function in terms of gain and phase at various excitation frequencies obtained by the two methods. Both methods produced the same transfer function, which confirmed that the heat release response to secondary fuel injection is independent of the combustor acoustic field.

Note that the phase of the transfer function drops linearly as a function of frequency, and at a frequency of 800Hz is approximately equal to –360deg, which equates to a pure time delay of approximately 1.25 ms. This pure time delay can be attributed to mechanical response of the fuel injector/actuator as well as the time required for the fuel to mix and react with the flame.

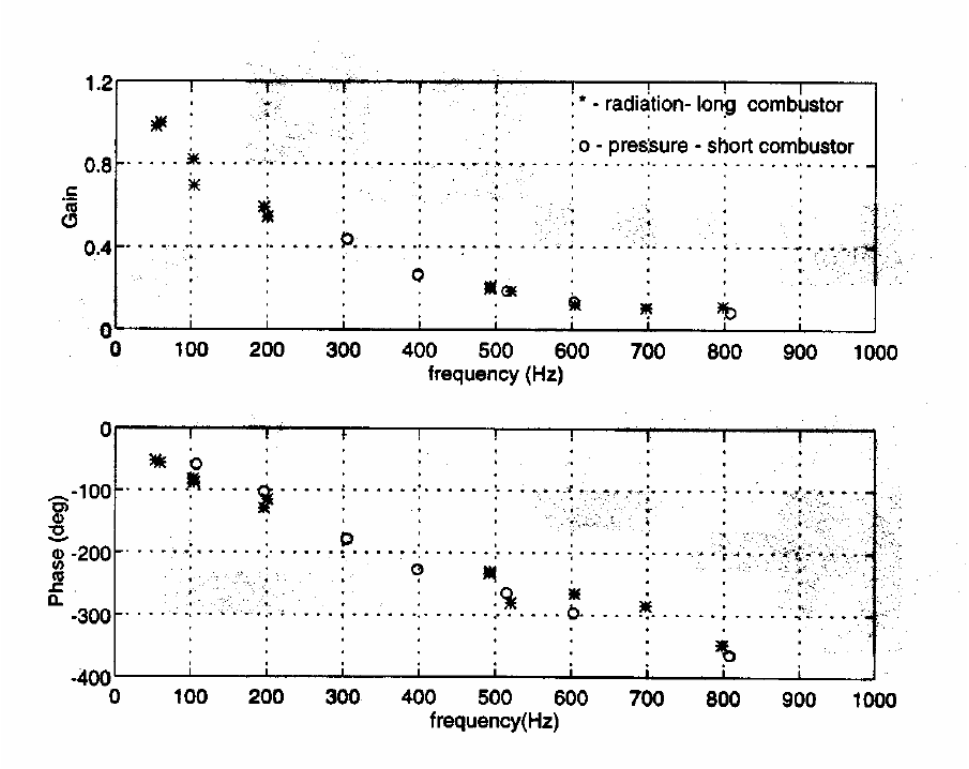

Figure B.4: Transfer function between actuator command and heat release obtained from radical radiation measurement with long combustor and pressure measurement in short combustor

After the gain and phase of the combustor response were determined using the open-loop test methods described above, these values were put into a lookup table. This lookup table was then used in closed-loop tests to demonstrate the ability of the active control system to control the combustion instability. Fig. B.5 shows the effect of closed-loop control on unstable pressure oscillations in the gas rocket simulator. In the top figure, the initially unstable combustor was exhibiting large amplitude pressure oscillations until approximately t = 0.1 sec, at which time the active control system was activated. Once the control was activated, the 360Hz pressure oscillations quickly vanished. The middle figure provides an indication of when the control was active. Once the 360Hz oscillations were mitigated, the controller stopped modulation of the fuel

valve. The bottom figure shows the observed frequency of the pressure signal. Until the pressure oscillations are removed at t=1.3 sec, the dominant frequency coincides with the first natural mode at 360Hz. When the 360Hz component is mitigated (by active control), random noise is observed at various frequencies ranging from 500 to 1500Hz. At several times during the actively controlled period, the first harmonic (720Hz) appears, especially during the time between t = 0.22 – 0.25sec. However, this mode never organizes itself to become a large amplitude instability.

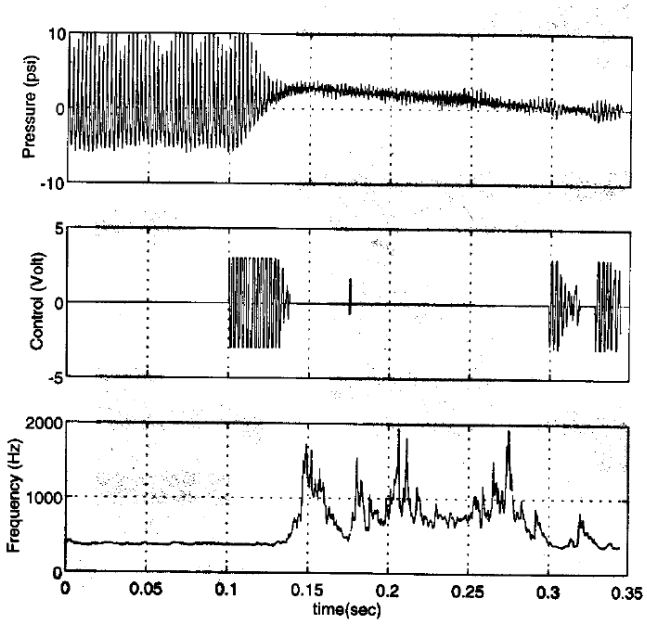

Figure B.5: Pressure oscillation control signal and observed frequency in the gas rocket simulator prior and after control implementation.

In summary, these experiments demonstrate the ability of the developed actuator to modulate fuel flow at frequencies of at least 800Hz. In open-loop tests, heat release modulations were measured up to 800Hz, and in closed-loop active control tests, the modulation capability at 360Hz was sufficient to control unstable oscillations at this frequency. For further information about these experiments, please see [66,67].

APPENDIX C

MEAN FUEL FLOW CONTROL

To control the mean flow rate of fuel through the actuator, a DC control loop is included in the active control circuit, as shown in Fig. C.1. This DC control loop serves two main purposes: a) compensate for thermal expansion of the magnetostrictive actuator, and b) compensate for "overdriving" that can occur when the fuel modulation amplitude is high, but the mean fuel flow rate is low.

Figure C.2 illustrates the concept of overdriving, and the mean flow compensation that is required to correct for it. In this illustration, a small amplitude control signal is initially applied to the actuator to control combustor pressure oscillations, thus resulting in mass flow fluctuations about the desired mean fuel flow rate. At time t=0.02, the amplitude of the control signal is increased (e.g., to attenuate a growth in the unstable oscillations), but the mean position of the actuator remains constant. Thus, the RMS amplitude of the fuel flow oscillations and the maximum flow rate during an oscillation period are increased. However, when the control signal approaches its maximum negative amplitude, at t=0.32 the actuator closes completely, and the fuel flow rate equals zero for a portion of the control period. When the actuator "bottoms out" in this manner, the result is slightly reduced RMS amplitude of the oscillations, and increased mean fuel flow through the actuator. Therefore, a mean fuel flow compensator is required, as shown in the block diagram in Fig. C.1.

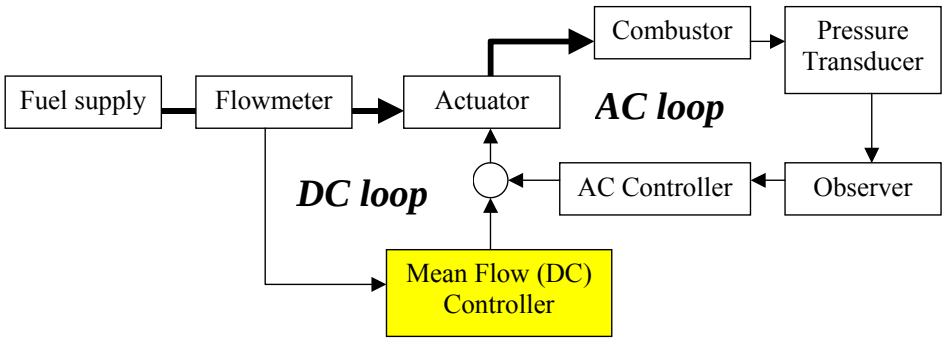

Figure C.1. Mean flow controller used to maintain the desired mean flow rate through the actuator

This compensator changes the mean actuator position to restore the mean flow rate of fuel through the actuator to the desired level. In Fig. C.2, the DC flow controller was abruptly turned on at t=0.042. However, during actual operation of the control system, the PI controller continuously adjusts the mean actuator position in order to minimize the error between the measured fuel flow rate and the desired flow rate. For the actuator configuration described in sections 2.2 and 2.3, the mean actuator position was adjusted by providing a DC bias to the actuator current. A similar FIA was also developed that used a servomotor-driven cam to change the mean position of the actuator for mean flow rate adjustments. In both cases, a simple PI controller is used for maintaining the desired mean fuel flow through the actuator.

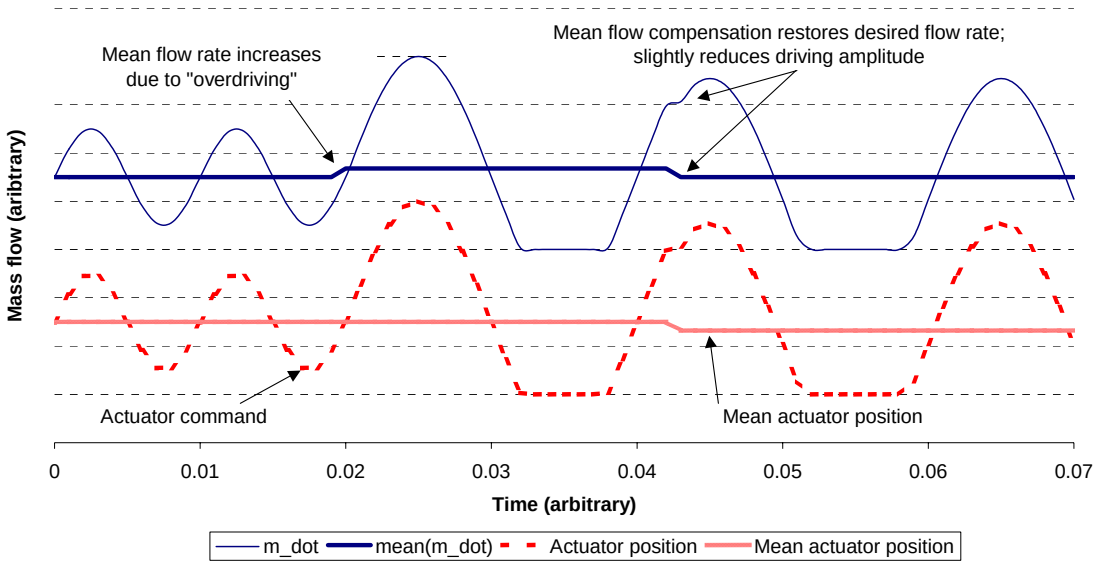

Figure C.2. Compensation for "overdriving" the reed valve fuel injector actuator

REFERENCES

1 Huppmann, H., Groetschel, U., Mueller, G., “Gas Turbines – Continuous Trend Toward Higher Performance – The Insurance Aspects”, International Machinery Insurer’s Association IMIA 16-70 (98), IMIA Conference, Interlaken, Germany, Sept. 1998.

2 Anex, R.P., Velnati, S., Meo, M., Ellington, R. and Sharfman, M., "Innovation and the Transformation to Clean Technologies: Life Cycle Management of Gas Turbine Systems," Proceedings of the 1999 NSF Design & Manufacturing Grantees Conference, Long Beach, CA, January 5-8, 1999

3 Keller, J.J., “Thermoacoustic Oscillations in Combustion Chambers of Gas Turbines,” *AIAA Journal* Vol. 33 (12), 1995, pp. 2280-2287.

4 Lieuwen, T., *Investigation of Combustion Instability Mechanisms in Premixed Gas Turbines*, Ph.D. Thesis, Georgia Tech, 1999.

5 Oyediran, A. Darling, D. Radhakrishnan, K. ,”Review of combustion-acoustic instabilities,” NASA Tech Memo n 107020 Aug 1995.

6 Culick, F.E.C., Yang, V., “Overview of combustion instabilities in liquid-propellant rocket engines,” *Progress in Astronautics and Aeronautics* v 169.

7 McManus, K.R. Poinsot, T. Candel, S.M., “Review of active control of combustion instabilities,” *Prog Energy Combust Sci* v 19 n 1 1993 p 1-29.

8 Rayleigh, L., *The Theory of Sound*, Dover Pub., New York, 1945.

9 Putnam, A.A., *Combustion Driven Oscillations in Industry*, J.M. Beer (Ed.), American Elsevier,New York (1971).

10 Zinn, B.T., (1986), Pulsating Combustion. In Weinberg, F. (ed.), *Advanced Combustion Method*s, Academic Press, 1986, chapter 2.

11 Lieuwen, T., Neumeier, Y., Zinn, B.T., “The Role of Unmixedness and Chemical Kinetics in Driving Combustion Instabilities in Lean Premixed Combustors, *Combust Sci Technol* v 135 n 1-6 1998.

12 Lieuwen, T., Zinn, B.T., “Theoretical Investigation of Combustion Instability Mechanisms in Lean Premixed Gas Turbines,” AIAA Paper 98-0641, *36th Aerospace Sciences Meeting*, Reno, NV, Jan. 1998.

13 Torres, H., Lieuwen, T.C., Johnson,C.E., Daniel, B.R., Zinn, B.T., "Experimental Investigation of Combustion Instabilities in a Gas Turbine Combustor Simulator," AIAA Paper # 99-0712, *37th Aerospace Sciences Meeting*, Reno, NV, January 1999.

14 Crocco, L., "Theoretical Studies on Liquid-propellant Rocket Instability," *Tenth Symposium (International) on Combustion*, pp. 1101-1128, The Combustion Institute, Pittsburgh, 1965.

15 Crocco, L., Cheng, S., *Theory of Combustion Instability in Liquid Propellant Rocket Motors,"*Butterworths Scientific Publications, London, 1956.

16 Harrje, D.J., Reardon, F.H.E., *Liquid Propellant Rocket Combustion Instability*, NASA report SP-194, 1972.

17 Akbari, P., Ghafourian, A., and Mazaheri, K., "Experimental Investigation of Combustion Instability in an Axisymmetric Laboratory Ramjet," AIAA 99-2103, *35th AIAA/ASME/SAE/ASEE Joint Propulsion Conference and Exhibit*, Los Angeles, June, 1999.

18 Peracchio, A.A., Proscia, W.M., "Nonlinear heat-release/acoustic model for thermoacoustic instability in lean premixed combustors," *ASME Paper 98-GT-269*.

19 Cohen, J.M., Anderson, T.J., "Experimental Investigation of Near-blowout Instabilities in a Lean, Premixed Step Combustor," AIAA Paper 96-0819, *34th Aerospace Sciences Meeting and Exhibit*, Reno, NV, Jan. 1996.

20 Richards, G.A., Janus, M.C., "Characterization of Oscillations During Premix Gas Turbine Combustion," ASME Paper 97-GT-244.

21 Hermann, J., Orthmann, A., Hoffmann, S., Berenbrink, P., "Combination of Active Instability Control and Passive Measures to Prevent Combustion Instabilities in a 260MW Heavy Duty Gas Turbine"

22 Billoud, G., Galland, M.A., Huynh Huu, C., Candel, S., "Adaptive Active Control of Combustion Instabilities", *Combust. Sci. and Tech.*, 1992, Vol. 81 pp. 257-283.

23 Gulati, A., Mani, R., "Active Control of Unsteady Combustion-induced Oscillation", *Journal of Propulsion and Power*, v8 n5, Sep-Oct 1992, pp. 1109-1115.

24 Neumeier, Y., Zinn, B.T., AIAA Paper 96-0758, *34th Aerospace Sciences Meeting and Exhibit*, Jan 15-18, 1996, Reno, NV.

25 Neumeier, Y., Markopolous, N., Zinn, B.T., "A Procedure for Real-time Mode Decomposition, Observation, and Prediction for Active Control of Combustion

Instabilities", *IEEE Paper 97318, Conference on Control Applications*, Hartford, CT, Oct 5-7, 1997.

26 Fleifil, M., Annaswamy, A.M., Hathout, J.P., Ghoniem, A.F., ``The Origin of Secondary Peaks with Active Control of Thermoacoustic Instability," *Combustion Science and Technology*, v133, pp. 227-260, June 1998.

27 Lieuwen, T.C., Zinn, B.T., "Experimental Investigation of Limit Cycle Oscillations in an Unstable Gas Turbine Combustor," AIAA Paper 2000-0707, *38th Aerospace Sciences Meeting and Exhibit*, Reno, NV, Jan. 2000.

28 Lieuwen, T.C., "Phase Drift Characteristics of Self Excited Combustion Driven Oscillations," to be published in *J. Sound Vibr.*

29 Sterling, J.D., Zukoski, E.E., "Nonlinear Dynamics of Laboratory Combustor Pressure Oscillations," *Combust. Sci. and Tech.*, v. 77 pp. 225-238, 1991.

30 Schadow, K.C. Gutmark, E., "Combustion instability related to vortex shedding in dump combustors and their passive control," *Energy Combust Sci* v 18 n 2 1992 p 117-132.

31 Marble, F.E., Cox, D.W., Jr., "Servo-Stabilization of Low-Frequency Oscillations in a Liquid BiPropellant Rocket Motor," *ARS Journal*, 23, 63, 1953.

32 Lee, Y.C., Gore, M.R., Ross, C.C., "Stability and Control of Liquid Propellant Rocket Systems," *ARS Journal*, 23, 75, 1953.

33 McManus, K.R., Vandsburger, U., Bowman, C.T., "Combustor Performance Enhancement Through Direct Shear Layer Excitation," *Combust. Flame*, v82, pp. 75-92, 1990.

34 Padamanabhan, K.T., Bowman, C.T., Powell, J.D., "Online adaptive optimal combustor control", *IEEE Transactions on Control Systems Technology*,

35 Richards, G.A., Yip, M.J., "Combustion Oscillation Control by Cyclic Fuel Injection", *J Eng Gas Turbines Power Trans ASME* v119 n2 pp. 340-343, 1997.

36 Seume, J.R. Vortmeyer, N. Krause, W. Hermann, J. Hantschk, C.-C. Zangl, P. Gleis, S. Vortmeyer, D. Orthmann, A. "Application of active combustion instability control to a heavy duty gas turbine," *J Eng Gas Turbines Power Trans ASME* v 120 n 4 Oct 1998.

37 Furlong, E.R., `Mihalcea, R.M., Webber, M.E., Baer, D.S., Hanson, R.K., "Diode-laser sensors for real-time control of pulsed combustion systems," *AIAA Journal*, v37 n6 1999, pp. 732-737.

38 Hathout, J.P., Annaswamy, A.M., Fleifil, M., Ghoniem, A.F., "Active Control of Thermoacoustic Instability Using a Model-Based Approach", *Proceedings of the 1997 ASME International Mechanical Engineering Congress and Exposition*, November, 1997, Dallas, TX.

39 Schadow, K.C., Gutmark, E., Parr, T.P., Wilson, K.J., "Suppression of Combustion Instabilities by Active Shear-Flow/Combustion Control", *International Symposium on Air Breathing Engines*, Nottingham, England, Sept. 1991.

40 Bloxsidge, G.J., Dowling, A.P., Hooper, N., Langhorne, P.J., "Active Control of Reheat Buzz", *AIAA Paper 87-0433,* 25th Aerospace Sciences Meeting, Reno, NV, Jan. 1987.

41 Langhorne, P.J., Dowling, A.P., Hooper, N., "Practical Active Control System for Combustion Oscillations", *J. Propulsion*, v6 n3, pp. 324-333.

42 Sivasegaram, S., Whitelaw, J.H., "Active Control of Combustors with Several Frequency Modes", *ASME Winter Annual Meeting*, Anaheim, CA, Nov 8-13, 1992.

43 Johnson,C.E., Neumeier, Y., Lieuwen, T.C., Zinn, B.T., "Experimental Determination of the Stability Margin of a Combustor Using Exhaust Flow and Fuel Injection Rate Modulations," *28th International Symposium on Combustion*, Edinburgh, 2000.

44 Sattinger, S.S., Amos, D.J., Darling, D.D., Neumeier, Y., Nabi, A., Zinn, B.T., "Sub-Scale Demonstration of the Active Feedback Control of Gas-Turbine Combustion Instabilities," *Proceedings of the 1998 International Gas Turbine & Aeroengine Congress & Exhibition*, Stockholm, Sweden, 1998.

45 Annaswamy, A.M. El Rifai, O.M. Fleifil, M. Hathout, J.P. Ghoniem, A.F., "Model-based self-tuning controller for thermoacoustic instability", *Combust Sci Technol* v 135 n 1-6 1998 Gordon & Breach Science Publ Inc Newark NJ USA p 213-240.

46 Koshigoe, Shozo Komatsuzaki, Toshihiko Yang, Vigor, "Adaptive control of combustion instability with on-line system identification", *J Propul Power* v 15 n 3 May-Jun 1999 AIAA Reston VA USA p 383-389.

47 Bowman, Craig T., and Kemal, Abid, "Active Adaptive Control of Combustion," *4th IEEE Conference on Control Applications*, 1995.

48 Kinsler, Frey, Coppens, and Sanders, *Fundamentals of Acoustics*, *fourth edition*, J. Wiley & Sons, 2000.

49 F.E Marble and S. M. Candel, *Seventeenth Symposium (International) on Combustion*, The Combustion Institute, Pittsburgh, PA, 1978, pp.761-769.

50 V. Yang and F.E.C. Culick, AIAA-83-0574, *AIAA 21st Aerospace Sciences Meeting*, 1983, Reno, Nevada.

51 G. J. Bloxsidge, A.P. Dowling and P.J. Langhorne, *J Fluid Mech* 193:445-473 (1988).

52 M. Fleifil, A.M. Annaswamy, Z.A. Ghoneim and A.F. Ghoniem, *Combust Flame* 106: pp. 487-510 (1996).

53 Zinn, B.T. and L. Narayanasuami, *Acta Astronautic* 9:303-315 (1982)

54 Matsui, Yasuji, *Combust. Flame* 43:199-209 (1981)

55 Poinsot, T., Le Chatelier, C., Candel, S.M., and Esposito, E., *J. Sound Vib* 107:265-278 (1986)

56 Panchenko, N.N., *Combust Explos Shock Waves* 26:699-701 (1991)

57 Lieuwen T., "Online Combustor Stability Margin Assessment Using Dynamics Pressure Data," *Proceedings of ASME/IGTI Turbo Expo 2004*, ASME Paper 2004-53149, Vienna, Austria, June, 2004.

58 Neumeier, Y., Zinn, B.T., "Experimental demonstration of active control of combustion instabilities using real time modes observation and secondary fuel injection," 26th International Symposium on Combustion, Naples, Italy, July, 1996.

59 Johnson, C.E., Neumeier, Y., Neumaier, M., Zinn, B.T., Darling D.D., Sattinger, S.S., " Demonstration of Active Control of Combustion Instabilities on a Full-Scale Gas Turbine Combustor," 2001-GT-0519, ASME Turbo Expo, New Orleans, LA, June 4-7, 2001.

60 Press, W.H., S.A. Teulosky, W.T. Vetterling, B.P. Flannery, *Numerical Recipes in C*, Cambridge University Press, New York, p. 636, 1992.

61 Hibshman, J.R., Cohen, J.M., Banaszuk, A., Anderson, T.J., Alholm, H.A., "Active Control of Combustion Instability in a Liquid-Fueled Sector Combustor," *44th ASME Gas Turbine and Aeroengine Technical Congress*, ASME Paper 99-GT-215, Indianapolis, IN, June, 1999.

62 Banaszuk, A., Jacobson, C.A., Khibnik, A.I., Mehta, P.G., "Linear and Nonlinear Analysis of Controlled Combustion Processes. Part I: Linear Analysis," *1999 Conference on Control Applications*, Hawaii, August, 1999.

63 Banaszuk, A., Jacobson, C.A., Khibnik, A.I., Mehta, P.G., "Linear and Nonlinear Analysis of Controlled Combustion Processes. Part II: Nonlinear Analysis," *1999 Conference on Control Applications*, Hawaii, August, 1999.

64 Coker, A., Neumeier, Y., Lieuwen, T., Zinn, B.T., Menon, S.: "Studies of Active Instability Control Effectiveness in a High Pressure, Liquid Fueled Combustor," *41st Aerospace Sciences Meeting and Exhibit*, AIAA-2003-1009, Reno, Nevada, 2003.

65 United States Patent No. 5,719,791, "Methods, Apparatus and Systems for Real Time Identification and Control of Modes of Oscillations," co-inventor: B. T. Zinn, Atlanta, GA.

66 Neumeier, Y., Zinn, B.T., "Experimental demonstration of active control of combustion instabilities using real time modes observation and secondary fuel injection," *26th International Symposium on Combustion*, Naples, Italy, July, 1996.

67 Neumeier, Y., Nabi, A., Arbel, A., M. Vertzberger, M. and Zinn, B.T., "Open Loop Performance of a Fast-Response, Actively Controlled Fuel Injector Actuator," *Journal of Propulsion and Power*, Vol. 13. No 6, November-December 1997 pp. 705-713.